# Characterizing the *Chlamydia trachomatis* inclusion membrane proteome

Mary Dickinson

A dissertation

submitted in partial fulfillment of the

requirements for the degree of

Doctor of Philosophy

University of Washington

2019

Reading committee

Kevin Hybiske, Chair

Lee Ann Campbell

David Sherman

Program Authorized to Offer Degree:

Pathobiology

University of Washington

## Abstract

Characterizing the *Chlamydia trachomatis* inclusion membrane proteome

Mary Dickinson

Chair of the Supervisory Committee:

Kevin Hybiske

Pathobiology Program, Department of Medicine

*Chlamydia trachomatis* is the most common cause of bacterial sexually transmitted infection, responsible for millions of infections each year. Despite this high prevalence, the elucidation of the molecular mechanisms of *Chlamydia* pathogenesis has been difficult due to limitations in genetic tools and its intracellular developmental cycle. Within a host epithelial cell, chlamydiae replicate within a vacuole called the inclusion. Many *Chlamydia*–host interactions are thought to be mediated by the Inc family of type III secreted proteins that are anchored in the inclusion membrane, but their array of host targets are largely unknown. To investigate how the inclusion membrane proteome changes over the course of an infected cell, we have adapted the APEX system of proximity-dependent biotinylation. APEX is capable of specifically labeling proteins within a 20 nm radius in living cells. We transformed *C. trachomatis* to express the enzyme APEX fused to known inclusion membrane proteins, allowing biotinylation and purification of inclusion-associated proteins. Using quantitative mass spectrometry against APEX labeled samples, we identified over 400 proteins associated with the inclusion membrane at early, middle, and late stages of epithelial cell infection. This system was

sensitive enough to detect inclusion interacting proteins early in the developmental cycle, at 8 hours post infection, a previously intractable time point. A spreadsheet of the proteins identified by APEX at each time point is included as the supplemental file Table S2–1.

Mass spectrometry analysis revealed a novel, early association between *C. trachomatis* inclusions and endoplasmic reticulum exit sites (ERES), functional regions of the ER where COPII-coated vesicles originate. Pharmacological disruption of ERES function severely restricted early chlamydial growth and the development of infectious progeny. Depletion of certain ERES proteins with RNA interference also reduced formation of infectious progeny. Most ERES proteins tested localized to small punctae that sometimes colocalized with the inclusion membrane, but two ERES proteins that were identified by APEX, PDCD6 and TFG, accumulated on the inclusion membrane in certain conditions. When intracellular calcium was elevated, PDCD6 strongly associated with the inclusion membrane. A truncated form of TFG accumulated on the inclusion membrane. Unlike other ERES proteins tested, depletion of PDCD6 caused enhanced *C. trachomatis* infectious progeny formation.

The work in this dissertation shows that APEX is a powerful in situ approach for identifying critical protein interactions on the membranes of pathogen-containing vacuoles. Furthermore, the data derived from proteomic mapping of *Chlamydia* inclusions has illuminated an important functional role for ERES in promoting chlamydial developmental growth.

# Table of Contents

# List of Figures

# List of Tables

## Acknowledgements

I've been very grateful for the support I've received from my friends and family throughout graduate school. I had many great teachers who helped me become interested in science and pursue graduate school. I am thankful for the help and feedback from current and past members of the Hybiske lab, especially Kevin who has been a very supportive mentor. Thanks to the other graduate students in the Pathobiology program, especially those in my year, who made graduate school a lot easier and more enjoyable. I want to thank my parents for helping me along the way and staying excited about what I've pursued. Thanks to my partner Zac for constantly providing me with support and encouragement throughout the past few years.

# Chapter 1 – Introduction

## *Chlamydia trachomatis* disease burden and developmental growth

*Chlamydia trachomatis* is the most common bacterial sexually transmitted infection; despite effective treatments, rates of infection continue to increase each year (1). Since *Chlamydia* infections are often asymptomatic, individuals may maintain and transmit the infection for extended periods of time (2). *Chlamydia* infections are especially impactful for women; they can cause ectopic pregnancy, infertility, and pelvic inflammatory disease. In the United States in 2016 there were 1.6 million cases of *Chlamydia* infection, of which 1.1 million were detected in females (3). *Chlamydia* infections can be treated with antibiotics, and unlike many bacteria, antibiotic resistance is not a major concern. The recommended antibiotics are a single dose of azithromycin or twice daily doxycycline for one week (4). Alternatives include erythromycin, levofloxacin, or ofloxacin (4). Since rates of *Chlamydia* infection continue to rise, preventative measures such as a vaccine may be necessary to decrease the prevalence of *Chlamydia*. There is currently no vaccine, and the lack of understanding of *Chlamydia* basic biology makes it more difficult to develop new strategies to reduce infection. A more thorough understanding of how *Chlamydia* survives and grows within the human host could provide valuable hypotheses for how to prevent infection.

A major challenge in studying *Chlamydia* is the difficulty of cultivating the bacteria in the laboratory. *Chlamydia* has a unique, biphasic developmental cycle that transitions between two forms, the infectious elementary body (EB) and the metabolically active reticulate body (RB) (3, Figure 1–1). This full cycle can only be completed inside of a host cell, so it is not possible to grow *Chlamydia* in broth culture or on agar plates. To begin an infection, an EB attaches and enters a host epithelial cell; in the host cell the EB is enclosed within a vacuole called the inclusion, which provides a separate environment within the host cell cytoplasm (5). It is unknown what environment the inclusion provides to allow growth, but inside the inclusion

*Chlamydia* can transition into the RB form and begin replicating. Starting at around 20 hours post infection (hpi) the RBs start to asynchronously transition back into the EB form (5). After 48-72 hpi *Chlamydia* are released from the host cell and can initiate new infections. Although *Chlamydia* is confined to the inclusion for the duration of the developmental cycle, there are many exchanges across this membrane bilayer to allow *Chlamydia* to secrete proteins into the host cell cytosol, as well as import nutrients into the inclusion.

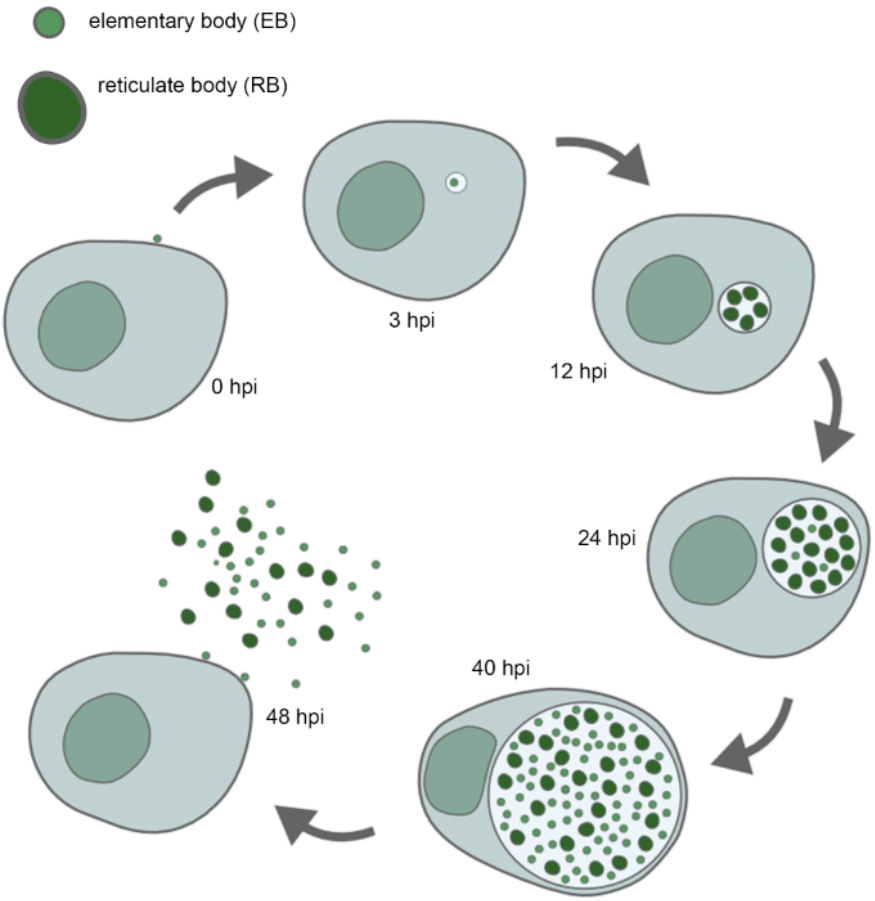


**Figure 1–1. *Chlamydia trachomatis* developmental cycle.**

*Chlamydia trachomatis* developmental forms and representative diagrams of inclusion size at specific hours post infection (hpi). The inclusion grows until around 48 hours when *Chlamydia* are released and can infect new cells.

### Inclusion development and nutrient acquisition

The inclusion membrane originates from the host cell membrane that surrounds the individual bacteria as they are taken up into the cell (6). This small, membrane-bound vacuole

surrounding *Chlamydia* expands to allow bacterial replication, and it is thought that the inclusion membrane is largely host-derived (6). The inclusion rapidly dissociates from the endocytic pathway, and does not acquire markers of endosomes or lysosomes such as EEA1, Lamp1 or Lamp2 (6). Inhibitor of vacuolar acidification Bafilomycin A1 has no effect on *Chlamydia* growth, unlike other intracellular bacteria that occupy acidic vacuoles like *Coxiella burnetii* (6). Within a few hours of infection, the inclusion traffics along microtubules to settle in the perinuclear region near the microtubule organizing center (MTOC) (7). This process requires *Chlamydia* transcription and translation, and also requires host dynein (7).

*Chlamydia* has a highly reduced genome making it dependent on the host cell for many essential factors (8). *Chlamydia* must acquire amino acids, nucleotides, and likely other macromolecules, but it is unknown how these are transported across the inclusion membrane (6). *Chlamydia* is known to interact with the endoplasmic reticulum (ER), golgi, lipid droplets, multivesicular bodies (MVBs) and high density lipoprotein (HDL) machinery to acquire lipids from the cell. During infection, the ER and the inclusion are closely apposed in certain regions, forming membrane contact sites. These contact sites are thought to facilitate acquisition of ceramide through the ceramide transfer protein CERT (9). It was shown that CERT depletion with RNA interference led to a reduction in *Chlamydia* infectious progeny. A CERT inhibitor reduced NBD-ceramide (6-((N-(7-Nitrobenz-2-Oxa-1,3-Diazol-4-yl)amino)hexanoyl)Sphingosine) uptake in a similar manner to brefeldin A (BFA) (10). It was proposed that ceramide uptake via CERT is essential for *Chlamydia* replication, while ceramide uptake via the golgi is dispensable (10). It is unclear why ceramide from these two sources would have a different effect on *Chlamydia* growth. Ceramide is processed into sphingomyelin inside the cell; SMS1 and SMS2 are proteins involved in sphingomyelin production at the golgi or plasma membrane, respectively. It was shown that SMS2, but not SMS1, is recruited to the inclusion membrane, yet knockdown of either SMS1 or SMS2 reduced chlamydial infectious

progeny by similar amounts (10). It is unclear why both would affect IFU, yet only one is recruited to the inclusion membrane.

The golgi becomes fragmented in infected cells, redistributing in mini-stacks around the inclusion (11). There is some evidence that golgi fragmentation is important for *Chlamydia* growth, but there is also evidence that it is dispensable. The interactions between the golgi and the inclusion were first studied in the context of sphingomyelin uptake (12). It was found that in an infected cell, fluorescently labeled ceramide is taken up into the golgi where it is processed into sphingomyelin and taken up by the inclusion from the trans-golgi (13,14). Treatment of infected cells with brefeldin A (BFA), which causes the golgi to collapse into the ER, causes significantly reduced incorporation of NBD-ceramide into the inclusion, yet BFA had no effect on *Chlamydia* replication (13). Similarly, it has been shown that cholesterol can be incorporated into the inclusion membrane and bacterial outer membrane, from a BFA-sensitive pathway (15). Just as with ceramide, BFA significantly reduced cholesterol uptake into the inclusion. Other data that contradicts the importance of the golgi for infection is that knockdown of GBF1, a target of BFA, enhanced the number of infectious progeny or inclusion forming units (IFU) (10). Knockdown of Rab1 and p115, which are important for vesicle tethering to the golgi, enhanced *Chlamydia* IFU (16). So while cholesterol and ceramide are trafficked to the inclusion from the golgi, this trafficking may not be very important for *Chlamydia* growth.

Lipid droplets are lipid storage organelles that contain neutral lipids, contained within a phospholipid monolayer (17). Several chlamydial secreted effectors localize to lipid droplets, and lipid droplets translocate into the inclusion lumen (17,18). It has been proposed that these lipid droplets serve as a source of energy in the form of fatty acids (17). Similarly it is thought that MVBs provide lipids for chlamydial growth (19). MVBs are formed from remodeling of the early endosome, forming an acidic endocytic organelle containing luminal vesicles (20). MVB protein markers CD63 and MLN64 are visible within the inclusion at 36 hpi when labeled by indirect immunofluorescence (19). Similarly, immunoelectron microscopy showed CD63 was associated

with the inclusion at 48 hpi (19). Growing *C. trachomatis* in the presence of exogenous CD63 antibody led to a large reduction in infectious progeny, and inhibitors of PI3K, which impair MVB function, also disrupted chlamydial growth (19). Disruption of MVBs also reduced sphingomyelin uptake into the inclusion (19).

HDL proteins ABCA1, CLA1, and ApoA1 are accumulated inside the inclusions of infected cells (21). ApoA1 localized to foci within the inclusion that colocalized with phosphatidylcholine, so it was hypothesized that this pathway is a mechanism to acquire phospholipids from the host cell (21). A small molecule that inhibits the transporter ABCA1 reduced uptake of phosphatidylcholine into the inclusion, and also decreased *Chlamydia* growth (21). Knockdown of ABCA1 also dramatically reduced *Chlamydia* growth (21).

### *Chlamydia* genetic manipulation

Recent advances in *C. trachomatis* genetic manipulation have provided new avenues for investigating *Chlamydia* basic biology. In 2011, the first stable transformation of *Chlamydia* was reported, providing a method for introducing genes into the bacteria on a modified version of the endogenous *Chlamydia* plasmid (22). Since then, a tetracycline-inducible plasmid system has been developed, for adjusting the timing and level of expression of introduced genes (23). These systems have allowed study of fluorescent *Chlamydia*, epitope-tagging of putative secreted *Chlamydia* inclusion membrane proteins (Incs) to test localization, as well as further testing of host protein-Inc interactions (24). There is currently no method to integrate genes into the chromosome, so if several different genes are introduced they have to go on a single plasmid, creating large vectors that are unstable or difficult to grow.

Although introducing genes is a valuable tool for studying *Chlamydia*, the inability to knockout genes has made confirming any predicted functions difficult. Several strategies have been developed in the past few years to make knockouts possible, though they remain

challenging, time consuming, and unlikely to work on essential genes. Nonetheless, the ability to knockout genes, determine a phenotype, then complement the gene to confirm the effect provides a fundamental, robust framework that is very new to the *Chlamydia* field. Already with the few knockouts made, many functions of one highly studied chlamydial protease, CPAF, have been shown to be an artifact of cellular lysis conditions used previously (25,26). A knockout of CPAF, as well as a complemented strain, have shown that CPAF is likely not as critical to chlamydial virulence as previously thought (26). Likely as the *Chlamydia* genetic field expands, previously identified functions may be called into question.

Two techniques have been developed to randomly disrupt genes in the chlamydial genome. One strategy that has been used to create functional knockouts of *Chlamydia* genes is chemical mutagenesis. *Chlamydia* can be treated with the DNA mutagen ethyl-methanesulfonate (EMS), causing single base mutations by switching cytosine to thymine (27). The level of mutagenesis can be adjusted so the genome of each individual bacterium has only a few base changes. This creates synonymous, non-synonymous, and nonsense mutations randomly throughout the genome. These mutants can be screened for interesting phenotypes, or sequenced to isolate mutations in genes of interest. Since the mutations are caused by single base changes, it is possible for these mutations to revert, especially if the mutation is highly deleterious to growth. Similarly, any genomes with stop codons disrupting essential genes will not be able to grow, so this technique will not work for all genes. Additionally, unless there is a stop codon at the beginning of a gene, it is difficult to assess how impaired the gene function is.

Two systems have been developed to specifically disrupt genes of interest. One technique that has been used is insertion of group II introns into the genome. These introns can be targeted to a gene of interest, where an antibiotic cassette integrates into the genome. This is a more thorough disruption than chemical mutagenesis, however it could have polar effects on genes that are in the same operon, causing disruption of multiple genes. This technique is also costly, it can be difficult to accurately target a certain gene, and it will not work on essential

genes. A technique called fluorescence-reported allelic exchange mutagenesis (FRAEM) has been used to exchange a fluorescent reporter and antibiotic cassette for a gene in the *Chlamydia* genome through homologous recombination (28,29). This requires creation of a plasmid with 3 kb flanking regions to the gene of interest, and with an already large plasmid used to transform *Chlamydia*, the resulting FRAEM plasmid is about 17 kb, making it very difficult to create and use. A new iteration of this plasmid has been created, containing cre recombinase to excise the antibiotic cassette following integration (30). This minimizes risks of polar effects, and would allow knockout of multiple genes following multiple rounds of transformation.

As chlamydial genetics advance, there are many more opportunities to use modern techniques to study pathogenesis. There has been some success with adaptation of dCas9 for gene knockdown, though thus far it is not stable enough to reliably deplete *Chlamydia* gene expression (31). With screening of Cas9 from different species, or alternative nucleases such as Cpf1, it may be possible to have a consistent way to knockdown protein levels. This would be useful even for essential genes that play critical roles during infection.

### *Chlamydia*–host interactions

*Chlamydia* uses the type III secretion apparatus to secrete effectors across the inclusion membrane. Of these effectors, 59 are predicted to localize to the inclusion membrane and are members of the Inc protein family (32). Given that the *C. trachomatis* genome encodes 894 proteins, the Incs represented a large portion of the genome and are thought to be critical for mediating many host-pathogen interactions. Despite the importance, determining any functions or binding partners for these Incs has been difficult.

Traditional biochemical techniques such as co-immunoprecipitation, yeast two-hybrid, and bacterial two-hybrid have identified binding partners of a few of the Incs. Yeast two-hybrid identified 14-3-3β as the first host protein that was found to bind a *Chlamydia* inclusion membrane protein, IncG (33). Rab4 was found to bind *Chlamydia* Inc CT229 (34). Co-

immunoprecipitation was used to show that IncA and CT813 interact with host SNARE proteins (35). CT223 binds the centrosomal protein CEP170 to alter microtubule organization (36). Limited antibodies and the lack of genetic tools for introducing tagged genes into *Chlamydia* made large scale identification of Inc binding partners difficult until recently.

There have been a handful of protein-protein interactions identified between *Chlamydia* effectors and proteins within the host, but it is likely that there are many more for the numerous type III secreted effectors that have no known binding partners. In addition to the type III secreted effectors, at least one type II secreted effector is transported into the host cytoplasm during infection (37). There are also many host proteins that associate with the inclusion membrane that have no known Inc binding partner. In addition to Rab4, Rab1, Rab6, and Rab11 are also recruited to the *C. trachomatis* inclusion membrane (37). The inclusion interacts with several components of the cytoskeleton; detyrosinated and acetylated microtubules, as well as actin and intermediate filaments redistribute around the inclusion membrane (38,39). In most cases these interactions are studied in isolation, but as we discover more host proteins associated with the inclusion membrane it may reveal connections between the proteins recruited by different Incs.

**Proteomics of inclusion-interacting proteins**

Two proteomics studies facilitated the discovery of new host proteins that interact with the inclusion membrane during infection. Mirrashidi et al. expressed 58 tagged Incs in HEK293T cells and used tandem affinity purification to pull down interacting proteins (40). This was done in the absence of infection so some interactions may not be maintained in a natural infection. This paper highlighted a new association between IncE and the retromer complex. They confirmed that IncE binds SNX5 and SNX6 during infection and SNX1, SNX2, SNX5, and SNX6 localize to the inclusion. Interestingly, knockdown of retromer components led to an increase in infectious progeny, suggesting that the retromer restricts *Chlamydia* growth.

Since this paper came out, at least one study has confirmed two other interactions from this data set between IncV (CT005) and ER resident proteins VAPA and VAPB (41).

In the other proteomics study, Aeberhard et al. developed a method to purify whole inclusions at 24 hpi (42). Following purification, they performed mass spectrometry on lysates of these whole inclusions. They expressed 26 of the proteins identified with fluorescent protein fusions or epitope tags and verified that at least 19 of these hits were associated with the inclusion membrane, showing fairly high accuracy of this method for identifying inclusion-associated proteins. Similar to the affinity purification study, they confirmed that retromer proteins SNX1, SNX2, SNX5 and SNX6 were recruited to inclusion membranes and knockdown of these proteins enhanced formation of infectious progeny.

These two proteomics studies have both identified many novel host proteins that may be associated with the *Chlamydia* inclusion membrane. Each strategy identified about 350 proteins, and combined there are 626 unique proteins with potential roles during infection. It is not clear why there was little overlap between the studies, but infection may alter the abundance of some of the proteins detected and the tandem affinity purification was not done in infected cells. There may have also been different conditions for pulldown of proteins vs inclusions. High abundance proteins associating with purified inclusions may have been more easily detected even if they don't directly bind an Inc. Additionally, Incs are known to bind each other so overexpression of a single Inc may not capture interactions that require the presence of multiple Inc binding partners. Overall these studies provide numerous opportunities for investigating host proteins that may associate with the inclusion membrane, but these data are hardly comprehensive. Since these two studies required pulldown of either tagged Incs or purified inclusion following cell lysis, it is likely that more transient or sensitive interactions would not be maintained. Also these were performed either in the absence of infection or at a single time point, but it is likely that the host factors associated with the inclusion change over time. Thus, while we have learned much about the inclusion membrane proteome, there is still a need for

investigation of how the inclusion membrane changes over time, as well as a way to identify interactions that are not as stable.

**Dissertation Summary**

Determining the host proteins that associate with the inclusion during infection could provide novel insight into the host pathways that are required for optimal *Chlamydia* growth. Identifying proteins that are associated with the inclusion early during infection would be particularly valuable, as this time point has been difficult to study by traditional molecular biology techniques. The goal of this dissertation was to identify novel host proteins associated with the inclusion membrane during different stages of infection. Chapter 2 discusses the approach used to identify inclusion-associated proteins with proximity-dependent biotinylation and mass spectrometry. Chapter 3 reveals one set of proteins identified by mass spectrometry were ER exit sites, and shows that these sites are functionally important for *Chlamydia* growth. Chapter 4 investigates a protein complex within ER exit sites that is strongly recruited to the inclusion membrane. Chapter 5 discusses a summary of the findings in this dissertation, final conclusions, and future directions for studying inclusion-associated proteins and ER exit sites in the context of *Chlamydia* infection.

# Chapter 2 – Identifying novel proteins associated with the inclusion membrane using proximity-dependent biotinylation

Text and figures in this chapter adapted from the article:

Mary Dickinson, Lindsey Anderson, Bobbie-Jo Webb-Robertson, Joshua Hansen, Richard Smith, Aaron Wright, Kevin Hybiske (2018) Proximity-dependent proteomics of the *Chlamydia trachomatis* inclusion membrane reveals functional interactions with endoplasmic reticulum exit sites. In review, PLOS Pathogens.

## Introduction

*Chlamydia trachomatis* is an obligate intracellular bacterium that infects mucosal epithelial cells of the endocervix and conjunctiva. It infects millions of people every year and is the etiological agent of ocular trachoma (1,43). Although *C. trachomatis* infections are effectively treated with antibiotics, the majority of infections are asymptomatic and go untreated (2). The consequences of long term infection can be severe, especially in chronically infected women that are at risk for developing pelvic inflammatory disease, ectopic pregnancy, or infertility as a consequence of infection (44). Chlamydiae undergo a biphasic developmental cycle, characterized by transitions between infectious elementary bodies (EB) and metabolically active reticulate bodies (RB) (5,45). During infection of a host cell, an EB attaches to and internalizes into a vacuole called the inclusion. Within the inclusion, EB–RB conversion and replication proceed, ultimately followed by asynchronous conversion to EB and exit from the host cell. Chlamydial growth within host cells is critically dependent on protein rearrangements on the inclusion membrane early during infection, and on extracting nutrients from the host cell. The mechanisms responsible for these processes are not well understood. The streamlined

genome of *Chlamydia* necessitates a dependency on the host cell for many nutrients, yet some of these molecules cannot freely permeate the inclusion membrane and import systems have not been identified (8). In addition, while much is known about chlamydial manipulation of host signaling, very little is known about the molecular processes necessary for *Chlamydia* to obtain nutrients from the host (45,46).

The inclusion membrane represents the major interface through which chlamydiae manipulate host cell function. In accordance with this, different chlamydial species encode 50-70 type III secreted inclusion membrane (Inc) proteins that are predicted to localize to the inclusion membrane throughout the chlamydial developmental cycle (47–52). The Inc family is a signature genetic feature of chlamydiae; however, their lack of sequence similarity with proteins from other bacteria has largely precluded bioinformatic prediction of molecular functions and potential host interaction targets. Two major proteomic studies in recent years have greatly advanced our knowledge of candidate host proteins associated with the inclusion membrane and with specific Inc proteins (40,42). These studies also highlighted molecular interactions that occur between the inclusion membrane and the retromer complex (40,42).

A comprehensive understanding of inclusion membrane modifications, and the host proteins recruited to the inclusion, has not been realized. Even less is known regarding the temporal dynamics of these interactions over the 48-72 hour *C. trachomatis* developmental cycle, and the factors that are critical for inclusion biogenesis. Molecular analysis of early inclusions has been particularly elusive due to their small size. Previous proteomic efforts provided major new insight into the inclusion membrane proteome; however they were unable to characterize protein compositions of early inclusions or identify temporal protein associations. The development of techniques to investigate the inclusion membrane proteome under native conditions, at multiple stages of infection, would accelerate the discovery of *Chlamydia*–host interactions. To this end, we used the APEX system of proximity-dependent biotinylation in *C. trachomatis*, as a flexible tool for exploring host-pathogen interactions. APEX

has been tested in *Chlamydia* by microscopy and western blot, and shown to be able to biotinylate proteins on the inclusion membrane when fused to inclusion membrane proteins IncF, IncA, or a truncated IncA (53). APEX is an ascorbate peroxidase that catalyzes a reaction between biotin-phenol and hydrogen peroxide, forming a phenoxyl radical that rapidly forms a covalent bond with a nearby amino acid (54,55). The labeling radius of APEX is less than 20 nm, and the reaction is carried out in living cells for only one minute; this allows highly spatially and temporally resolved biotinylation of proteins in situ. In combination with mass spectrometry, APEX has been used to map the mitochondrial matrix, outer membrane, and inner membrane space, as well as the endoplasmic reticulum (ER) membrane and several other subcellular locations of mammalian cells (55–58). Recently, APEX was used to study how protein interactions with G-protein-coupled receptors change after activation, highlighting its experimental utility for studying protein interaction dynamics (59). We engineered a *C. trachomatis* strain that contained an Inc protein fused to APEX, and under the control of an inducible promoter. Using this strain, we expressed Inc-tagged APEX on the inclusion membranes of cells infected with *C. trachomatis* at three stages of growth. Subsequent quantitative mass spectrometry defined the proteomes of inclusion membrane interacting proteins at early, middle, and late stages of chlamydial development.

## Results

### Development of the APEX *in situ* proximity labeling system for *C. trachomatis*

We sought to develop the APEX system for identifying inclusion interacting proteins, with the primary goal of determining how these interactions evolve during *Chlamydia* infection of host cells. Previous mass spectrometry studies of the inclusion membrane were either done in the absence of infection, or only at a later stage of infection after mechanical manipulations

(40,42). These studies also used techniques that required lysing open the host cells and pulling down Incs or whole inclusions in an in vitro environment, which may have disrupted weaker, more transient protein-protein interactions. With the recent development of a transformation system for *Chlamydia*, a wide range of techniques are now possible (22,24). Leveraging this advance, we infected cells with a *C. trachomatis* L2/434 strain engineered to express Inc-APEX fusion proteins, to enable the capture of inclusion membrane interacting proteins in live cells, at multiple times during infection. The Inc-APEX fusion protein localized to inclusion membranes, with APEX exposed in the host cell cytosol. The APEX system is highly sensitive, has defined the proteomes of cellular compartments refractory to other techniques, and APEX enzymatic function was shown to remain intact when tagged to a chlamydial Inc protein (53,54,57).

We transformed *C. trachomatis* to express different Inc proteins (IncB, IncA, IncC, InaC, and CT223) tagged to APEX and tested protein biotinylation levels by western blot, and their localization by immunofluorescence microscopy. Although IncB, IncC, and CT223 are known to localize to microdomains in the inclusion membrane, when overexpressed and fused to APEX they often localized around the entire inclusion membrane (Figure S2–1A). IncC-APEX was seen in microdomains in some inclusions, and distributed around the inclusion membrane in others (Figure S2–1B). IncB-APEX and CT223-APEX did not appear to be in microdomains; CT223-APEX was observed both on the inclusion membrane as well as inside bacteria, while IncB-APEX was exclusively observed on the inclusion membrane (Figure S2–1A). These results are slightly different than localization seen by overexpression of flag-tagged Incs, where IncB-flag, CT223-flag, and IncC-flag localized to microdomains. It is possible that APEX interfered with endogenous binding partners of these Incs, or expression levels were different than in a previous study (52). IncA-APEX was not secreted very efficiently, but this appears to be an issue with our construct, as IncA-APEX has been previously tested (53). To determine whether overexpression had a negative effect on *Chlamydia* growth we infected HeLa cells with *Chlamydia* strains expressing Inc-APEX fusions and induced expression with 1 ng/mL anhydrotetracycline (ATc)

at the start of infection, then measured inclusion diameter at 24 hours post infection (hpi). Strains expressing IncA-APEX and IncB-APEX resulted in the largest inclusions as measured by diameter; IncA-APEX was not secreted efficiently so we did not go forward with this strain, but IncB-APEX had a clear localization around the inclusion membrane (Figure S2–1C). We also tested if IncB-APEX overexpression affected endogenous Inc localization using immunofluorescence microscopy. By comparing uninduced or IncB-APEX expressing *C. trachomatis* we did not observe any differences in IncA localization, and microdomains marked with CT223 appeared normal (Figure S2–2A,B). There was a slight decrease in inclusion diameter with the IncB-APEX *Chlamydia* when grown in the presence of ATc, indicating overexpression had some detrimental effects on inclusion growth (Figure S2–2C). Since IncB-APEX distributed evenly around the inclusion membrane and did not cause expansion of endogenous microdomains, we deemed it the most suitable whole inclusion membrane probe, rather than identifying microdomain-specific proteins (52,60).

To further ensure that the results of IncB-APEX were generalizable, we performed preliminary mass spectrometry analysis with the two Incs that gave the highest amount of biotinylation by western blot (IncB and CT223). We determined that IncB-APEX identified more host proteins when overexpressed, in concordance with the western blot data, and IncB-APEX detected all the proteins that were found by the CT223-APEX fusion with the exception of two proteins. This fits with previous uses of APEX, where the proteomic results were localization-specific, rather than representing binding partners of the protein fused to APEX. We therefore chose to focus on IncB-APEX for the rest of our experiments. In subsequent mass spectrometry experiments IncB-APEX identified the two proteins that were identified by CT223-APEX in the first trial, confirming that these proteins were not unique to CT223. Furthermore, IncB is constitutively expressed during infection, ensuring that any chaperones necessary for proper secretion will be present at any time points tested (60–62).

For mass spectrometry experiments we used *C. trachomatis* L2/434 transformed with a tetracycline inducible plasmid encoding IncB-APEX (Figure 2–1A). At specific time points, biotin-phenol and hydrogen peroxide were added to catalyze protein biotinylation, and resulting labeled proteins were pulled down using streptavidin and identified by mass spectrometry (Figure 2–1B). We confirmed that protein biotinylation required IncB-APEX expression, biotin phenol, and hydrogen peroxide (Figure 2–1C). Furthermore, the profile and depth of labeled proteins in cells infected with the IncB-APEX expressing *C. trachomatis* strain were distinct from cells infected with a strain expressing an untagged APEX that was not secreted (Figure 2–1C). Staining of infected, labeled cells with a fluorescent streptavidin probe demonstrated that biotinylated proteins were enriched on inclusion membranes at 8, 16 and 24 hpi (Figure 2–1D). Biotinylated proteins at 8 hpi manifested as distinct foci which were always outside of the bacterial outer membrane, indicating that IncB-APEX is being secreted.

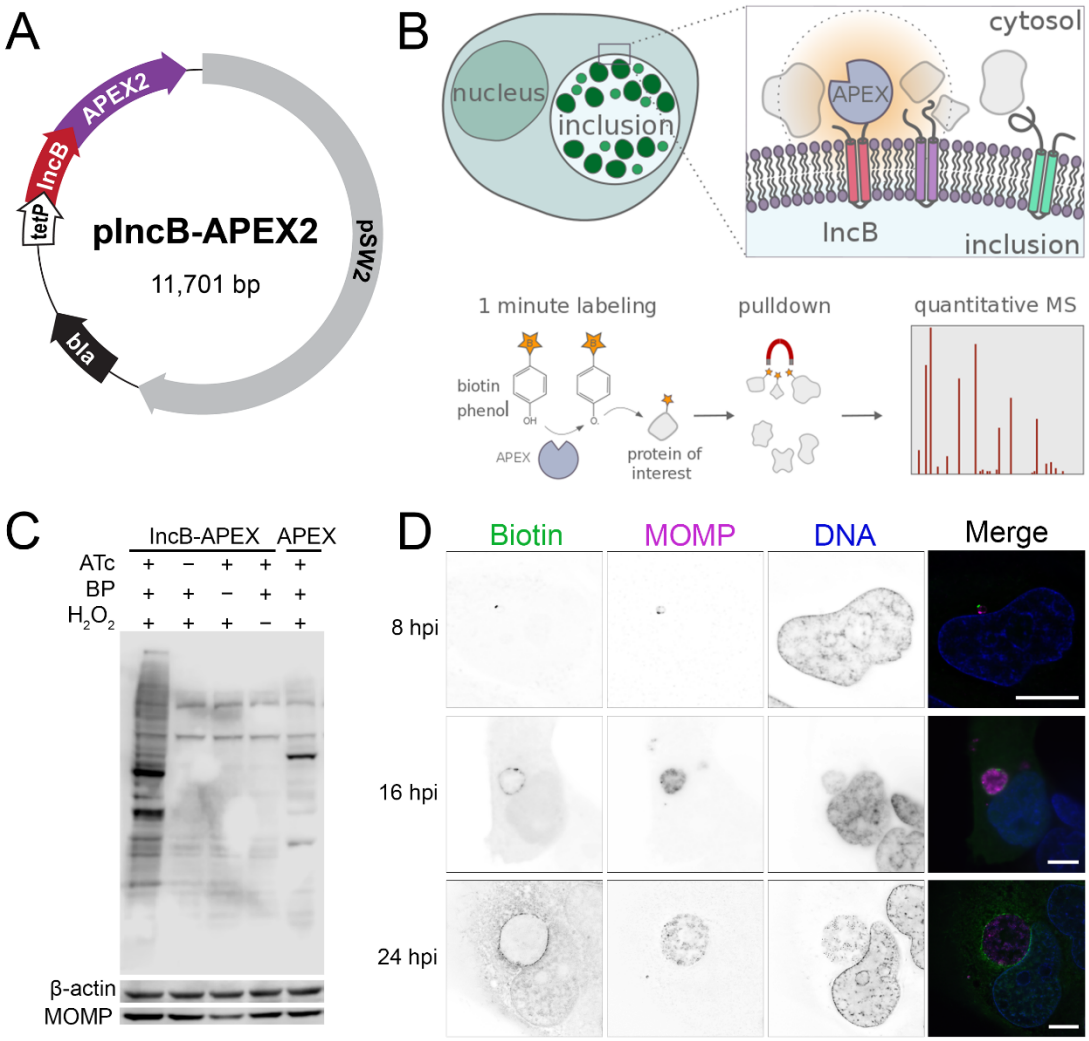


**Figure 2–1. In situ proteomic labeling of the *C. trachomatis* inclusion membrane.**

(A) Plasmid used to transform *C. trachomatis* L2 and localize APEX to the inclusion membrane. IncB-APEX2 fusion expression was under the control of a tetracycline inducible promoter. (B) Schematic for APEX localization and biotinylation reaction. Cells were infected with *C. trachomatis* expressing IncB-APEX for 8, 16, or 24 hours, expression was induced by anhydrotetracycline, and incubation with biotin-phenol and hydrogen peroxide for 1 minute catalyzed biotinylation of proteins within ~20 nm of APEX. Biotinylated proteins were enriched using streptavidin coated agarose resin and relative abundance estimated using mass spectrometry-based proteomics. (C) Western blot analysis of cells infected for 16 hours with *Chlamydia* expressing IncB-APEX (first four columns) or untagged APEX (last column). Blots were probed with streptavidin-HRP to detect biotinylated proteins. Anti beta-actin and anti MOMP antibodies were used as human and *Chlamydia* loading controls, respectively. BP, biotin-phenol; ATc, anhydrotetracycline. (D) Immunofluorescence microscopy of cells infected with *C. trachomatis* IncB-APEX and after 1 min inclusion membrane protein labeling at 8, 16, and 24 hpi. Representative images are shown. Biotin labeled proteins were identified by streptavidin-Alexa 488, *Chlamydia* were labeled with an anti-MOMP antibody, DNA labeled with DAPI. Single channel images are displayed in inverted grayscale. Merged panels display all three color channels. Scale bars = 16 μm.

**Identification of inclusion interacting proteins by quantitative mass spectrometry**

HeLa cells were infected with IncB-APEX *C. trachomatis*, with 1 ng/ml anhydrotetracycline added at the start of infection to induce expression (23). At 8, 16, or 24 hpi, infected cells were incubated with biotin-phenol for 30 min, and protein biotinylation was catalyzed by the addition of hydrogen peroxide for 1 minute. Following reaction quenching, cells were immediately pelleted and frozen for further processing. Control cells were treated identically to experimental cells, minus the addition of hydrogen peroxide. For each infection time point, biotinylated proteins were prepared from six biological replicates and six controls for enrichment and analysis by mass spectrometry.

Mass spectrometry of IncB-APEX-labeled samples identified 452 unique host proteins and 15 chlamydial proteins across the three time points analyzed. The presence of these proteins exhibited notable dynamics over the times tested, for example some only present at a single time point, and others maintained throughout infection (Figure 2–2A). Among host proteins recruited to *C. trachomatis* inclusions, 89 were significantly enriched at 8 hpi, 178 proteins at 16 hpi, and 396 proteins at 24 hpi. There were 37 proteins that maintained enrichment at all three time points (Figure 2–2A). Of the 15 chlamydial proteins labeled by IncB-APEX, 11 were annotated as Incs (Figure 2–2B, Incs highlighted in green). Another, CT610 (CADD), does not have a canonical Inc structure but has been shown to be secreted with an inclusion membrane localization (63). Of the remaining three *Chlamydia* proteins, two are found in high abundance in the bacteria and thus may be due to labeling by pre-secreted IncB-APEX. A complete list of proteomic data is contained in Table S2–1.

To develop an understanding of the general roles of proteins identified by IncB-APEX labeling, and to confirm that our approach labeled pathways and cellular components that *Chlamydia* is known to interact with, we analyzed proteomic data against annotation databases.

Pathway overrepresentation analysis was performed using InnateDB with KEGG pathways, and the representation of subcellular locations in the data set was determined using the Human Protein Atlas database (64–66). KEGG pathway analysis showed that many of the identified proteins were associated with cellular pathways known to play roles during *Chlamydia* infection, including 'bacterial invasion of epithelial cells' and endocytosis (Figure 2–2C). Proteins associated with ER processing were significantly enriched at all three time points. Proteins involved in glycolysis and the pentose phosphate pathway were significantly enriched at 8 hpi. Analysis of subcellular localization annotations for IncB-APEX labeled proteins revealed a general spatial context consistent with the known perinuclear residence of the inclusion (Figure 2–2D,E) (46). Ontology analysis indicated that early in *C. trachomatis* infection, at 8 hpi, inclusions acquired proteins normally localized to the cytosol, nucleus, plasma membrane, ER, and vesicles. Growth and maturation of the inclusion, at 16 and 24 hpi, was accompanied by a sustained enrichment of proteins associated with early inclusions, as well as an emergence of interactions with cytoskeleton associated proteins: actin, microtubules, centrosomes, the MTOC, and intermediate filaments. Although there are limitations to the accuracy of annotations in KEGG or localization databases, the pathway overrepresentation analysis highlights expected enrichments in the IncB-APEX dataset, as well as potential new associations that could be relevant to *Chlamydia* growth.

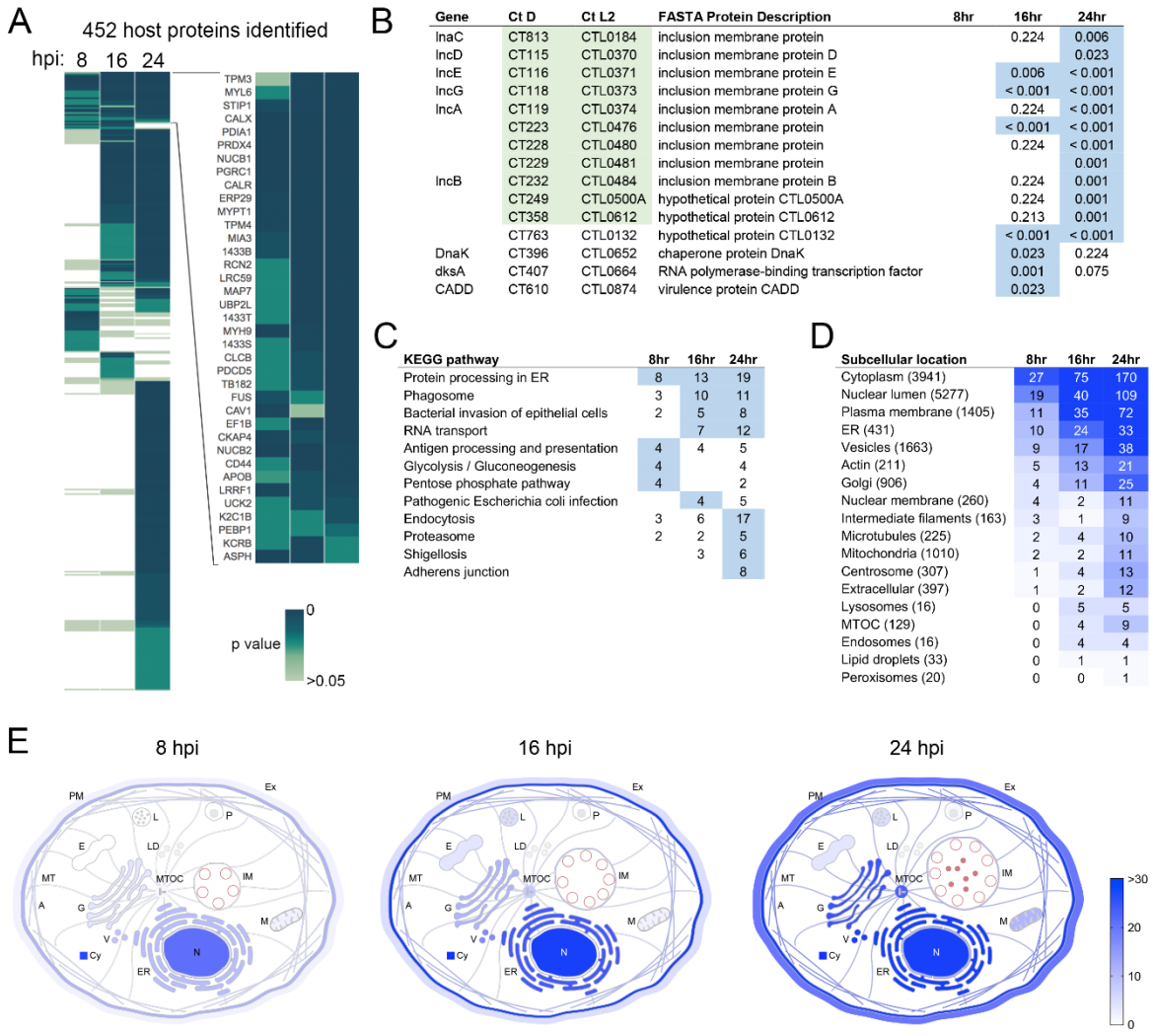


| Gene | Ct D | Ct L2 | FASTA Protein Description | 8hr | 16hr | 24hr |
|---|---|---|---|---|---|---|
| InaC | CT813 | CTL0184 | inclusion membrane protein | | 0.224 | 0.006 |
| IncD | CT115 | CTL0370 | inclusion membrane protein D | | | 0.023 |
| IncE | CT116 | CTL0371 | inclusion membrane protein E | | 0.006 | < 0.001 |
| IncG | CT118 | CTL0373 | inclusion membrane protein G | | < 0.001 | < 0.001 |
| IncA | CT119 | CTL0374 | inclusion membrane protein A | | 0.224 | < 0.001 |
| | CT223 | CTL0476 | inclusion membrane protein | | < 0.001 | < 0.001 |
| | CT228 | CTL0480 | inclusion membrane protein | | 0.224 | < 0.001 |
| | CT229 | CTL0481 | inclusion membrane protein | | | 0.001 |
| IncB | CT232 | CTL0484 | inclusion membrane protein B | | 0.224 | 0.001 |
| | CT249 | CTL0500A | hypothetical protein CTL0500A | | 0.224 | 0.001 |
| | CT358 | CTL0612 | hypothetical protein CTL0612 | | 0.213 | 0.001 |
| | CT763 | CTL0132 | hypothetical protein CTL0132 | | < 0.001 | < 0.001 |
| DnaK | CT396 | CTL0652 | chaperone protein DnaK | | 0.023 | 0.224 |
| dksA | CT407 | CTL0664 | RNA polymerase-binding transcription factor | | 0.001 | 0.075 |
| CADD | CT610 | CTL0874 | virulence protein CADD | | 0.023 | |

| KEGG pathway | 8hr | 16hr | 24hr |
|---|---|---|---|
| Protein processing in ER | 8 | 13 | 19 |
| Phagosome | 3 | 10 | 11 |
| Bacterial invasion of epithelial cells | 2 | 5 | 8 |
| RNA transport | | 7 | 12 |
| Antigen processing and presentation | 4 | 4 | 5 |
| Glycolysis / Gluconeogenesis | 4 | | 4 |
| Pentose phosphate pathway | 4 | | 2 |
| Pathogenic Escherichia coli infection | | 4 | 5 |
| Endocytosis | 3 | 6 | 17 |
| Proteasome | 2 | 2 | 5 |
| Shigellosis | | 3 | 6 |
| Adherens junction | | | 8 |

| Subcellular location | 8hr | 16hr | 24hr |
|---|---|---|---|
| Cytoplasm (3941) | 27 | 75 | 170 |
| Nuclear lumen (5277) | 19 | 40 | 109 |
| Plasma membrane (1405) | 11 | 35 | 72 |
| ER (431) | 10 | 24 | 33 |
| Vesicles (1663) | 9 | 17 | 38 |
| Actin (211) | 5 | 13 | 21 |
| Golgi (906) | 4 | 11 | 25 |
| Nuclear membrane (260) | 4 | 2 | 11 |
| Intermediate filaments (163) | 3 | 1 | 9 |
| Microtubules (225) | 2 | 4 | 10 |
| Mitochondria (1010) | 2 | 2 | 11 |
| Centrosome (307) | 1 | 4 | 13 |
| Extracellular (397) | 1 | 2 | 12 |
| Lysosomes (16) | 0 | 5 | 5 |
| MTOC (129) | 0 | 4 | 9 |
| Endosomes (16) | 0 | 4 | 4 |
| Lipid droplets (33) | 0 | 1 | 1 |
| Peroxisomes (20) | 0 | 0 | 1 |

**Figure 2–2. Global analysis of the inclusion membrane interaction proteome throughout the *C. trachomatis* developmental cycle.**

(A) Heatmap of inclusion membrane interacting proteome identified by APEX at 8, 16, and 24 hpi. Data from 6 replicate experiments per time point were averaged and compared against 6 replicate controls at similar times. Colors represent *p*-values, proteins not detected have no color. Enlarged section of heatmap shows proteins significantly enriched at all time points. Significance determined by t-test or g-test, $p < 0.05$. (B) *C. trachomatis* ORFs identified on the inclusion membrane, with p values displayed for their presence in 6 replicate samples for each time point. Locus tags highlighted in green represent annotated Inc proteins. Values highlighted in blue represent *p* values < 0.05. (C) KEGG pathway overrepresentation analysis of inclusion membrane proteome (65). Overrepresentation determined by hypergeometric algorithm with Benjamini Hochberg method for multiple test correction. Values highlighted in blue represent *p* values < 0.05. (D) Subcellular location enrichments of APEX identified proteins. Color intensity reflects the number of proteins for each location annotation pulled from the Human Protein Atlas database (66). Numbers in parentheses indicate the total number of reference proteins contained under that annotation in the Human Protein Atlas database. (E) Spatial distribution of inclusion interacting proteins from 8-24 hpi using Human Protein Atlas annotations and manual entry of Inc proteins. Color intensity indicates the number of proteins assigned to

location annotations. A, actin filaments; Cy, cytosol; E, endosomes; ER, endoplasmic reticulum; Ex, extracellular/secreted; G, Golgi apparatus; IM, inclusion membrane; L, lysosomes; LD, lipid droplets; M, mitochondria; MT, microtubules; MTOC, microtubule organizing center; N, nucleus; P, peroxisomes; PM, plasma membrane; V, vesicles.

We used the STRING database to identify known molecular interactions between identified proteins, plotted all proteins with at least one interacting partner (Figure 2–3A). This allowed analysis of the potential recruitment of multiprotein interaction complexes to the *C. trachomatis* inclusion. Highly interconnected protein communities were identified using the Louvain method of community detection. From this analysis, major protein networks emerged, encompassing innate immune signaling, the nuclear membrane, vesicular traffic, the cytoskeleton, nucleoside metabolism, and ER chaperones. Since the inclusion is anchored in the perinuclear region, the nuclear membrane was likely labeled along the edge of the inclusion that borders the nucleus. Temporal analysis of these interactions revealed a dramatic recruitment of glycolytic proteins to early inclusions, for example aldolases, transketolase, pyruvate kinase, glucose-6-phosphate isomerase, and peroxiredoxin (Figure 2–3B). Inclusion maturation was marked by a significant expansion of protein networks related to the MTOC and centrosome, innate immune signaling, proteasome regulation, and clathrin assembly (Figure 2–3B). Network analysis also allowed identification of host factors that may potentially interact with known host–Inc interactions, for example VAPA association with IncV (41) and the potential expanded interaction with S10AG and S10AE.

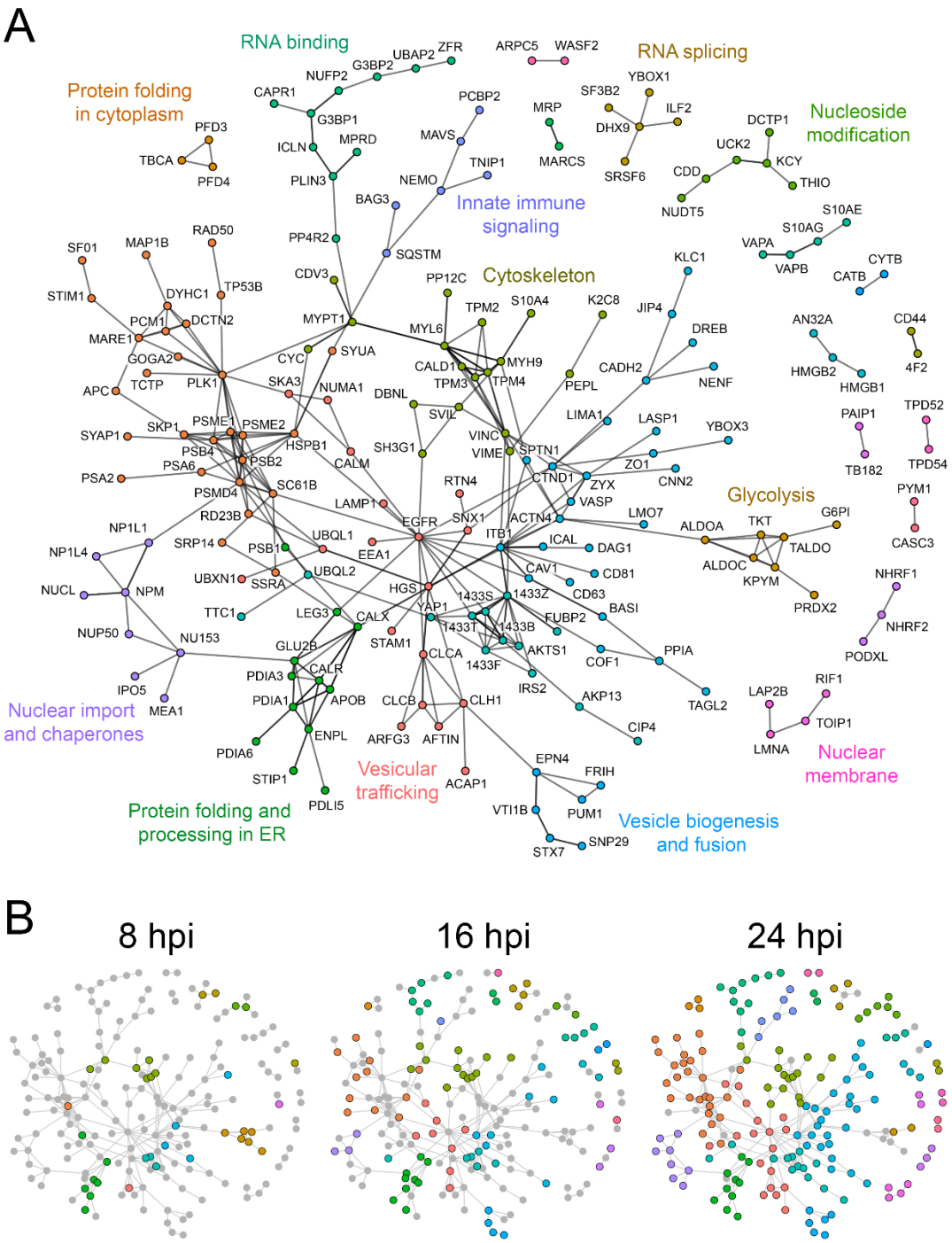


**Figure 2–3. Network analysis of *C. trachomatis* inclusion membrane interacting proteins.**

(A) Interactions between host proteins identified by APEX proteomic labeling were obtained from StringDB (67), and visualization map was generated using R with the tidygraph package (68). Colors represent more interconnected protein communities within the network. The interaction map in A represents the global extent of inclusion membrane interactions identified over the chlamydial developmental cycle. Edges between protein nodes represent interactions

that were curated in StringDB either from published experiments or other databases. Proteins which do not have characterized interaction partners (i.e. single nodes) and translation related proteins were omitted for clarity. (B) Temporal dynamics of inclusion membrane protein interaction networks over the developmental cycle. Protein networks present in 8, 16, and 24 hpi proteomic data sets are represented by colored nodes. Gray nodes depict proteins present in the global interaction map (A) but absent from a specific stage of infection.

**Functional validation of targets recruited to early inclusions**

Because *C. trachomatis* inclusions at 8 hpi are so small, validation of host protein recruitments by fluorescence microscopy is difficult. We reasoned that proteins associated with early inclusion membranes might play important roles in mediating the biogenesis of the inclusion. To validate the functional participation of inclusion-associated proteins towards *Chlamydia* developmental growth, we performed RNA interference (RNAi) on 64 of the 89 proteins present in the 8 hpi interaction dataset. HeLa cells were grown in a 96 well plate format, transfected with siRNA oligonucleotides for 48 h, and infected with *C. trachomatis* L2 to determine the impact of protein depletion on bacteria growth. At 48 hpi, EB were harvested from siRNA treated cells and analyzed for inclusion forming units (IFU) on fresh cells. Knockdown of 16 proteins (25%) resulted in a >1.5 fold change in infectious progeny formation, as compared to the mean IFU of the plate and a nontargeting siRNA control (Figure 2–4A). A change of 1.5 fold was highlighted due to use in a previous siRNA screen (69). As a positive control, depletion of MAP1LC3B resulted in decreased *C. trachomatis* IFU, consistent with reported findings (69). Overall, 10 protein knockdowns resulted in a >1.5 fold decrease in IFU (Figure 2–4A top), and 6 protein knockdowns led to a >1.5 fold increase in IFU (Figure 2–4A bottom). We verified knockdown by qRT-PCR for the targets with at least 1.5 fold difference in IFU (Figure S2–3). Proteins whose depletion resulted in decreased IFU were frequently targets identified by IncB-APEX at multiple stages of *Chlamydia* development (Figure 2–4A). In contrast, many of the proteins whose knockdown led to increased IFU production were more transiently recruited to inclusions, with enrichments primarily detected at early inclusions

(Figure 2–4A). Collectively, the RNAi data show IncB-APEX identified proteins at the inclusion membrane that functionally impacted chlamydial growth.

Our mass spectrometry data provided an opportunity for comparison with those generated by previous studies, to develop a more comprehensive understanding of the protein networks recruited to the inclusion membrane. First, we compared our IncB-APEX data set to two previous mass spectrometry experiments that conducted analysis on purified inclusions (labeled as 'inclusion-MS' in Figure 2–4B) (42), and affinity purified Incs expressed in 293 cells (labeled as 'AP-MS' in Figure 2–4B) (40). Furthermore, proteins were manually cross-referenced against the literature to identify evidence-based reports of proteins recruited to inclusions or inclusion membrane proteins (labeled with PMID in Figure 2–4C). Overall, 16 proteins were identified by all three MS approaches to interact with inclusions, and the present study now provides temporal data for when these interactions occur during host cell infection (Figure 2–4B, upper half). Ten of the 16 proteins were previously reported to be recruited to inclusion membranes by immunofluorescence microscopy (Figure 2–4C). The remaining 6 proteins identified by all 3 MS approaches–ASPH, LRRF1, LRC59, TMOD3, CLINT1, and BAP31–represent priority targets for further study in the context of *Chlamydia* infection. IncB-APEX labeling contained 60 additional proteins that were identified on 24 hpi inclusions by inclusion-MS (Table S2–1) (42). Thirteen proteins from IncB-APEX data correlated with Inc specific data obtained from AP-MS, thus adding in situ context to previously described molecular interactions (Figure 2–4B, lower half) (40). Finally, IncB-APEX identified 31 proteins previously shown by microscopy to be in close proximity to inclusions during infection (Figure 2–4C). This substantiates the efficacy of the APEX approach and additionally provides important new temporal information for how these host targets are dynamically recruited to the inclusion membrane by *Chlamydia*.

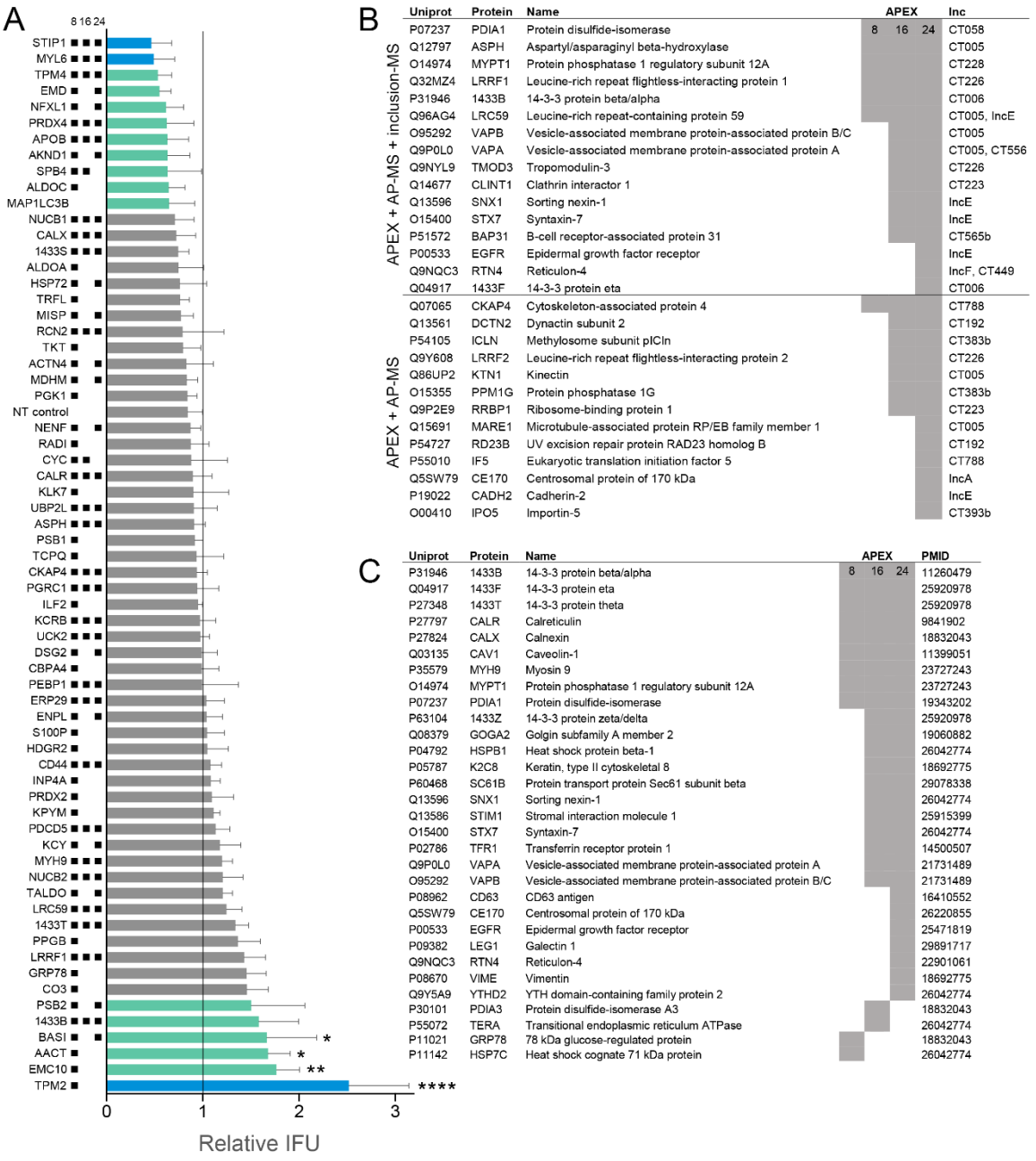


**Figure 2–4. RNAi validation of inclusion interacting proteins and comparison to previous data sets.**

(A) IFU determination following RNAi depletion of 64 proteins identified from early (8 hpi) inclusions. Cells were transfected with siRNA corresponding to targets shown on the y-axis, infected with *C. trachomatis* L2, and harvested for IFU determination at 48 hpi. Bars, mean(SD); n = 3; IFU shown relative to mean IFU of plate. Black squares next to RNAi targets (y-axis) indicate which time points the protein was enriched in APEX mass spectrometry data. Teal bars correspond to at least 1.5 fold increase/decrease compared to the mean, blue bars are over 2 fold increase/decrease compared to the mean. Significance was determined by one-way ANOVA with Dunnett's multiple comparisons test, comparing to mean infectivity of plate; *, $p <$

0.05; **, $p < 0.01$; ****, $p < 0.0001$. (B) Summary of all proteins shared between APEX data and two previous inclusion mass spectrometry data sets (40,42). Lower table describes all proteins that overlap between APEX and AP-MS Inc-specific interactions (40). Shaded boxes represent significant enrichment found by APEX. (C) Summary of APEX identified proteins with reported microscopy-based associations with *Chlamydia* inclusions. PMID entries refer to the publications used to provide this evidence.

## Discussion

Establishment and maintenance of the inclusion is critical to *Chlamydia*'s ability to infect and grow within host cells. Bioinformatic analysis of the *C. trachomatis* genome predicts over 50 type III secreted Inc transmembrane proteins (8,47,49); however, little is known about the broad spectrum of host proteins that are recruited to the inclusion membrane. Recent proteomic studies have provided a major, initial snapshot of proteins that comprise mature inclusions (42) and that associate with exogenously expressed Inc proteins (40). However, we still lack an understanding of host factors recruited to inclusions in their endogenous host cell setting, how the inclusion membrane interactome changes throughout the developmental cycle, and in particular what signaling pathways are critical for inclusion biogenesis. To advance knowledge in these important unexplored areas, we developed the APEX proximity-dependent biotinylation platform for *Chlamydia*, to allow type III mediated expression of Inc proteins, fused to APEX, on the inclusion membrane. Using this approach, we obtained proteomic data for the dynamic recruitment of 452 host proteins to *C. trachomatis* inclusion membranes; this work strengthens existing proteomic datasets and additionally provides new insight into the *Chlamydia*–host interactions that shape the chlamydial intracellular inclusion niche. APEX proximity dependent proteomics represents a powerful tool for investigating host–pathogen interactions. Previous work has demonstrated the efficacy of tagging IncA and IncF with APEX (53), and we urge the field to exploit this system to accelerate our understanding of the molecular functions of chlamydial type III secreted proteins.

A major finding of this study was the population of proteins assembled on early inclusions, as this subset is predicted to contain proteins important for regulating processes that shape inclusion biogenesis. Our data show that early inclusions, containing only a few bacteria, were enriched in proteins associated with the early secretory pathway and distinct cellular processes. In accordance with the need of chlamydiae to scavenge nutrients and energy from the host cell, proteins important for glycolysis were identified, including aldolases, transaldolase, transketolase, peroxiredoxins, and pyruvate kinase. Although these proteins were largely not identified at later time points, it is unclear if they are no longer in close proximity to the inclusion, or they represent a much smaller percentage of the inclusion membrane proteome at later times and were simply not detected. In addition, a large number of ER proteins were proximity labeled by the inclusion membrane, for example protein disulfide isomerase, calreticulin, calnexin, endoplasmin, apolipoprotein B-100, STIP1, and EMC10. Finally, members of the 14-3-3 protein family, serpins, and several cytoskeletal proteins—alpha-actinin-4, emerin, myosins, MYPT1, tropomyosins—were found to interact with inclusion membranes. Depletion of many of these early association factors led to alterations in chlamydial growth, as measured by the production of IFU. We elected to perform a high throughput RNAi screen in order to test candidate proteins from the 8 hpi proteomic data. This approach contained single siRNA oligonucleotides for each target, so follow-up studies would have to use independent sequences to ensure off-target effects did not affect IFU. Similarly, we did not assess the effect of knockdown on chlamydial entry into the cell so that could be another factor that impacted IFU. Among proteins recruited to early inclusions, RNAi knockdown of tropomyosins yielded unexpectedly large and disparate effects on bacteria growth. Knockdown of TPM2 enhanced IFU by over 2 fold, while knockdown of TPM4 resulted in close to 2 fold reduced IFU. Although tropomyosins affect actin filament stability, the different forms are thought to be functionally distinct.

Our study provides a third proteomic mapping of the inclusion membrane interactome, with each effort exploiting unique approaches and technological systems. We now have the opportunity to synthesize these proteomic datasets to derive a list of 'high confidence' interactions, and develop an understanding of multiprotein interactions that may occur with specific *C. trachomatis* Incs. Six proteins represented high confidence proteins recruited to early inclusions, three of which were previously shown to be recruited to inclusions: PDIA1 (PDI) (70), ASPH, MYPT1 (71), LRRF1, 14-3-3β (33), and LRC59. By 16 hpi, seven additional high confidence proteins were found to interact with inclusion membranes across all three proteomic studies: VAPA (10), VAPB (72), TMOD3, SNX1 (42,46), STX7 (42), BAP31, and CLINT1. Finally, 24 hpi *C. trachomatis* inclusions were consistently enriched with three additional host proteins: EGFR (73), 14-3-3ζ (27), and RTN4 (74). Interestingly, BAP31, ASPH, and LRC59 are normally associated with the ER; LRC59 additionally interacts with FGF, and *C. trachomatis* EB have been shown to interact with FGFR on the cell surface (75). The inclusion proteome data can be used to predict protein networks that associate with particular Incs. For example, our data revealed the recruitment of DYHC1, PCM1, MARE1, MAP1B, and PLK1 on the inclusion membrane, and these interactions may be mediated through CT192, an Inc protein shown by AP-MS to also directly interact with DCTN2 (40). Finally, our study indicated that chlamydial proteins constitute a small portion of the overall inclusion membrane proteome, as compared to host proteins. Only 11 Inc proteins were identified across all time points, suggesting that additional Incs are likely expressed at lower levels; Incs may also be difficult to detect compared to many more abundant host proteins. The chlamydial protease CPAF has been shown to degrade certain host proteins post-cell lysis (25,26). It is possible CPAF degraded some proteins post-lysis and these would be missed by mass spectrometry. IncB has no known binding partners, but many Incs have been shown to dimerize or bind other Incs (76). This suggests another possibility that most Incs are sequestered into heteromeric complexes, such that even with induced overexpression, IncB based proximity labeling was unable to access the full

repertoire of Incs present on the inclusion membrane. This outcome may also represent a limitation of the APEX approach for capturing all proximal proteins on inclusion membranes. Some growth attenuation was observed for the IncB-APEX expressing strain, and IncB-APEX overexpression may perturb the distribution of endogenous Incs. Future efforts by the field should therefore focus on determining what extent of the inclusion membrane interactome is Inc-specific, and which Incs control the recruitments of host targets.

## Materials and Methods

### Antibodies and reagents

All reagents were purchased from Thermo Fisher Scientific (Rockford, IL) unless otherwise noted. Primary antibodies used in this study and their catalog numbers: IncA (gift from Daniel Rockey), CT223 (gift from Daniel Rockey), MOMP (Virostat, Westbrook, ME; 1621), Flag (Millipore Sigma; F1804). Secondary antibodies used: Donkey anti-Rabbit HRP, Donkey anti-Goat Alexa 594, Goat anti-Mouse DyLight 594, Goat anti-Rabbit Alexa 488, Streptavidin Alexa 488.

### Cell culture and *Chlamydia* infections

HeLa 229 cells (ATCC) or McCoy cells (obtained from Walt Stamm) were grown in Roswell Park Memorial Institute 1640 (RPMI; Gibco) medium supplemented with 10% fetal bovine serum (HyClone) and 2 mM L-glutamine (HyClone) at 37°C, 5% $CO_2$. *Chlamydia trachomatis* LGV L2 434/Bu was grown in HeLa 229 cells for 48 hours, then infected cells scraped into sucrose phosphate buffer (5 mM glutamine, 0.2 M sucrose. 0.2 M phosphate), lysed using bead bashing, and cell debris cleared by centrifugation at 300 × g for 10 minutes. Supernatant containing *Chlamydia* aliquoted and stored at -80°C. HeLa cells were infected with

*Chlamydia* diluted in Hank's buffered salt solution (HBSS; Gibco) at an MOI ~1 for 2 hours at room temperature. Cells were washed with HBSS, then incubated at 37°C in RPMI.

**Plasmid constructs and generation of transformed *Chlamydia* strains**

Plasmids were isolated using the Qiaprep Spin Miniprep kit or the HiSpeed Plasmid Midi kit (Qiagen, Germantown, MD).

*Chlamydia* plasmid expressing IncB-APEX2 (referred to as IncB-APEX in text) fusion was made in a modified version of the pASK-GFP parent vector provided by Scott Hefty (23), where GFP was replaced with IncB-APEX2 (55) and the mKate2 sequence was removed. Plasmid grown in dam- *E. coli* (C2925; NEB, Ipswich, MA) prior to *Chlamydia* transformation. Plasmid transformed strains of *C. trachomatis* L2 were generated using established procedures (22). Three different dilutions (undiluted, 1:2, 1:10) of *C. trachomatis* L2 stocks were made in 50 µL calcium chloride buffer (20 mM Tris pH 7.4, 100 mM CaCl2). In the same buffer, 3 ug plasmid was diluted to 50 µL and added to diluted *Chlamydia*. The 100 µL *Chlamydia*–plasmid mixture was incubated for 30 minutes at room temperature. McCoy cells were trypsinized and diluted to a final concentration of 4 x $10^7$ cells/ml in calcium chloride buffer. After 30 minute incubation, 100 µL diluted McCoy cells were added to *Chlamydia* and DNA mixture, and incubated for 20 minutes. In a 6 well plate, 100 µL McCoy cells, plasmid, and *Chlamydia* mixture were added to 2 mL medium. At 12-15 hours post infection, cells were washed and medium added containing 2.5 U/mL Penicillin G (Millipore Sigma) and 1 ug/mL cycloheximide. Cells were incubated for 48 hours, then *Chlamydia* passaged onto fresh McCoy cells. After first passage, cells were grown in medium containing 10 U/mL Penicillin G and 1 ug/mL cycloheximide. Transformants were passaged at least 2 more times, every 48 hours, until inclusions were apparent. Stocks of transformed *Chlamydia* were frozen at -80°C as described above.

**Biotin-phenol labeling in live cells**

Biotin-phenol labeling of *Chlamydia* infected cells was adapted from described a protocol (77). HeLa cells were grown in 8 well chamber slides (for immunofluorescence detection of biotinylation; Nunc Lab-Tek), or a T75 flask (for western blot and mass spectrometry), then infected with *C. trachomatis* L2 expressing IncB-APEX at an MOI of approximately 1. Cells were incubated in RPMI containing 1 ng/mL anhydrotetracycline (ATc; Acros Organics, New Jersey) and 1 ug/mL cycloheximide (Gold Biotechnology, St. Louis, MO). At 30 minutes prior to time point, 2.5 mM biotin-phenol (Iris Biotech, Marktredwitz, Germany) in RPMI was added to cells. At each time point, 30% hydrogen peroxide diluted to 100 mM working stock in Dulbecco's phosphate-buffered saline (DPBS; Gibco) was added to cells at a final concentration of 1 mM, and allowed to incubate with gentle rocking for 1 minute at room temperature. Labelling solution was aspirated and cells were rinsed 3 times in quenching solution (10 mM sodium ascorbate, 5 mM Trolox, 10 mM sodium azide in DPBS). For immunofluorescence, normal fixation and staining protocols were followed. For western blot and mass spectrometry, cells were scraped into quenching solution and centrifuged for 5 minutes at 3,000 x g, 4°C. Cells were lysed by resuspending in ice cold RIPA buffer (50 mM Tris, 150 mM NaCl, 0.1% SDS, 0.5% sodium deoxycholate, 1% triton X-100, pH 7.5) with Halt protease inhibitor cocktail (Pierce) and quenchers (10 mM sodium ascorbate, 5 mM Trolox, 10 mM sodium azide). Lysate was incubated for 2 minutes on ice, then sonicated 3 x 1 second at 20% amplitude, and clarified by centrifugation for 10 minutes at 15,000 x g, 4°C. Part of the lysate was reserved for western blot, and remaining lysate for each sample was snap frozen until mass spectrometry processing.

**Protein purification for mass spectrometry**

Protein concentrations for individual samples were measured by BCA. The samples were normalized to 2 mg/mL for enrichment. Labeled protein lysates were enriched with streptavidin

agarose resin (Thermo Fisher Scientific, Rockford, IL). The resin was prepped for enrichment by placing the resin in a Bio-Rad chromatography column (Bio-Rad, Hercules, CA) on a vacuum manifold. The resin was washed with 0.5% SDS in PBS (1 mL, repeat 2×), 6 M urea in 25 mM ammonium bicarbonate ($NH_4HCO_3$) (1 mL, repeat 2×), and PBS (1 mL, repeat 4×). The resin was transferred to 4 mL cryovials using two 1 mL aliquots of PBS. An additional 0.5 mL of PBS was added to each tube followed by 1000 μg of protein (in 1.2% SDS in PBS). The total volume of each tube was set to 3.0 mL, giving a final SDS concentration of 0.2%. Tubes were rotated end over end for 4 hr at room temperature. Following streptavidin capture of biotinylated proteins, the solution was transferred into the Bio-Rad columns, and the solution was removed. The resin was washed with 0.5% SDS in PBS (1 mL, repeat 2×), 6 M urea in 25 mM $NH_4HCO_3$ (1 mL, repeat 2×), Milli-Q water (1 mL, repeat 2×), PBS (1 mL, repeat 8×), and 25 mM $NH_4HCO_3$ (1 mL, repeat 4×). The enriched resin was transferred to sealed 1.5 mL tubes using two 0.5 mL aliquots of 25 mM $NH_4HCO_3$. Samples were centrifuged at 10,500 x g, and the supernatant was discarded. 6M Urea was added to the resin for each sample followed by 100 mM TCEP (20uL) and place on a thermomixer for 30 min (1200 rpm at 37°C). After the samples were reduced, 200 mM iodoacetamide (20uL) was added to alkylate the proteins. The resin was placed back on the thermomixer for 45 min (1200 rpm at 50°C) and covered in foil. Following alkylation, the samples were returned to the Bio-Rad column and rinsed with PBS (1mL, repeat 8×) and 25 mM $NH_4HCO_3$ (1 mL, repeat 4×). The enriched resin was transferred to sealed 1.5 mL tubes using two 0.5 mL aliquots of 25 $NH_4HCO_3$. Samples were centrifuged at 10,500 x g, and the supernatant was discarded. Enriched biotinylated proteins were prepared for LC–MS/MS analysis. 25mM $NH_4HCO_3$ (200 μL) was added to the resin for each sample, along with trypsin solution. Resin solutions were placed on the thermomixer at 37 °C set at 1200 rpm set for overnight. Following trypsin digestion, the tryptic peptides were collected, and the resin washed once with 25 mM $NH_4HCO_3$ (150 μL). Volatiles were then removed from the combined tryptic peptide supernatant using a speed vacuum. The dried peptides were reconstituted in 25 mM

$NH_4HCO_3$ (40 µL) and heated for 10 min at 37 °C with mild agitation. To remove any solid particulates, samples were centrifuged at 53,000 x g for 20 min at 4 °C. From each ultracentrifuge vial was removed 25 µL for MS analysis. Samples were stored at −20 °C until analysis.

**Mass spectrometry and bioinformatic analysis of proteomic data**

Biotinylated tryptic peptides were enriched and separated using in-house reverse-phase resin columns by LC and analyzed on a Thermo Fisher Velos Orbitrap MS as described previously (78). Instrument data were acquired for 100 min, beginning 65 min after sample injection into the LC. Spectra was then collected from 400-2,000 *m/z* at a 100k resolution, following by data-dependent ion trap generation of MS/MS using the top six most abundant ions, a collision energy of 35%, and a dynamic exclusion time of 30 s for discriminating against previously analyzed ions. MS/MS spectra were searched using the MSGF+ algorithm and a tag-free quantitative accurate mass and time (AMT) tag approach for subsequent unique peptide to protein mapping using LC-MS peak feature detection, as described previously (79) with the following modifications. Identified features from each MS dataset were filtered on an FDR of less than or equal to 1%. Unique fragments, requiring a minimum of six amino acids in length, were filtered using an MS-GF threshold of $\leq 1 \times 10^{-9}$, corresponding to an estimated false-discovery rate (FDR) <1% at a peptide level. Resulting relative peptide abundances, in replicate across 48 biological samples including control samples, were log transformed and the data were processed for quality control. Elimination of statistical outliers was confirmed using a standard Pearson correlation at a sample level (80). Parameters for removing inadequate data for qualitative statistics required a minimum of two observations for a peptide across all groups to be compared quantitatively or identified in at least half the biological replicates for a given condition group using previously described methods (81). Peptides were normalized using median centering, adjusting for overall differences in abundances across samples. Statistical

comparisons were made between control and biotinylated groups at each time point and evaluated for quantitative differences using a standard 2-sample t-test and a qualitative difference (presence/absence markers) g-test. Statistical test used for each protein is shown in table S2. Additional evaluations were done in a similar manner for comparison of conditions across time.

For KEGG pathway analysis, UniProt identifiers of proteins were uploaded into InnateDB pathway analysis, then processed using the pathway overrepresentation analysis tool. The recommended settings were used for the analysis: hypergeometric algorithm, Benjamini Hochberg *p* value correction method. Only pathways with $p < 0.05$ after Benjamini Hochberg correction were listed.

To assign subcellular localization ontologies to proteins, the Human Protein Atlas database (version 18) was used (66). Subcellular localization data for all proteins were downloaded, and data for proteins in the IncB-APEX data set were extracted. Only subcellular locations with enhanced, supported, or approved reliability scores were used. Proteins with more than one annotated location were counted for each location. Highly similar categories were condensed, for example nuclear speckles, nucleoli, nucleoli fibrillar center, and nucleoplasm were all counted as nuclear lumen.

Network analysis of APEX proteins was done using annotations from StringDB (version 10) (67). Only interactions with evidence from experiments or databases were considered, with a confidence score of at least 0.700 (high confidence). Proteins with no interaction partners were excluded. Annotated interactions were downloaded for the proteins each time point, and these data were compiled into a list of all interactions at different time points using Microsoft Excel. To make the graph more readable, proteins involved in translation were excluded. These data were imported into RStudio software, and plotted using the tidygraph package (68). Graph layout was arranged using the Fruchterman Reingold algorithm, and subsets of closely interacting protein communities were detected using the Louvain method. General categories of

some of the protein communities were assigned based on similarities between the UniProt descriptions of proteins in that particular community. If there were only 2 proteins in a group, or there was no consensus between the UniProt descriptions, no category was assigned.

To compare to the AP-MS (40) and inclusion-MS (42) protein lists, full data sets were obtained from the supplemental data of each study. Proteins were matched based on UniProt identifiers, and all three data sets were combined using RStudio and Microsoft Excel (Table S2–1). For the AP-MS data, MIST scores are listed (closer to 1 is better). All Inc proteins that were found to interact with the host protein were listed, with the MIST score from the first listed Inc retained. For APEX and inclusion-MS, *p* values are listed.

**siRNA transfections**

For siRNA transfections, HeLa cells were plated in 24 well or 96 well plates to 60-80% confluence. For 24 well plates, 50 µL Opti-MEM (Gibco) medium containing 5 pmol siRNA oligonucleotides and 1.5 µL Lipofectamine RNAiMAX was added to each well. Following transfection, cells were incubated for 48 hours at 37°C prior to infection or protein analysis by western blot. For 96 well plate experiments, knockdowns were done in duplicate, with 10 µL Opti-MEM containing 1 pmol siRNA oligonucleotides and 0.3 µL Lipofectamine RNAiMAX added per well. Oligonucleotides were purchased from Dharmacon. Dharmacon siGenome individual oligonucleotides were used for all knockdowns.

**Quantitative PCR analysis**

For qRT-PCR confirming siRNA knockdown, HeLa cells were plated in 24 well plates, and transfected with siRNA oligos as described above. Cells were incubated for 48 hours, then cell pellets were frozen until RNA extraction.

RNA was extracted using the Qiagen RNeasy mini kit (Qiagen). cDNA was made using the iScript cDNA synthesis kit (Bio-Rad). qRT-PCR reactions were set up with SsoAdvanced

Universal SYBR Green Supermix (Bio-Rad) and run on the StepOnePlus Real-Time PCR system (Applied Biosystems, Foster City, CA). GAPDH was used as the housekeeping gene, and the ΔΔCT method was used to calculate relative expression.

**Immunofluorescence microscopy**

For immunofluorescence microscopy, cells were rinsed in HBSS, then fixed for 15 minutes in 3.7% paraformaldehyde in HBSS. Cells were rinsed 2 times in HBSS, then permeabilized with 0.5% triton X-100 for 15 minutes, and blocked in 1% bovine serum albumin (BSA) in PBS for 20 minutes. Samples were incubated with primary antibodies for 1 hour at room temperature in blocking buffer, then rinsed 3 times in blocking buffer, then incubated 45 minutes at room temperature with secondary antibodies in blocking buffer. DAPI was used to stain DNA, and added during the secondary antibody step. For biotin labeling, Streptavidin-Alexa 488 was incubated for 30 minutes at room temperature. Cells were imaged on a Nikon Ti-E inverted microscope and images were captured on a Hamamatsu camera controller C10600. Images were processed using Volocity software (PerkinElmer, Waltham, MA).

**Western blot analysis**

For western blot analysis of biotinylated proteins (77), 6x protein loading buffer was added to lysates, samples were boiled for 5 minutes, followed by cooling on ice. 15 µl lysate was loaded and run on 10% SDS gel in Tris running buffer by SDS-PAGE. Proteins were transferred from gels onto Immobilon PVDF membrane (Millipore Sigma) with a Pierce G2 fast blotter in Pierce 1-Step transfer buffer, then blocked with 3% BSA in TBST overnight at 4°C. Blots were incubated with streptavidin-HRP in 3% BSA in TBST for 30 minutes at room temperature, washed 4 x 5 minutes in TBST, incubated with chemiluminescent substrate (Li-Cor 92695000, Lincoln, NE) for 5 minutes, and imaged using a C-DiGit blot scanner (Li-Cor). For western blot analysis of RNAi knockdowns, cell pellets were lysed in ice cold RIPA buffer (50 mM Tris, 150

mM NaCl, 0.1% SDS, 0.5% sodium deoxycholate, 1% triton X-100, pH 7.5) with Halt protease inhibitors (Pierce) for 30 minutes on ice, with vortexing every few minutes. Lysates were centrifuged for 20 minutes at 14,000 x g, and supernatant added to 4x laemmli buffer (Bio-Rad, Hercules, CA). Lysates were run by SDS-PAGE on 5-15% or 5-20% mini-PROTEAN TGX stain free gels (Bio-Rad), transferred to Immobilon PVDF membrane (Millipore Sigma), blocked for 1 hr in 5% milk-TBST, and labeled with antibody and digitally imaged as described above.

**Inclusion forming unit analysis**

Infected HeLa cells were lysed at 48 hpi by incubating in water for 20 minutes followed by pipetting to disrupt cells. Serial dilutions of lysate were plated onto fresh HeLa monolayers in a 96 well plate. At 24 hpi, cells were fixed and stained with DAPI and an anti-MOMP antibody. Using immunofluorescence microscopy, 10-15 fields per well were taken at 20x magnification. Inclusions and nuclei in each field were counted using the Fiji distribution of ImageJ (82). The overall percentage of infected cells was used to compare IFU between conditions, and the relative IFU calculated for each experiment by comparing to control.

**Supplemental Information**

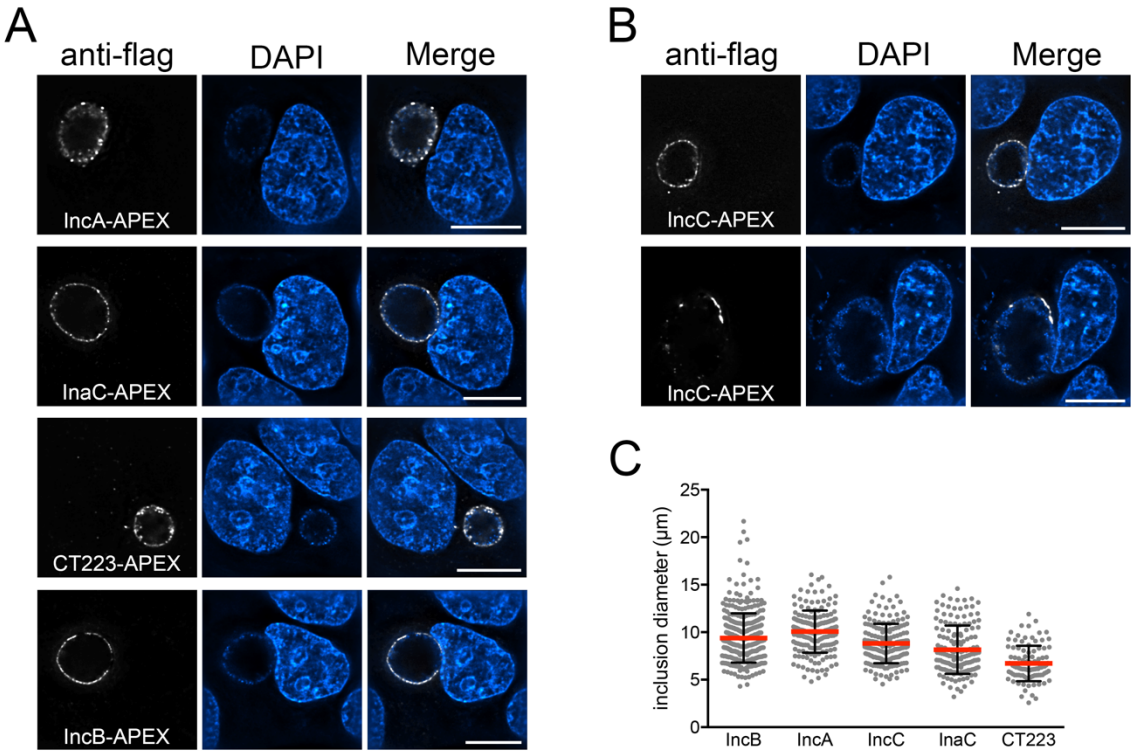


**Figure S2–1. Overexpression of different Inc-APEX fusions causes unique localizations and effects on inclusion growth.**

(A) HeLa cells were infected with *C. trachomatis* transformed with plasmids containing several known Incs fused to APEX and a flag tag. 1 ng/mL ATc was added at the start of infection, cells were fixed at 24 hpi and stained with anti-flag (white) and DAPI (blue). Images shown are single planes of deconvolved z-series. Scale bars = 16 µm. (B) Cells were infected with *C. trachomatis* transformed to express IncC-APEX with a flag tag, cells were treated as described in A. IncC-APEX was sometimes distributed evenly around the inclusion (top images), while in other inclusions it had a microdomain localization pattern (bottom images). Scale bars = 16 µm. (C) Cells were infected and fixed as described in A, and inclusion diameter was measured. Incs listed are referring to the Inc fused to APEX in the *Chlamydia* transformant tested. Each dot represents one inclusion, red line represents mean diameter with SD in black. Mean diameter values in left to right order were 9.40 µm, 10.07 µm, 8.82 µm, 8.16 µm, 6.71 µm.

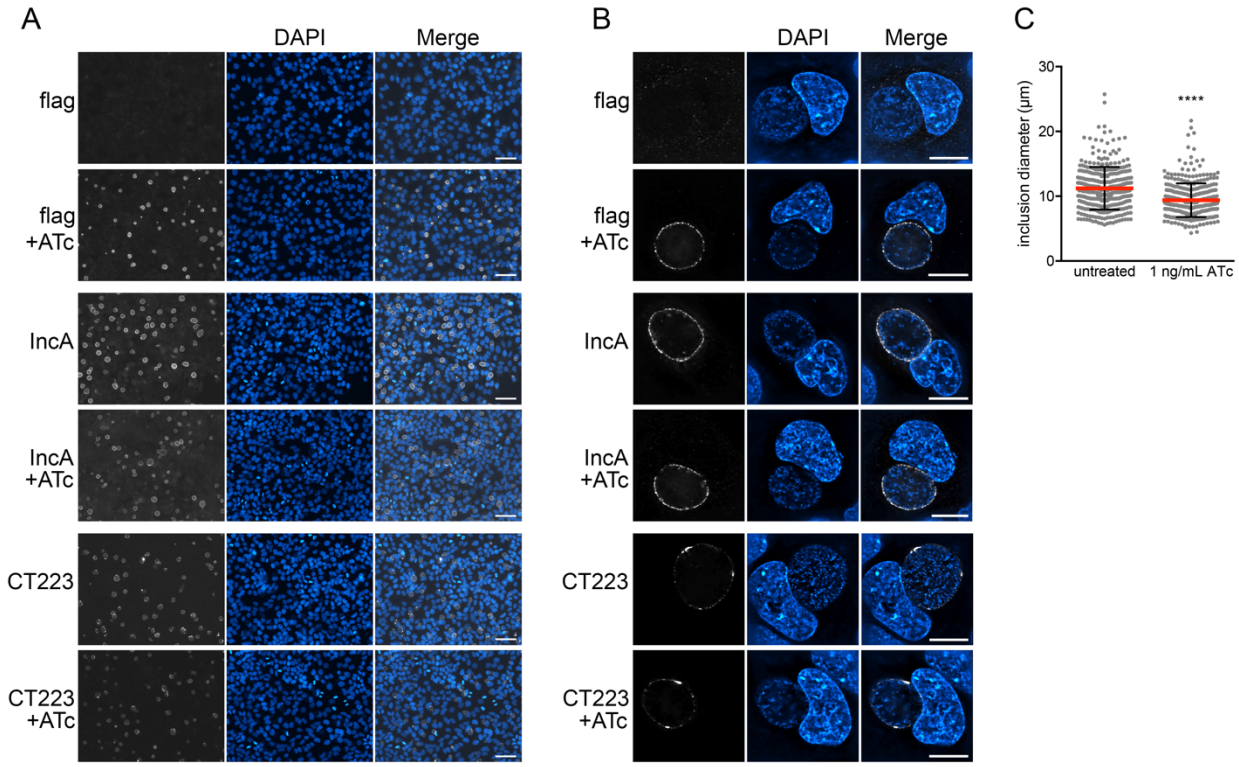


**Figure S2–2. IncB-APEX overexpression requires ATc and does not disrupt endogenous IncA or CT223 localization.**

HeLa cells were infected with *C. trachomatis* transformed with tet inducible IncB-APEX plasmid. Cells were grown in normal conditions or with 1 ng/mL ATc (rows labeled +ATc). At 24 hpi, cells were fixed and stained with anti-flag, anti-IncA, or anti-CT223 antibodies and DNA was labeled with DAPI. Images are 20x magnification (A, scale bars = 32 µm) or single plane from 60x deconvolved z-series (B, scale bars = 16 µm). (C) Same samples as described in A, B, plot of inclusion diameters with or without 1ng/mL ATc. Each dot represents one inclusion, measurements taken from two independent experiments. Significance determined by two-tailed Mann-Whitney test, red line shows mean (SD); ****, $p < 0.0001$. Mean diameter for untreated inclusions was 11.22 µm and 9.40 µm for inclusions treated with 1 ng/mL ATc.

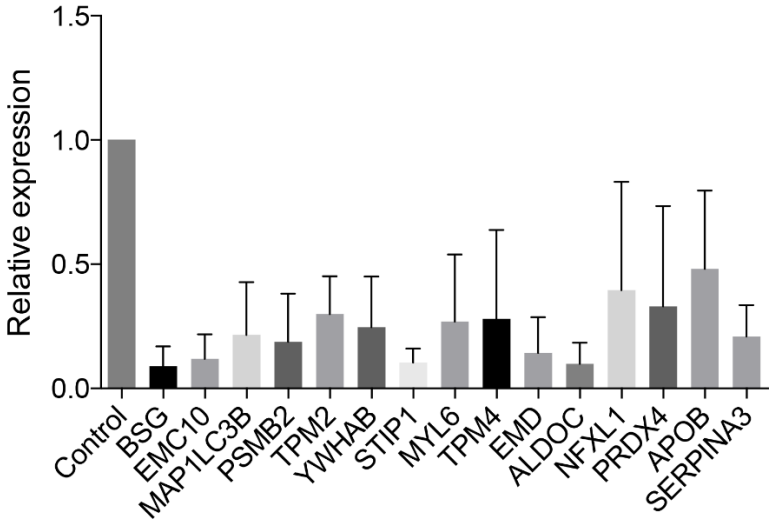


**Figure S2–3. mRNA expression of targets that alter Chlamydia IFU by at least 1.5 fold is reduced following siRNA treatment.**

HeLa cells were transfected with siRNA oligos corresponding to the genes listed in graph or non-targeting control. Relative expression was measured using qRT-PCR using the ΔΔCT method at 48 hours post transfection.

# Chapter 3 – Endoplasmic reticulum exit sites are required for *Chlamydia trachomatis* growth

Text and figures in this chapter adapted from the article:

Mary Dickinson, Lindsey Anderson, Bobbie-Jo Webb-Robertson, Joshua Hansen, Richard Smith, Aaron Wright, Kevin Hybiske (2018) Proximity-dependent proteomics of the *Chlamydia trachomatis* inclusion membrane reveals functional interactions with endoplasmic reticulum exit sites. In review, PLOS Pathogens.

## Introduction

Proteomics of proteins in close proximity to the inclusion membrane using the enzyme APEX (discussed in Chapter 2) showed that many ER proteins were enriched at the inclusion membrane. Although the *C. trachomatis* inclusion has previously been shown to form membrane contact sites with the ER, APEX identified a novel subset of ER proteins that are required for ER exit site (ERES) function. ER exit sites are the domain of the ER where cytoplasmic coat protein complex II (COPII) vesicles originate for transport of cargo to the ER-golgi intermediate compartment (ERGIC). From the ERGIC, cargo is transported to the golgi in COPI coated vesicles, and from the golgi cargo can be transported to other organelles or secreted from the cell. Although the golgi has been studied extensively in the context of *Chlamydia* infection, ERES have not been studied, and could be a novel interaction between the host secretory pathway and *Chlamydia*.

The core proteins required for COPII budding that are conserved among eukaryotic cells are Sar1, Sec23, Sec24, Sec31, and Sec13 (83). First guanosine triphosphate (GTP) bound Sar1 is recruited to ER membranes, where it embeds into the membrane and induces budding initiation

by causing membrane curvature (83). Sar1 can then recruit the Sec23-Sec24 heterodimer, which not only forms the inner coat of COPII vesicles, but Sec23 also acts as a GTPase activating protein for Sar1 (83). Full Sar1 GTPase activity occurs upon the arrival of the outer coat proteins Sec31 and Sec13. Following full assembly of these 5 components, there is cargo loading followed by vesicle scission, forming a 60-70 nm vesicle (83). In mammalian cells there are more proteins involved, many of which have enigmatic roles in vesicle formation (83,84). Even for the core proteins, many paralogs have evolved; there are two Sar1 paralogs, two Sec23 paralogs, two Sec31 paralogs, and 4 Sec24 paralogs (83). It is unknown if these paralogs provide unique functions or have evolved to have tissue-specific roles (83). Sec12 is a guanine exchange factor for Sar1, causing Sar1 activation (84). cTAGE5 can bind Sec12 and helps concentrate it at ERES (85). The protein Sec16 is thought to act as a scaffolding protein; it binds several different COPII proteins and seems to localize to ERES upstream of other COPII components (84). It has recently been shown that Tango1 is required for proper Sec16 localization to ERES (86).

ERES have been studied in the context of *Brucella abortus* and *Legionella pneumophila* infection (87,88). COPII components were found to associate closely with Legionella during infection, and a dominant negative version of Sar1 reduced *Legionella* replication (88). It is unclear how much of this is due directly to ER exit sites versus downstream effects on the golgi, as the same study showed that Arf1 was also required for replication, and BFA caused a reduction in bacterial growth (88). For *Brucella*, the dominant negative Sar1 reduced bacterial replication, as well as the acquisition of ER membranes that is important for maturation of the *Brucella* containing vacuole (87). Unlike *Legionella*, BFA and expression of a dominant negative Arf1 had no effect on *Brucella* growth, indicating a different mechanism of ERES interaction for the two pathogens (87).

In the context of *Chlamydia* infection, IncB-APEX proteomic analysis revealed a significant enrichment of ER associated proteins near inclusion membranes throughout infection. These findings are consistent with previous reports of membrane contacts between

inclusions and the ER (9,74). IncB-APEX data showed that ER protein associations were present near early inclusions, at 8 hpi, and additionally highlighted an enrichment of markers for ER exit sites (ERES). ERES are specialized subdomains of the ER from which COPII coated vesicles bud and traffic to the ER-Golgi intermediate compartment (ERGIC) (84). Sec16, TANGO1, TFG, and peflin, were identified on inclusion membranes by IncB-APEX, with TANGO1 present at all three time points (Table S2–1). In support of an intimate association between ERES and inclusions, five members of the p24 family, proteins which regulate ERES organization and are packaged into COPII vesicles (89), were identified by inclusion-MS and AP-MS (40,42). In this chapter we investigated the role of ERES function on *Chlamydia* growth through both chemical inhibition and RNA interference of select ERES proteins.

## Results

### Recruitment of ERES proteins Sec16 and Sec31 to *C. trachomatis* inclusions

To validate the association of ERES with the inclusion membrane, we used immunofluorescence microscopy to investigate the spatial relationship between the ERES marker Sec16 and the inclusion membrane. In uninfected cells, Sec16 was distributed in a normal pattern throughout the cytoplasm in small punctae, with a dense cluster of Sec16 in perinuclear ER membranes (Figure 3–1A). In *C. trachomatis* infected cells, Sec16 redistributed in a punctate pattern around the inclusion at 24 hpi (Figure 3–1A). Several Sec16 punctae closely abutted inclusion membranes defined by IncA (Figure 3–1A, inset). Sec16 was also recruited to inclusions at 14 hpi (Figure S3–1). We further examined the ectopic distribution of Sec16 in live cells using HeLa cells transfected with Sec16-GFP and infected with a *C. trachomatis* strain expressing mCherry, and observed a similar association of Sec16 with inclusions (Figure S3–2). Next, we tested whether the COPII coat protein Sec31 associated with inclusion membranes in a similar manner, and as would be expected for functional ERES. Like

Sec16, Sec31 was redistributed around inclusion membranes, with some Sec31 foci appearing to overlap with the inclusion membrane (Figure 3–1B, Figure S3–1). Together, these data demonstrate that structural and regulatory ERES proteins are recruited to inclusion membranes. It is unclear if these ERES proteins are on the ER, on COPII vesicles, or on the inclusion membrane. The localizations of ERES, ERGIC, and cis Golgi network are closely related in mammalian cells. Secretory cargo in COPII-coated vesicles leave the ER at ERES, quickly fuse with the ERGIC, and then are packaged into COPI-coated vesicles for transport to the Golgi. To check if the Golgi was necessary for the distribution of ERES to *Chlamydia* inclusions, we resolved the localization of the Golgi and ERES in infected cells with or without Brefeldin A (BFA) treatment (Figure S3–3). In untreated cells, the general localization of Sec31 and Golgi were similar, although the individual components did not colocalize. After BFA treatment, the Golgi was dispersed, whereas Sec31 remained distributed in close proximity to inclusions.

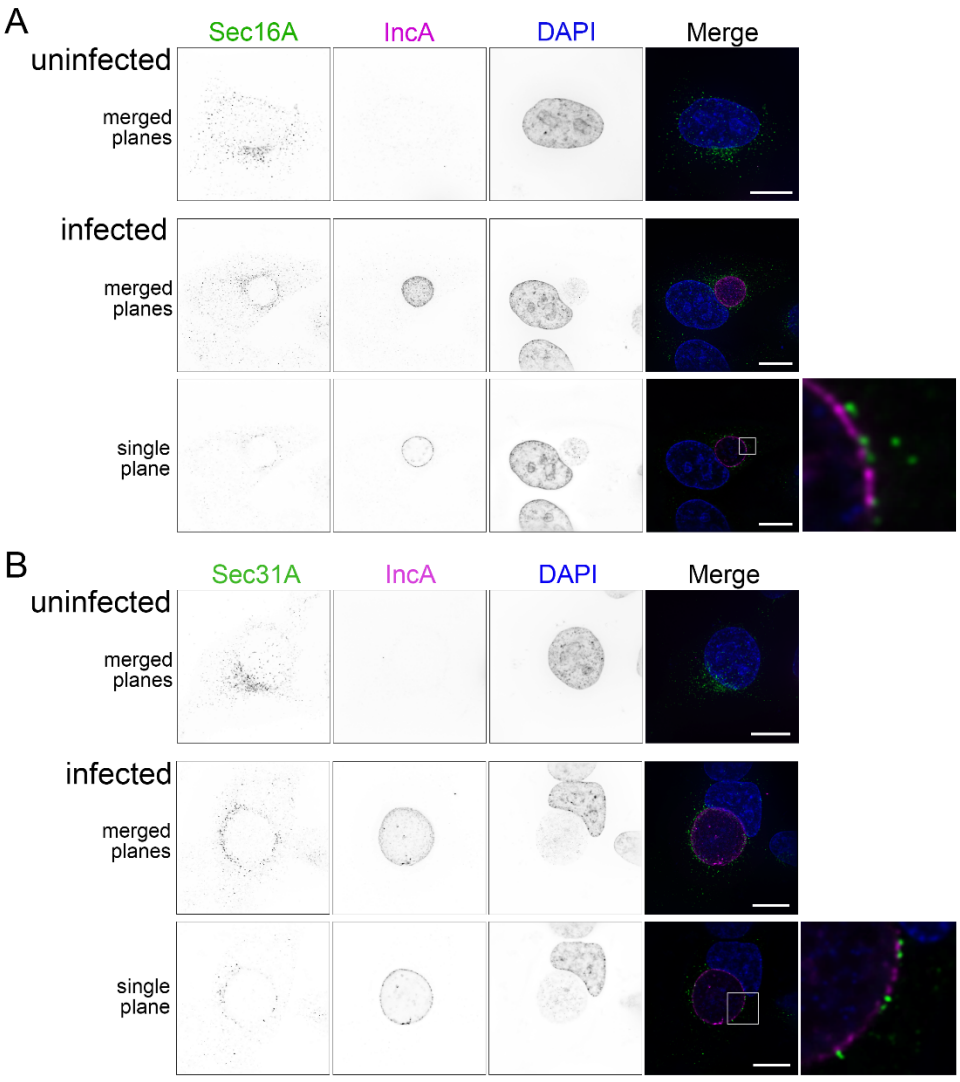


**Figure 3–1. ERES proteins Sec16A and Sec31A are recruited to the *C. trachomatis* inclusion.**

(A) Immunofluorescence microscopy of cells showing cellular distribution of Sec16A (anti-Sec16A, first column, green in merge), *Chlamydia* IncA (anti-IncA, second column, magenta in merge), and DNA (DAPI, third column, blue in merge). (B) Distribution of the COPII outer coat protein Sec31A (anti-Sec31A, first column, green in merge), IncA, and nuclei. Single channel images are displayed in inverted grayscale. Merged panels display all three color channels. Protein distribution in uninfected HeLa cells are shown in the top row. Deconvolved images from cells infected with *C. trachomatis* L2 at 24 hpi are shown as a summation of *z*-series images (merged planes) or a single *xy* plane. Enlargements (far right) represent the regions marked with white boxes. Scale bars = 16 µm.

## Chemical inhibition of ERES cargo loading restricts *C. trachomatis* developmental growth

We next tested if functional ERES were required for *Chlamydia* infection, by using a specific inhibitor of ERES export, FLI-06 (90,91). FLI-06 is a cell permeable, reversible inhibitor of ERES cargo loading and the early secretory pathway. The molecular target of FLI-06 target is unknown; however, the compound has been shown to prevent cargo recruitment to ERES. Any cargo already recruited is secreted, but no new cargo can be loaded into exit sites. First, we investigated how the localization of Sec16 and Sec31 were affected by incubation of *C. trachomatis* infected cells with FLI-06. Treatment of infected cells for 4 h with FLI-06, from 20-24 hpi, abrogated the recruitment of both of these ERES proteins to inclusions, resulting in diffuse localization similar to that seen in uninfected cells treated with FLI-06 (Figure 3–2A, Figure S3–4). Similar effects were observed with live cells expressing Sec16-GFP (Figure S3–2). The number of Sec31 punctae that overlapped with IncA were counted, and confirmed that treatment with FLI-06 resulted in significantly reduced COPII coat protein recruitment to inclusion membranes (Figure 3–2B). These data are consistent with the hypothesis that Sec16 and Sec31 recruitment to inclusions is a functional consequence of COPII vesicle formation, and not a byproduct of their proximity to ER membranes.

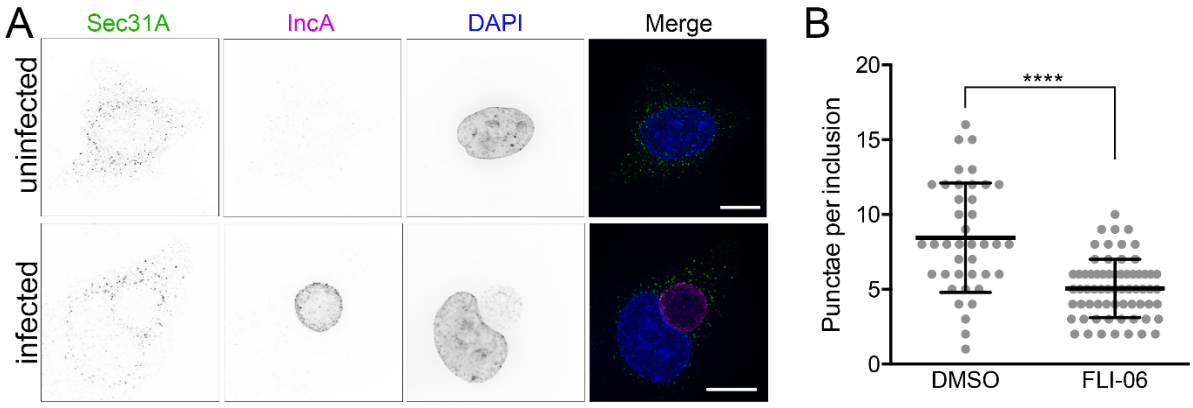


**Figure 3–2. Inhibition of ERES cargo loading abrogates ERES recruitment to the inclusion.**

(A) Treatment of *C. trachomatis* infected cells with FLI-06 disrupted the recruitment of COPII coat protein Sec31A to inclusion membranes. Immunofluorescence microscopy of cells showing cellular distribution of Sec31A (anti-Sec31A, first column, green in merges), inclusion membrane protein IncA (anti-IncA, second column, magenta in merges), and DNA (DAPI, third column, blue in merges). Representative deconvolved merged z-series images of uninfected cells are shown in upper panels, and cells infected with *C. trachomatis* L2 at 24 hpi are shown in lower panels. 10 µM FLI-06 treatment for 4 h, from 20-24 hpi, resulted in Sec31A distribution similar to that of uninfected cells, and away from inclusion membranes. Scale bars = 16 µm. (B) Quantification of Sec31 in cells infected and treated with FLI-06 as described in A. Sec31 punctae that were touching or overlapping with IncA in untreated or FLI-06 treated cells were counted using Volocity to assess the number of overlapping spots per inclusion. At least 20 inclusions were analyzed per condition, for two independent experiments. Each dot represents an inclusion, lines represent mean (SD). Significance determined by unpaired t-test with Welch's correction, ****, $p < 0.0001$.

To explore this outcome further, we tested the effect of FLI-06 on chlamydial developmental growth. *C. trachomatis* infected cells were treated with three concentrations of FLI-06 at distinct stages of infection: 2.5, 18, 24, and 40 hpi (Figure 3–3A). Following treatment, the effects of FLI-06 on primary infection and infectious progeny formation were determined by measuring inclusion diameter and IFU, respectively, at 48 hpi for all treatment groups (Figure 3–3B,C). We measured a significant, dose-dependent reduction in inclusion diameter for infected cells treated starting at 2.5 or 18 hpi (Figure 3–3B, Figure S3–5). Inhibitory effects were most pronounced with 10 µM of FLI-06, a concentration previously shown to block the recruitment of VSVG cargo to ERES (90,91). The effects of FLI-06 were

reversible, as treatment of infected cells at 18 hpi followed by washout at 24 hpi resulted in a recovery of inclusion growth at 48 hpi (Figure 3–3B). For cells treated with 10 μM FLI-06 at 2.5 hpi, fully formed inclusions at 48 hpi were rarely observed, indicating that early stages of *Chlamydia* and inclusion growth are reliant on COPII vesicle production from ERES. Two to 10-fold lower concentrations of FLI-06 resulted in dose-dependent phenotypes, thus strengthening the support that the effects of FLI-06 were biological.

The impact of FLI-06 on *C. trachomatis* IFU formation was more pronounced. Treatment of infected cells with 10 μM FLI-06 at 2.5 hpi resulted in no infectious progeny production, and a 99.8% or 95.6% reduction in *Chlamydia* IFU was observed in cells treated with 10 μM FLI-06 at 18 or 24 hpi, respectively (Figure 3–3C). Similar to the effects on primary infection, the impact of FLI-06 on *Chlamydia* growth was dose dependent. Cells pulsed with FLI-06 from 18-24 hpi partially recovered from the treatment, though IFU was reduced by 57.0% compared to untreated cells; this indicates that replication was reduced even during a 6 hour treatment. No effect on IFU production occurred when FLI-06 was applied to cells at 40 hpi, indicating that FLI-06 is not directly toxic to *Chlamydia* and that the effects of ERES on chlamydial inclusions were not on EB viability or infectivity. The potent effects of ERES disruption on inclusions at 18 hpi, when inclusions contain mostly RB, were consistent with an inhibitory effect that most heavily impacts RB growth. The application of FLI-06 at 18 hpi prevented the population of bacteria at that stage from converting into infectious EB by 48 h. Taken together, the data demonstrate that early *C. trachomatis* inclusions acquire vital cellular components from ERES-derived COPII vesicles for their complete developmental growth.

**Chemical inhibition of ERES cargo sorting reduces *Chlamydia* growth**

Since FLI-06 blocks secretion from ERES, it has severe effects on downstream steps of the secretory pathway and disrupts the Golgi (90). *Chlamydia* is known to acquire

sphingomyelin and cholesterol from the trans Golgi network. To test whether Golgi disruption contributed to the effects of FLI-06 on chlamydial growth, we used a chemical inhibitor with a different mechanism from FLI-06. Sodium phenylbutyrate (4PBA) has been used for many years to relieve ER stress by preventing accumulation of misfolded proteins within the ER. Recently it was shown that the secretion of misfolded proteins during 4PBA treatment happens through decreased selectivity of COPII cargo. 4PBA binds the p24 family of proteins, which provide cargo specificity for COPII vesicles, concentrating secreted proteins into vesicles while excluding ER resident proteins (92). COPII vesicles in cells treated with 4PBA show dramatically increased levels of ER resident proteins, along with decreased levels of normal COPII cargo (92).

We repeated the same experiments done with FLI-06 using 4PBA instead, and saw similar results on both inclusion diameter and IFU (Figure 3–3D,E). When 4PBA was added very early during infection, inclusions were significantly smaller (Figure 3–3D) and almost no viable EB were produced (Figure 3–3E). Consistent with 4PBA having a less severe effect on ERES compared to FLI-06, IFU of cells treated at 18 or 24 hpi with the highest dose of 4PBA was 79.5% or 59.25% reduced, respectively, much less severe than cells treated with FLI-06 at the same times. IFU was not affected when cells were treated with 4PBA from 18-24 hpi then washed off, or when cells were treated starting at 40 hpi, supporting that 4PBA is not directly toxic to *Chlamydia*. Since 4PBA allows protein secretion and still affects *Chlamydia* growth, this indicates that the effects of FLI-06 were unlikely to be a nonspecific effect of blocking protein secretion of the ER or Golgi, and COPII cargo regulation is important for the *Chlamydia* developmental cycle.

When FLI-06 or 4PBA were added early during infection, the inclusion diameter and IFU correlated well, with both being significantly lower than the control. When added at 24 hpi, however, both inhibitors did not significantly affect inclusion diameter, yet IFU for FLI-06 was reduced by 95.6% and for 4PBA was reduced by 59.25% (Figure 3–3C,E). We tested whether the

reduction in IFU was due to fewer bacteria present, or if it resulted from disrupted RB-EB conversion. We infected cells with *C. trachomatis*; at 24 hpi we added 10 μM FLI-06, 5 mM 4PBA, or 0.5 μg/mL chloramphenicol, then incubated until 48 hpi, extracted genomic DNA and used qPCR to measure *Chlamydia* genome copy number (Figure 3–3F). As expected, chloramphenicol inhibited *Chlamydia* replication and caused a 67.7% reduction in the number of bacterial genomes present, compared to the control. FLI-06 caused a 40.4% reduction in genome copy number, and 4PBA genome copy number was not significantly different from the control. This indicates that adding FLI-06 at 24 hpi caused some reduction in bacterial replication, but the drastic reduction in IFU must at least in part be due to reduced bacterial infectivity after treatment. 4PBA had a less severe effect on IFU, and the genome copy number supports that replication was not significantly reduced when added at 24 hpi, but there is a reduction in bacterial infectivity.

Given other known effects of 4PBA, it is possible that its effect on *Chlamydia* growth was due to decreased ER stress rather than dysregulation of COPII cargo. Because FLI-06 blocks secretion from the ER, it is also possible that ER stress was induced during FLI-06 treatment and resulted in a detrimental effect on *Chlamydia* growth. We checked if ER stress is induced during *C. trachomatis* infection under normal conditions, or after 4PBA or FLI-06 treatment. We compared ER stress in uninfected or *Chlamydia*-infected HeLa cells at 24 hpi after a 4 hour treatment with FLI-06, 4PBA, or thapsigargin, a well described inducer of ER stress (93). ER stress was assessed by mRNA expression of CHOP, BIP, and spliced XPB1. No significant differences were found between ER stress levels in infected cells and uninfected cells for all conditions tested (Figure 3–3G). Although CHOP, BIP, and sXBP1 expression were increased in FLI-06 treated cells, this increase was not statistically significant. Thapsigargin was able to induce much higher expression of CHOP, BIP, and sXBP1. Overall, these data indicate that it is unlikely that 4PBA or FLI-06 are acting by altering the levels of ER stress in infected cells.

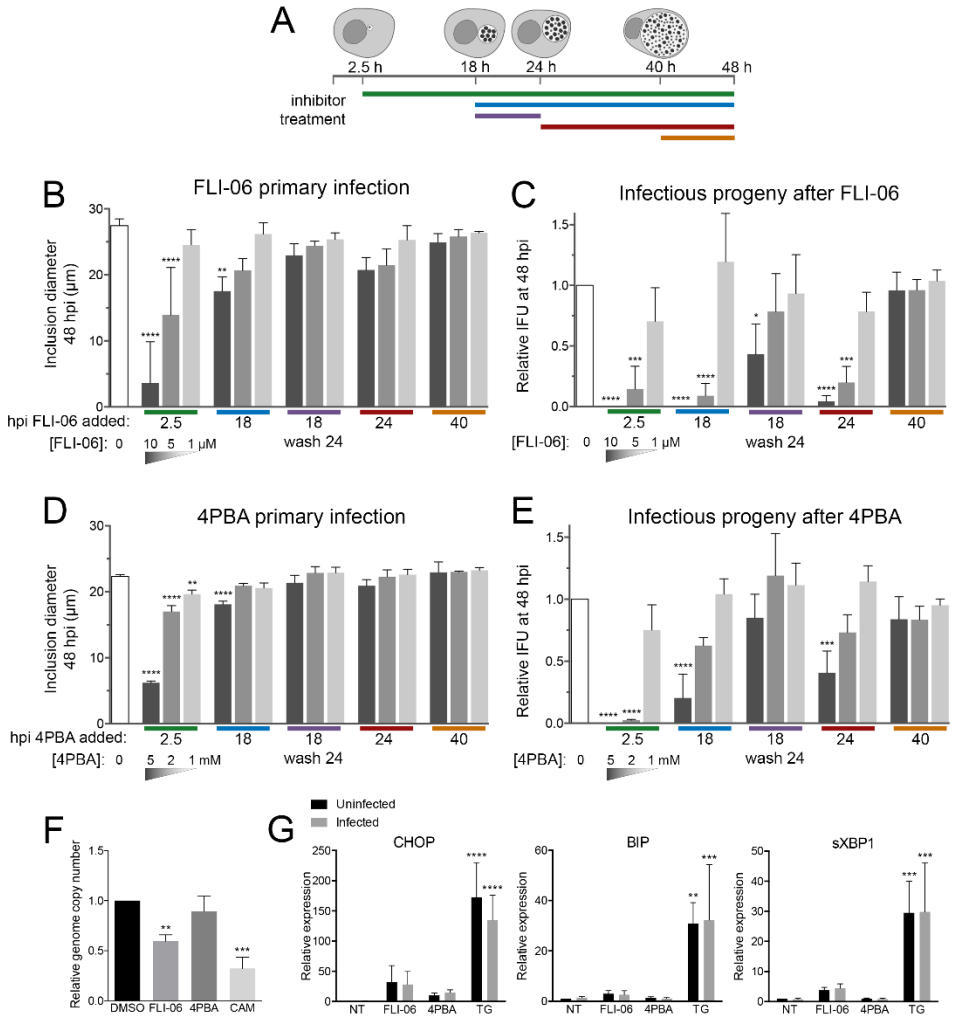


**Figure 3–3. Inhibition of ERES cargo loading or specificity reduces *C. trachomatis* developmental growth.**

(A) Experimental design used to test the impact of ERES disruption on *Chlamydia* developmental growth. Colored bars mark the times when FLI-06 or 4PBA was applied to infected cells. All cells were harvested for IFU determination at 48 hpi. The effects of ERES inhibition were determined for (B,D) primary infection, through measuring the diameters of inclusions at 48 hpi, or (C,E) IFU production at 48 hpi. Bars denote the mean (n = 3; SD); white bars correspond to untreated controls; gray bars are inhibitor treated in decreasing concentration, 10 µM, 5 µM, or 1 µM FLI-06 and 5 mM, 2 mM, 1 mM 4PBA. Colored bars on x-axis correspond to the inhibitor application key in A. Significance determined by one-way ANOVA with Dunnett's multiple comparisons test, comparing to untreated control. *, $p < 0.05$; **, $p < 0.01$; ***, $p < 0.001$; ****, $p < 0.0001$. (F) Infected cells were treated from 24-48 hpi with 10 µM FLI-06, 5 mM 4PBA, or 0.5 µg/mL chloramphenicol (CAM). Genomic DNA was extracted and genome copy number was determined by using quantitative PCR for the GroEL2 gene. Significance was determined by one-way ANOVA with Dunnett's multiple comparisons test, comparing to control. **, $p < 0.01$; ***, $p < 0.001$. (G) Relative expression of genes upregulated during ER stress in infected or mock infected cells after treatment with 10 µM FLI-06, 5 mM 4PBA, or 1 µM thapsigargin from 20-24 hpi. Gray bars are infected, black are uninfected.

Expression was determined using quantitative PCR. Significance was determined using a two-way ANOVA with Dunnett's multiple comparisons test. There was no significant difference between infected and uninfected cells, thapsigargin treatment was significantly different from the control. Uninfected treatments were compared to uninfected control, infected treatments compared to infected control. **, $p < 0.01$; ***, $p < 0.001$; ****, $p < 0.0001$.

### *Chlamydia* interactions with ERES are distinct from other interactions with the ER and Golgi

*C. trachomatis* inclusions form membrane contact sites with the ER, and whether ERES are recruited by the same mechanism is unclear (9,74). Previously, the lipid transfer protein CERT was shown to be a key component of ER membrane contact sites with inclusions (9,10); however, CERT did not colocalize with ERES markers (Figure 3–4A), indicating that ERES are likely an additional type of ER–inclusion interaction. Since FLI-06 and 4PBA act on the ER, it is possible they could indirectly affect *Chlamydia* growth by reducing contacts between the inclusion membrane and ER. To test this, we overexpressed fluorescent protein tagged CERT or the ER resident protein PDI, and saw no difference in their recruitment to inclusion membranes after treatment with FLI-06 or 4PBA (Figure 3–4A,B). BFA was included as a control to ensure any effects were due to the ER rather than post-ER trafficking steps.

CERT recruitment to the inclusion membrane is thought to facilitate non-vesicular ceramide trafficking, whereas the Golgi provides a vesicular route for ceramide uptake into the inclusion. To ensure that these inhibitors did not act through downstream effects on the Golgi, we evaluated Golgi morphology in infected cells treated with 4PBA, FLI-06, or BFA from 20-24 hpi. As expected, the Golgi marker GM130 was distributed around the inclusion in control cells and those treated with 4PBA, while cells treated with BFA and FLI-06 had faint, diffuse GM130 staining (Figure S3–6). Although the Golgi was not disrupted by 4PBA, it is possible that there is still an effect on the acquisition of Golgi derived vesicles by *Chlamydia*. To test this, we used fluorescently labeled NBD-C6-ceramide as a marker for sphingomyelin uptake into the

inclusion, as described previously (12). HeLa cells were infected with *C. trachomatis* and grown for 22 hours. Cells were then treated with either 10 μM FLI-06, 5 mM 4PBA, or 3 μg/mL BFA for 1 hour, then incubated for 30 minutes with NBD-ceramide, followed by 1.5 hours back-exchange in the presence of ERES inhibitors or BFA. Fluorescence microscopy was used to assess mean fluorescence of the inclusions with different treatments. Similar to previous studies, treatment with BFA reduced ceramide uptake by 58.0% (Figure 3–4C). FLI-06 reduced uptake by about the same amount, 52.9%, indicating that although FLI-06 disrupts the Golgi, it does not affect chlamydial ceramide acquisition any more than BFA. Since BFA has no effect on IFU, it is unlikely that the reduction in IFU seen following FLI-06 treatment is due to the disruption of the Golgi. This is further supported by 4PBA having no discernible effect on ceramide uptake (Figure 3–4C).

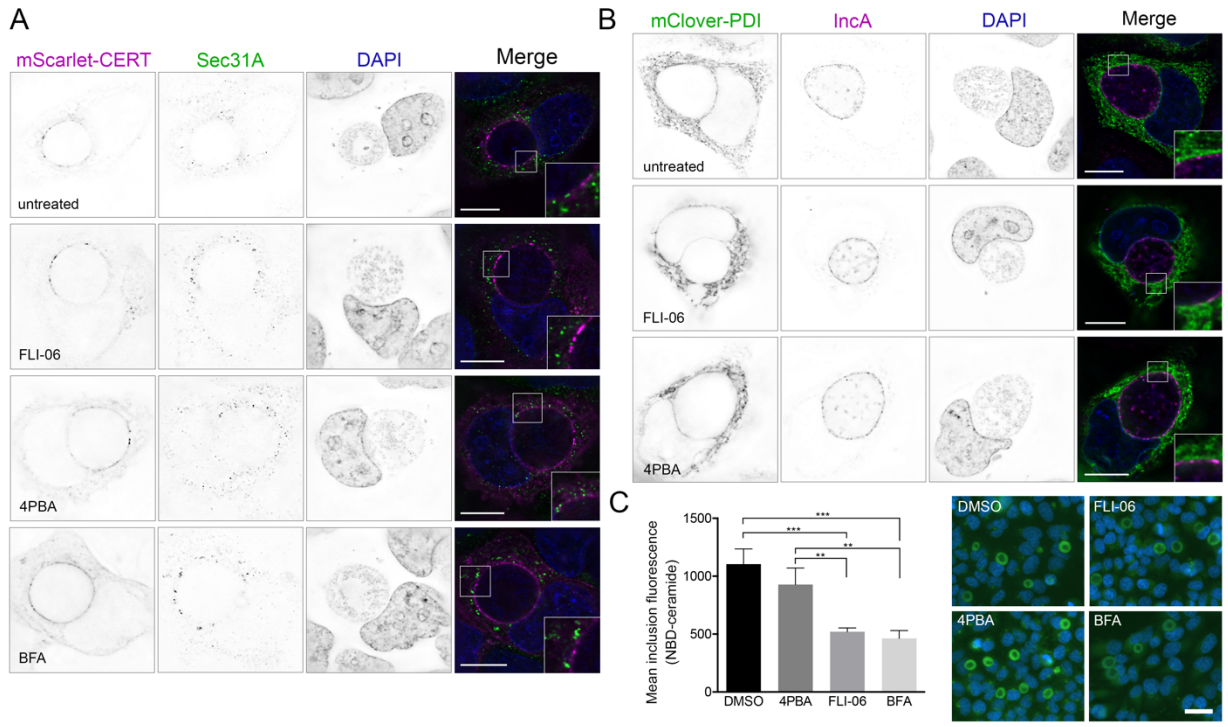


**Figure 3–4. Membrane contact sites and ceramide uptake are maintained during inhibition of ERES.**

Cells were infected with *C. trachomatis*, then transfected with a plasmid expressing pmScarlet-CERT (A, purple in merge) or pmClover3-PDI (B, green in merge). At 20 hpi, DMSO, 10 µM FLI-06, 5 mM 4PBA, or 3 µg/mL BFA were added to cells. At 24 hpi, cells were fixed and stained with anti-Sec31A (A, green in merge) or anti-IncA (B, purple in merge). DNA was stained with DAPI (blue in merge). Images are single planes from deconvolved z-series. Scale = 16 µm. (B) Inset shows regions along the inclusion membrane where PDI was closely apposed or overlapping IncA. (C) Average inclusion fluorescence after incubation with NBD-C6-Ceramide. Representative images shown on right, NBD-ceramide in green, DAPI in blue. Significance determined by one-way ANOVA with Tukey's multiple comparison test. Any comparisons not shown were not significant. **, $p < 0.01$; ***, $p < 0.001$.

## Depletion of ERES regulatory proteins disrupts *Chlamydia* growth

We next sought to determine the specific ERES and COPII associated proteins necessary for providing factors critical for chlamydial growth. Using RNAi, we knocked down the expression of Sec16A and TANGO1, proteins which are required for efficient COPII transport (86). We additionally knocked down cTAGE5 and Sec12; Sec12 is the guanine exchange factor for Sar1 GTPase, which in turn regulates COPII vesicle formation (94). Sec12 also interacts with

cTAGE5 at ERES, and it has been shown that cTAGE5 can recruit Sec12 to COPII budding sites (85). Bet3, a key component of the TRAPP complex that functions in COPII vesicle tethering and fusion at the ERGIC, was also knocked down (95).

HeLa cells were transfected with siRNA oligos and incubated for 48 hr prior to infecting with *C. trachomatis*. At 48 hpi, cells were lysed and chlamydial IFU was quantified on fresh HeLa monolayers. Knockdown of Sec12 and cTAGE5 resulted in a 49.1% and 58.4% reduction in IFU, respectively (Figure 3–5A, Figure S3–7). Simultaneous knockdown of both Sec12 and cTAGE5 reduced IFU by 85.2%. Surprisingly, Sec16A and TANGO1 depletion had no effect on IFU. Bet3 disruption also had no effect on IFU; however, this result was expected since Bet3/TRAPP functions downstream of ERES and COPII vesicle formation, as a tethering complex on the ERGIC and cis-Golgi. ERES proteins typically exhibit similar subcellular localizations, and we used immunofluorescence microscopy to determine if Sec12 had a similar distribution as other key COPII components during *Chlamydia* infection. Sec12 colocalized with Sec31 in infected cells (Figure 3–5B), and both proteins remained closely associated after treatment with FLI-06 or 4PBA (Figure S3–8). Sec12 also overlapped with IncA in distinct punctae, similar to the overlap seen with Sec31 or Sec16 and IncA (Figure 3–5C). While it is unclear why Sec12 and cTAGE5 depletion affect IFU while Sec16 and Tango1 have no effect, it seems that *Chlamydia* may require a specific cargo or function of ERES rather than general COPII vesicular trafficking. It is also possible that there is redundancy in the roles of Sec16 and Tango1 during infection. Future efforts will need to resolve whether the basis of this interaction is to provide COPII vesicular cargo to inclusions, or to allow *Chlamydia* to interfere with an ERES-mediated process critical for infection.

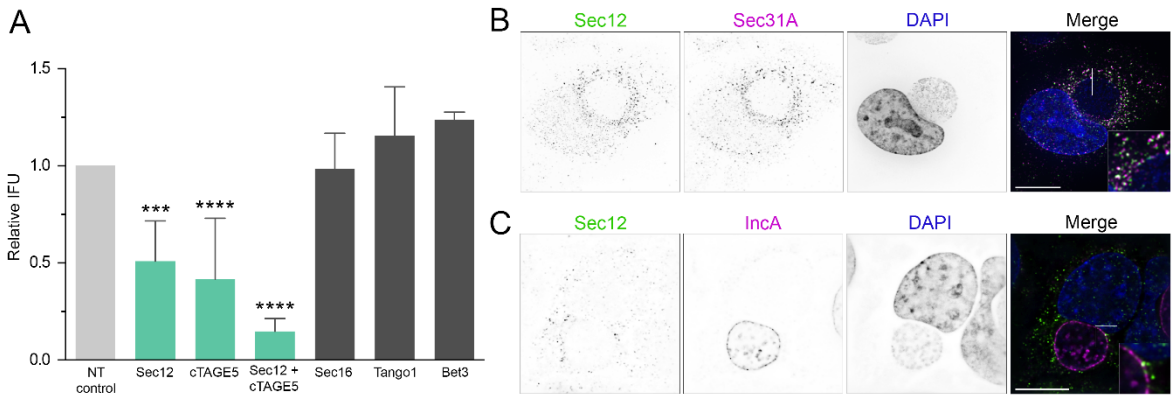


**Figure 3–5. RNAi depletion of ERES regulatory proteins Sec12 and cTAGE5 disrupt *Chlamydia* growth.**

(A) Cells were treated with siRNA oligonucleotides and incubated for 48 hours, then infected with *C. trachomatis* L2. At 48 hpi, cells were lysed and infectious *Chlamydia* EB from each sample group were tested for IFU by infecting new cells. IFU values were compared to scramble siRNA treated, infected cells. Significance determined by one-way ANOVA with Dunnett's multiple comparisons test, compared to control IFU. Bars, mean (SD);***, $p < 0.001$; ****, $p < 0.0001$; n ≥ 3. (B) Sec12 (anti-Sec12, green in merge) colocalizes with Sec31 (anti-Sec31A, purple in merge) in infected cells. Representative deconvolved merged z-series image. Scale bar = 16 µm. (C) Sec12 (anti-Sec12, green in merge) overlaps with IncA (anti-IncA, purple in merge) in a similar manner to Sec16 or Sec31. Single plane from deconvolved z-series image. Scale bar = 16 µm.

## Discussion

In this study, we also report the novel interaction between *C. trachomatis* inclusions and ER exit sites. Importantly, functional disruption of ERES cargo loading or specificity using chemical and genetic approaches resulted in major defects on inclusion and chlamydial growth. The ERES associated proteins Sec16, TANGO1, peflin, and TFG, were identified by IncB-APEX as inclusion membrane associated proteins, and follow up investigations confirmed the recruitment of Sec16 and the COPII coat protein Sec31 to the cytosolic surface of inclusion membranes. Inclusion–ERES interactions seem to be distinct from previously described IncD- and IncV-mediated ER–inclusion membrane contact sites (MCS) (9,10,41,72,74), since the ER membrane protein CERT, which interacts with IncD at MCS, did not colocalize with ERES proteins. Localization of CERT and ER marker PDI was unaffected by inhibition of ERES using

FLI-06 or 4PBA. In this regard, our findings strengthen the theme of inclusion membrane and ER interactions as playing important roles for inclusion biology and function during infection. Atlastin-3 and reticulon-4, which play roles in regulating ER morphology and structure (96,97), were also identified by our data and inclusion-MS (42). In addition to ERES and COPII components, inclusion membrane interactions contain ERGIC-53 and VIP36 (42), two homologous proteins which are primarily localized to the ERGIC and function to regulate COPII vesicle fusion, and ER-ERGIC-Golgi syntaxins 5 and 18 (42). We propose a model wherein *C. trachomatis* inclusions intimately interact with COPII mediated ERES to ERGIC vesicular traffic (Figure 3–6).

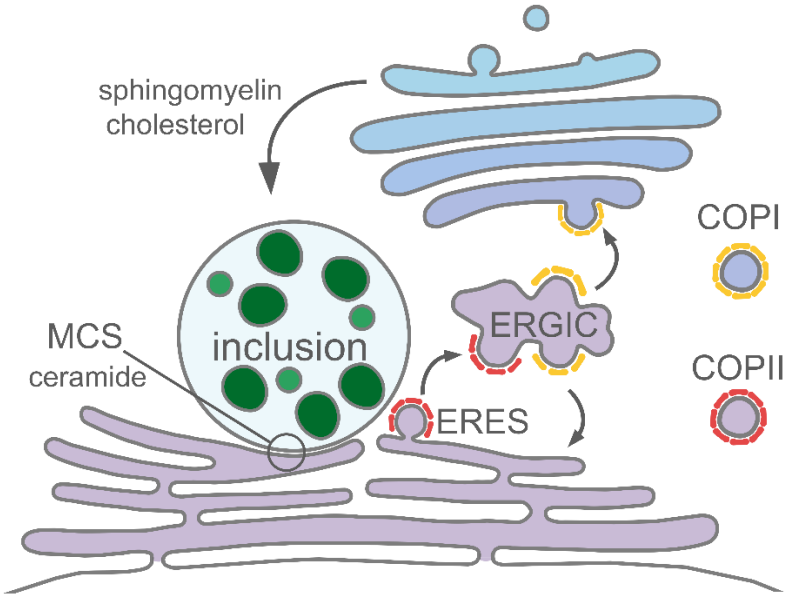


**Figure 3–6. Model for interactions between the *Chlamydia* inclusion and the early secretory pathway.**

Our findings support a model wherein the inclusion membrane is situated in cells in close proximity to ERES domains. Normal COPII vesicle traffic from ERES are delivered to the ERGIC in mammalian cells, followed by COPI vesicle traffic to the Golgi complex. Inclusion–ERES interactions constitute a larger theme of physical and functional interactions between the inclusion and ER.

Reasons for the importance of Sec12 and cTAGE5, but not Sec16 or Tango1, in the interaction between ERES and inclusion membranes are at this time unclear. Recent work by

others has shown that nutrient starvation induced Sec12 and cTAGE5 relocation to the ERGIC followed by generation of autophagosome membrane precursors (98,99). There are likely many other roles of ERES that have not yet been described, and the molecular mechanisms of ERES and ERGIC regulation are incompletely understood. FLI-06 blocks cargo recruitment to ERES, but unfortunately there are no known proteins involved in this step of COPII trafficking. The targets of 4-PBA, the p24 (also called TMED) family, would be very interesting to study in the context of *Chlamydia* infection, especially since five of these proteins were found by AP-MS or inclusion-MS (40,42). These experiments may prove challenging, however, as there are 11 members and they are thought to have functional redundancy.

Collectively, the functional and proteomic data show that complete developmental growth of *Chlamydia* requires efficient COPII vesicle production from ERES throughout the developmental cycle. One attractive nutritive benefit for *Chlamydia* is the acquisition of lipids, as supported by evidence that chlamydiae acquire phosphatidylcholine and other phospholipids from host cells (100,101), recruit lipid droplets to inclusions (18), redirect cholesterol to inclusions (15), and require functional host fatty acid synthesis machinery (18,102). Much of our understanding for ERES secretory mechanisms has come from studying the assembly of large cargo into COPII vesicles; for example procollagen, pre-chylomicrons, and very low-density lipoproteins (103). For export of these bulky cargo, cTAGE5 and TANGO1 are essential. In our system, cTAGE5 disruption impaired IFU production, whereas TANGO1 knockdown had no discernible effect. An explanation for these findings is elusive, notably because only a preliminary functional characterization of these regulatory proteins exists. Interestingly, cTAGE5 and the TANGO-related gene MIA2 can form a fusion protein (TALI) that binds TANGO1 and facilitates the recruitment of apolipoprotein B containing lipid complexes to ERES (104). Based on our proteomic data, apolipoprotein B is recruited to inclusion membranes throughout the developmental cycle.

## Materials and Methods

### Antibodies and reagents

All reagents were purchased from Thermo Fisher Scientific (Rockford, IL) unless otherwise noted. Primary antibodies used in this study and their catalog numbers: Sec12 (Western blot, PA5-53125), Sec12 (Immunofluorescence, gift from Kota Saito), cTAGE5 (PA5-29515), Sec31A (Cell Signaling, Danvers, MA; 13466S), Bet3 (TRAPPC3; PA5-55841), Sec16A (Bethyl Laboratories, Montgomery, TX; A300-648A-M), TANGO1 (MIA3; Millipore Sigma, St. Louis, MO; SAB2700012), GM130 (R&D Systems, AF8199SP), IncA (gift from Daniel Rockey), CT223 (gift from Daniel Rockey), MOMP (Virostat, Westbrook, ME; 1621), Flag (Millipore Sigma; F1804). Secondary antibodies used: Donkey anti-Rabbit HRP, Donkey anti-Goat Alexa 594, Goat anti-Mouse DyLight 594, Goat anti-Rabbit Alexa 488.

### Cell culture and *Chlamydia* infections

HeLa 229 cells (ATCC) or McCoy cells (obtained from Walt Stamm) were grown in Roswell Park Memorial Institute 1640 (RPMI; Gibco) medium supplemented with 10% fetal bovine serum (HyClone) and 2 mM L-glutamine (HyClone) at 37°C, 5% $CO_2$. *Chlamydia trachomatis* LGV L2 434/Bu was grown in HeLa 229 cells for 48 hours, then infected cells scraped into sucrose phosphate buffer (5 mM glutamine, 0.2 M sucrose. 0.2 M phosphate), lysed using bead bashing, and cell debris cleared by centrifugation at 300 × g for 10 minutes. Supernatant containing *Chlamydia* aliquoted and stored at -80°C. HeLa cells were infected with *Chlamydia* diluted in Hank's buffered salt solution (HBSS; Gibco) at an MOI ~1 for 2 hours at room temperature. Cells were washed with HBSS, then incubated at 37°C in RPMI.

**Plasmid constructs**

Plasmids were isolated using the Qiaprep Spin Miniprep kit or the HiSpeed Plasmid Midi kit (Qiagen, Germantown, MD).

Mammalian plasmid pmScarlet-CERT was made in the pEGFP-N1 backbone, with Gibson Assembly used to replace EGFP with mScarlet. mScarlet was amplified from the pmScarlet-C1 plasmid, which was a gift from Dorus Gadella (Addgene plasmid # 85042) (105). CERT was inserted at the N terminus of mScarlet using the XhoI and AgeI restriction sites. The pmClover3-PDI plasmid was made in the pEGFP-N1 backbone. Gibson Assembly was used to replace EGFP with mClover3, and PDI was inserted at the N terminus of mClover3 using Gibson Assembly. mClover3 was amplified from pKanCMV-mClover3-18aa-actin, which was a gift from Michael Lin (Addgene plasmid # 74259) (106). Plasmid pmGFP-Sec16L was a gift from Benjamin Glick (Addgene plasmid # 15776) (107).

**siRNA and plasmid transfections**

For siRNA transfections, HeLa cells were plated in 24 well or 96 well plates to 60-80% confluence. For 24 well plates, 50 µL Opti-MEM (Gibco) medium containing 5 pmol siRNA oligonucleotides and 1.5 µL Lipofectamine RNAiMAX was added to each well. Following transfection, cells were incubated for 48 hours at 37°C prior to infection or protein analysis by western blot. For 96 well plate experiments, knockdowns were done in duplicate, with 10 µL Opti-MEM containing 1 pmol siRNA oligonucleotides and 0.3 µL Lipofectamine RNAiMAX added per well. Oligonucleotides were purchased from Dharmacon. Dharmacon siGenome smartpools of 4 different oligonucleotide sequences were used for Sec16, Tango1, and Bet3 knockdowns. Dharmacon siGenome individual oligonucleotides were used for all other knockdowns.

For mammalian plasmid transfections, HeLa cells were plated in 4 well chamber slides (Nunc Lab-Tek), and infected with *C. trachomatis* L2. Immediately after infection, each well

was transfected with 50 µL Opti-MEM containing 500 ng plasmid and 1.5 µL Lipofectamine 2000.

**Quantitative PCR analysis**

For qRT-PCR confirming siRNA knockdown, HeLa cells were plated in 24 well plates, and transfected with siRNA oligos as described above. Cells were incubated for 48 hours, then cell pellets were frozen until RNA extraction.

For qRT-PCR measuring ER stress, HeLa cells were grown in 6 well plates and infected with *C. trachomatis* for 20 hours. At 20 hpi, 10 µM FLI-06, 5 mM 4PBA, 1 µM thapsigargin or DMSO was added in fresh medium. At 24 hpi, cells were trypsinized and cell pellets frozen until RNA extraction.

RNA was extracted using the Qiagen RNeasy mini kit (Qiagen). cDNA was made using the iScript cDNA synthesis kit (Bio-Rad). qRT-PCR reactions were set up with SsoAdvanced Universal SYBR Green Supermix (Bio-Rad) and run on the StepOnePlus Real-Time PCR system (Applied Biosystems, Foster City, CA). GAPDH was used as the housekeeping gene, and the ΔΔCT method was used to calculate relative expression.

For *Chlamydia* genome copy number analysis HeLa cells were infected with *C. trachomatis* for 24 hours, then 10 µM FLI-06, 5 mM 4PBA, 0.5 µg/mL chloramphenicol, or DMSO was added in fresh medium. At 48 hpi, cell pellets were trypsinized, centrifuged at 300 x g for 5 minutes, then *Chlamydia* genomic DNA was extracted using the DNeasy Blood and Tissue kit (Qiagen). qPCR was done with primers to GroEL2.

**Immunofluorescence and live cell microscopy**

For immunofluorescence microscopy, cells were rinsed in HBSS, then fixed for 5 minutes in ice cold methanol (Images with anti-Sec12 only, for methanol fixation permeabilization was skipped) or 15 minutes in 3.7% paraformaldehyde in HBSS. Cells were rinsed 2 times in HBSS,

then permeabilized with 0.5% triton X-100 for 15 minutes, and blocked in 1% bovine serum albumin (BSA) in PBS for 20 minutes. Samples were incubated with primary antibodies for 1 hour at room temperature in blocking buffer, then rinsed 3 times in blocking buffer, then incubated 45 minutes at room temperature with secondary antibodies in blocking buffer. DAPI was used to stain DNA, and added during the secondary antibody step. For imaging of live cells, media was replaced with HBSS before imaging. Cells were imaged on a Nikon Ti-E inverted microscope and images were captured on a Hamamatsu camera controller C10600. Images were processed using Volocity software (PerkinElmer, Waltham, MA).

Sec31A punctae overlapping the inclusion were counted manually using Volocity software. Spots that overlapped with IncA, or were touching IncA were counted as on the inclusion membrane. Region where inclusion is adjacent to nucleus was excluded from analysis. Images used for counting were 60x magnification, deconvolved z-series. Planes were examined individually to ensure overlap was in the same z dimension. At least 20 inclusions in control and FLI-06 treated cells were analyzed, for each of two independent experiments.

Ceramide trafficking to the inclusion was measured as previously described, with slight modifications (13). HeLa cells were infected with *C. trachomatis* at an MOI < 1 for 22 hours. Warm media containing 10 μM FLI-06, 5 mM 4PBA, 3 μg/mL BFA, or DMSO was added to the cells for 1 hour at 37°C. NBD-ceramide was complexed to BSA by adding 10 μM NBD-ceramide to HBSS with 0.7% fatty acid free BSA (Millipore Sigma) and vortexing thoroughly. After 1 hour incubation with inhibitors, cells were rinsed 1 time with HBSS, then NBD-ceramide/BSA was added and cells incubated for 30 minutes at 4°C. Cells were rinsed two times in HBSS, then incubated for 1.5 hours at 37°C in serum free media with 0.7% fatty acid free BSA with same inhibitors as before. After 1.5 hours, stained nuclei using Hoechst and took images with fluorescence microscope. Analyzed 5 microscopy fields per condition using Volocity software. For each field, made 30 identical circles that fit inside nuclei to get mean background fluorescence, outlined 20 inclusions (100 total per replicate) by hand to measure mean

fluorescence inside inclusion. Outlines were done in Hoechst channel only to avoid bias, measurements were taken from NBD channel only. Background fluorescence was subtracted from inclusion fluorescence to get measurements shown in graph. Data compiled from three independent experiments.

**Western blot analysis**

For western blot analysis of RNAi knockdowns, cell pellets were lysed in ice cold RIPA buffer (50 mM Tris, 150 mM NaCl, 0.1% SDS, 0.5% sodium deoxycholate, 1% triton X-100, pH 7.5) with Halt protease inhibitors (Pierce) for 30 minutes on ice, with vortexing every few minutes. Lysates were centrifuged for 20 minutes at 14,000 x g, and supernatant added to 4x laemmli buffer (Bio-Rad, Hercules, CA). Lysates were run by SDS-PAGE on 5-15% or 5-20% mini-PROTEAN TGX stain free gels (Bio-Rad), transferred to Immobilon PVDF membrane (Millipore Sigma) with a Pierce G2 fast blotter in Pierce 1-Step transfer buffer, blocked for 1 hr in 5% milk-TBST, and labeled with primary antibody in blocking solution for 1 hour, rocking. Washed 4 x 5 minutes in TBST, then incubated with secondary antibody for 45 min-1 hour in blocking solution, rocking. Rinsed 3 x TBST, then incubated with chemiluminescent substrate (Li-Cor 92695000, Lincoln, NE) for 5 minutes, and imaged using a C-DiGit blot scanner (Li-Cor).

**Inclusion forming unit analysis**

Infected HeLa cells were lysed at 48 hpi by incubating in water for 20 minutes followed by pipetting to disrupt cells. Serial dilutions of lysate were plated onto fresh HeLa monolayers in a 96 well plate. At 24 hpi, cells were fixed and stained with DAPI and an anti-MOMP antibody. Using immunofluorescence microscopy, 10-15 fields per well were taken at 20x magnification. Inclusions and nuclei in each field were counted using the Fiji distribution of ImageJ (82). The macro used to count inclusions and nuclei in images is provided in supplemental methods. The

overall percentage of infected cells was used to compare IFU between conditions, and the relative IFU calculated for each experiment by comparing to control. For FLI-06 experiments, HeLa cells in 24 well plate were infected with *C. trachomatis* L2 at an MOI around 1. FLI-06 was resuspended in DMSO to a concentration of 20 mM and frozen at -80°C until use. For treating cells, FLI-06 in DMSO was diluted 1:2000 in normal cell medium to make a final concentration of 10 μM FLI-06 and serial dilutions were used to make medium with 5 μM and 1 μM FLI-06. At 2.5, 18, 24, or 40 hours post infection, medium was aspirated from different wells in the plate and replaced with pre-warmed medium containing three different FLI-06 concentrations. Control well medium was aspirated and replace with fresh pre-warmed medium. For the 18 hour time point, two wells per concentration were prepared, one of which was aspirated and washed with HBSS at 24 hpi, then incubated in fresh medium. Since the stability of FLI-06 was unknown, medium in wells treated at 2.5 hpi was refreshed at 24 hpi, with identical concentrations of FLI-06. At 48 hpi, primary infection was imaged on microscope and 10-15 brightfield images were taken per well at 20x magnification and inclusion diameter was measured using Volocity software. After images were taken, cells were lysed for IFU assay as described above. IFU was adjusted based on number of inclusions per field in primary infection due to differences in cell growth with the inhibitor.

**Statistical analysis**

Statistical analysis was performed using GraphPad Prism software. Comparisons between IFU, inclusion diameter, or genome copy number were analyzed using one-way ANOVA with Dunnett's test for multiple comparisons. Comparison for number of Sec31 punctae on the inclusion membrane with or without FLI-06 treatment were analyzed using an unpaired t-test with Welch's correction. Ceramide uptake after treatment with inhibitors was analyzed using a one-way ANOVA with Tukey's multiple comparisons test. ER stress in infected and uninfected cells after treatment with inhibitors was analyzed using a two-way ANOVA with Dunnett's

multiple comparisons test. Graphs indicate mean and standard deviation, statistical significance is indicated as follows: *, $p < 0.05$; **, $p < 0.01$; ***, $p < 0.001$; ****, $p < 0.0001$.

**Supplementary Information**

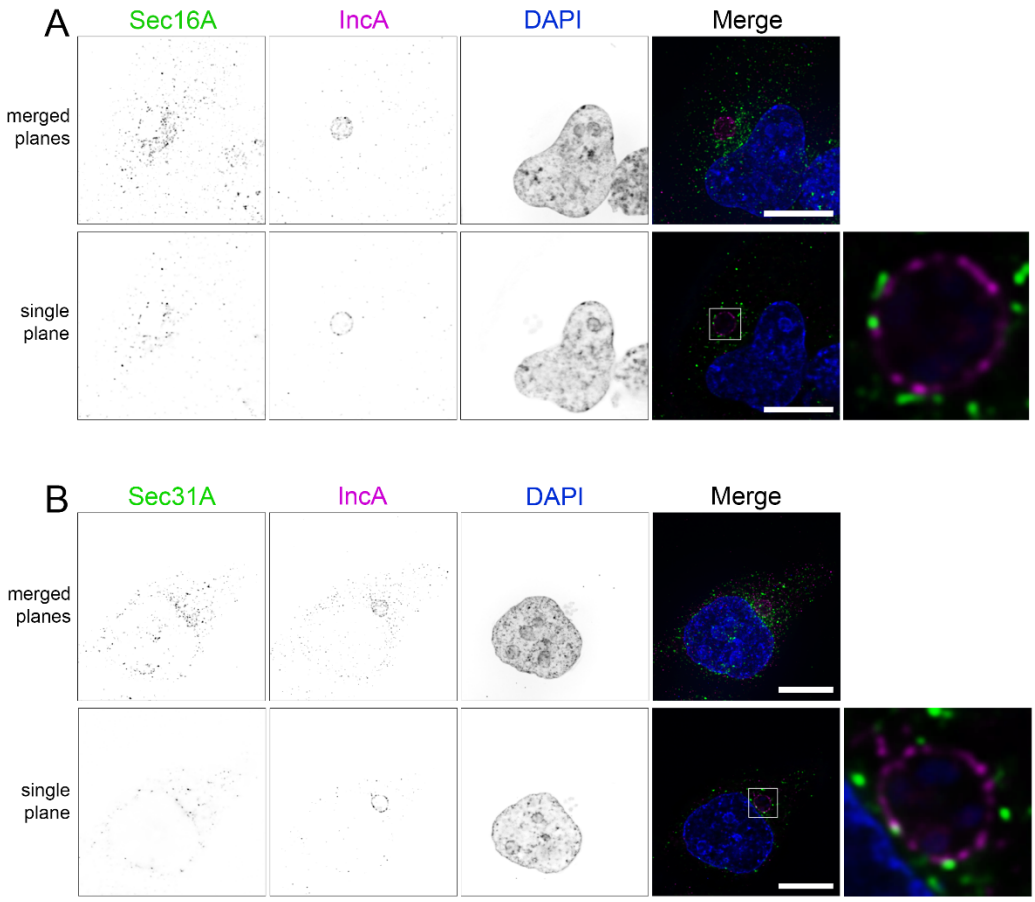


**Figure S3–1. Sec16A and Sec31A associate with the inclusion membrane early in infection.**

HeLa cells infected with *C. trachomatis* L2 were fixed at 14 hpi and stained with anti-Sec16A (A) or anti-Sec31A (B), anti-IncA, and DAPI. Top rows of A and B are deconvolved and merged z-series images; bottom rows are single deconvolved planes. Scale bars = 10 μm.

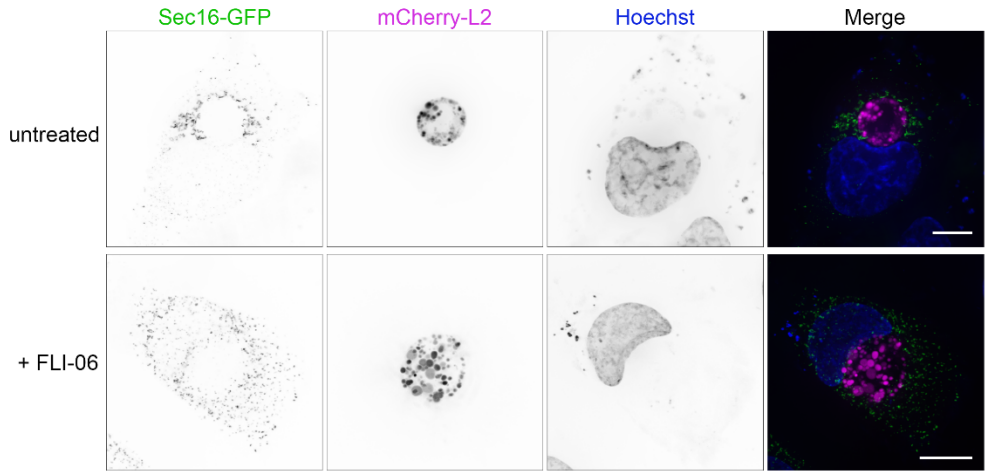


**Figure S3–2. Sec16 is recruited to *C. trachomatis* inclusions in living cells, and FLI-06 abrogates the association.**

HeLa cells were transfected with a Sec16-GFP plasmid and infected with mCherry expressing *C. trachomatis* L2. DNA was labeled with Hoechst and cells were imaged live at 24 hpi. In top row, Sec16-GFP shows a similar localization to antibody staining (Figure 3–1A), with an enrichment near the inclusion membrane. Bottom row shows cells treated with 10 µM FLI-06 from 20-24 hpi, resulting in diffuse Sec16-GFP punctae throughout the cell. Scale bars = 16 µm, images are deconvolved merged z-series.

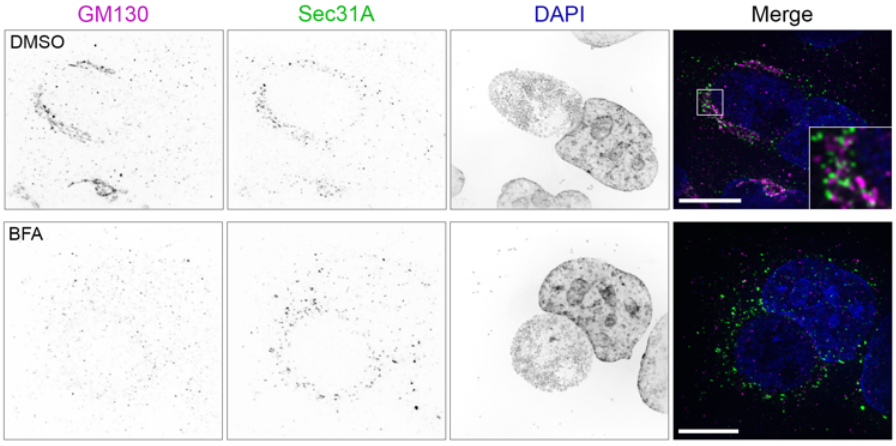


**Figure S3–3. ERES are distributed around the inclusion even during Golgi disruption.**

HeLa cells were infected with *C. trachomatis* and treated with either DMSO or 3 µg/mL BFA from 20-24 hpi. Cells were fixed at 24 hpi and stained with GM130 (anti-GM130, purple in merge) to mark the Golgi, Sec31A (anti-Sec31A, green in merge) to mark ERES, and DAPI for DNA (blue in merge). Scale = 16 µm, images are deconvolved merged z-series.

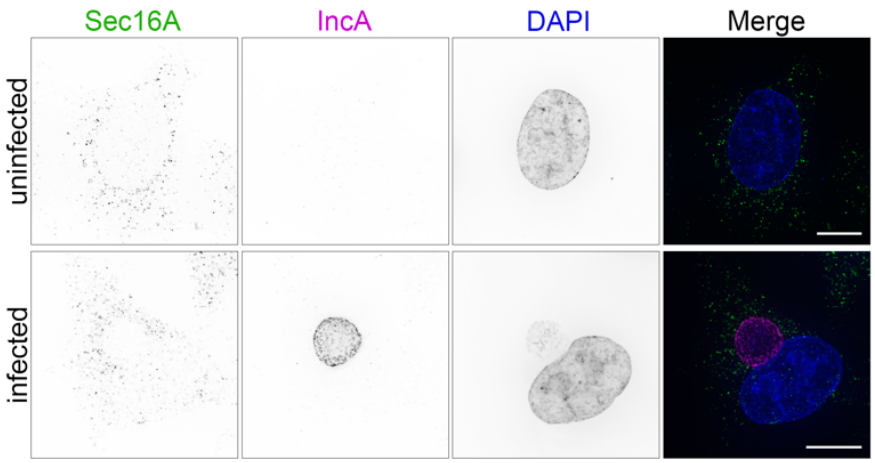


**Figure S3–4. ERES marker Sec16A is more diffuse following FLI-06 treatment.**

HeLa cells were infected with *C. trachomatis* and incubated with FLI-06 from 20-24 hpi, then fixed and processed for immunofluorescence. Sec16A (anti-Sec16A, green in merge), IncA (anti-IncA, purple in merge), and DNA (DAPI, blue in merge) were labeled, showing an altered localization of ERES in the presence of FLI-06. Scale = 16 µm, images are deconvolved merged z-series.

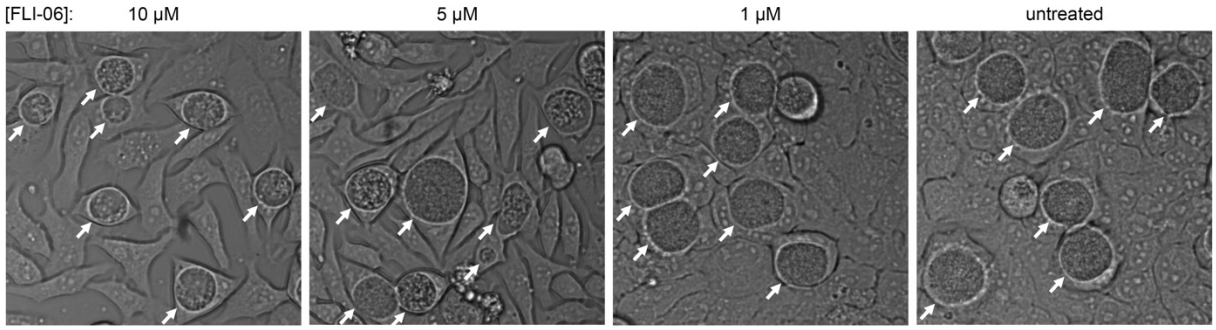


**Figure S3–5. Inclusion growth impacted following FLI-06 treatment.**

Brightfield images at 20x magnification of infected cells treated with FLI-06 starting at 18 hpi, at indicated concentrations, and measured at 48 hpi. At 10 and 5 µM FLI-06, inclusion morphology appears smaller with bacteria less uniformly distributed, compared to the 1 µM or untreated cells. Arrows indicate inclusions.

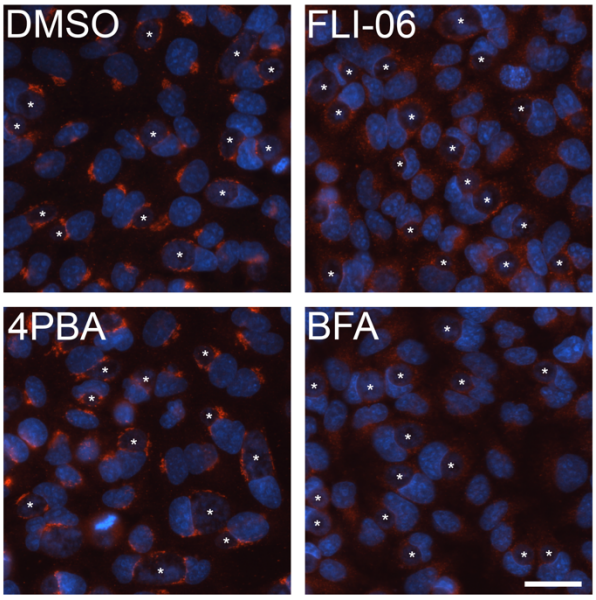


**Figure S3–6. Golgi is disrupted by BFA and FLI-06 but not 4PBA.**

HeLa cells were infected with *C. trachomatis* for 20 hours; 10 μM FLI-06, 5 mM 4PBA, or 3 μg/mL BFA were added from 20-24 hpi, then cells were fixed and processed for immunofluorescence. Golgi marker GM130 (anti-GM130, red) and DNA (DAPI) are shown at 20x magnification. Inclusions marked with stars, scale bar = 32 μm.

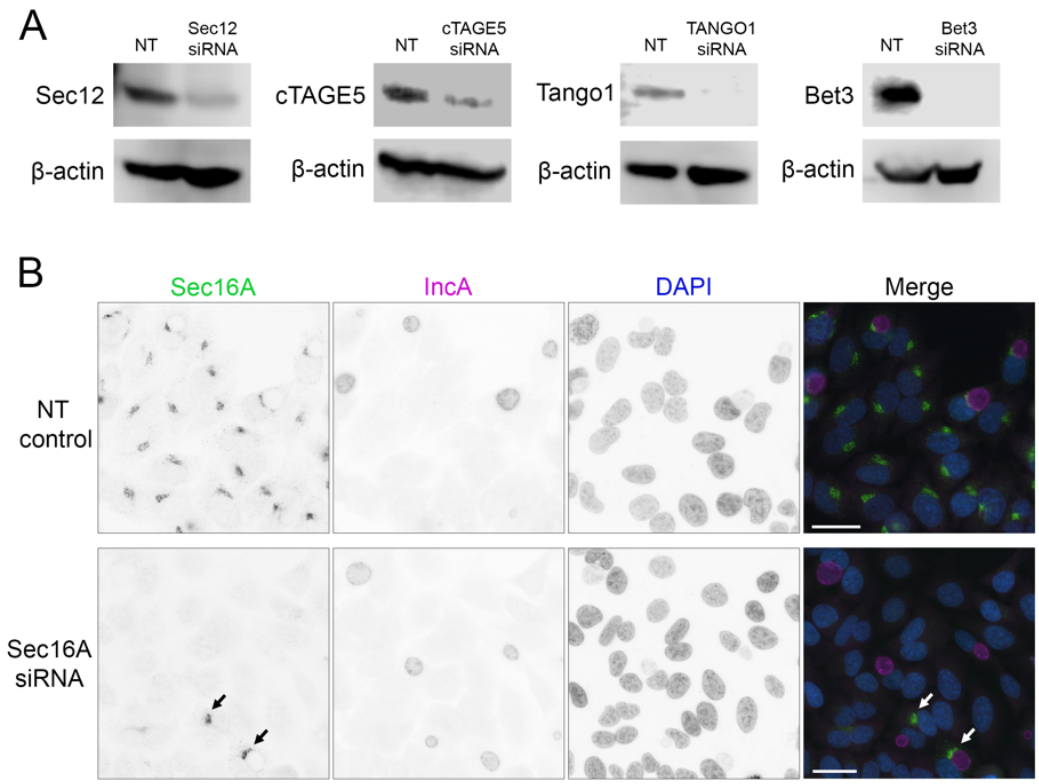


**Figure S3–7. Western blots and microscopy for ERES RNAi.**

(A) Western blots were used to confirm siRNA knockdown at the protein level. HeLa cells were transfected with siRNA oligonucleotides and incubated for 48 hours, then protein levels assessed by western blot. Knockdown was compared to cells transfected with a non-targeting (NT) control oligonucleotide. Beta-actin was used as a loading control. We were unable to detect Sec16A by western blot, so knockdown was confirmed by immunofluorescence microscopy. (B) HeLa cells were transfected with either the Sec16A siRNA oligonucleotide or NT control, incubated for 48 hours, then infected with *C. trachomatis* L2. Cells were fixed at 24 hpi and stained with anti-Sec16A, anti-IncA, and DAPI. Images are 20x magnification. In control cells, Sec16A (green in merge) is visible in every cell, while in the Sec16A targeting siRNA treated cells, most cells have no visible Sec16A. Knockdown efficiency was less than 100%, as shown by two cells with visible Sec16A expression (arrows). Scale bars = 30 μm.

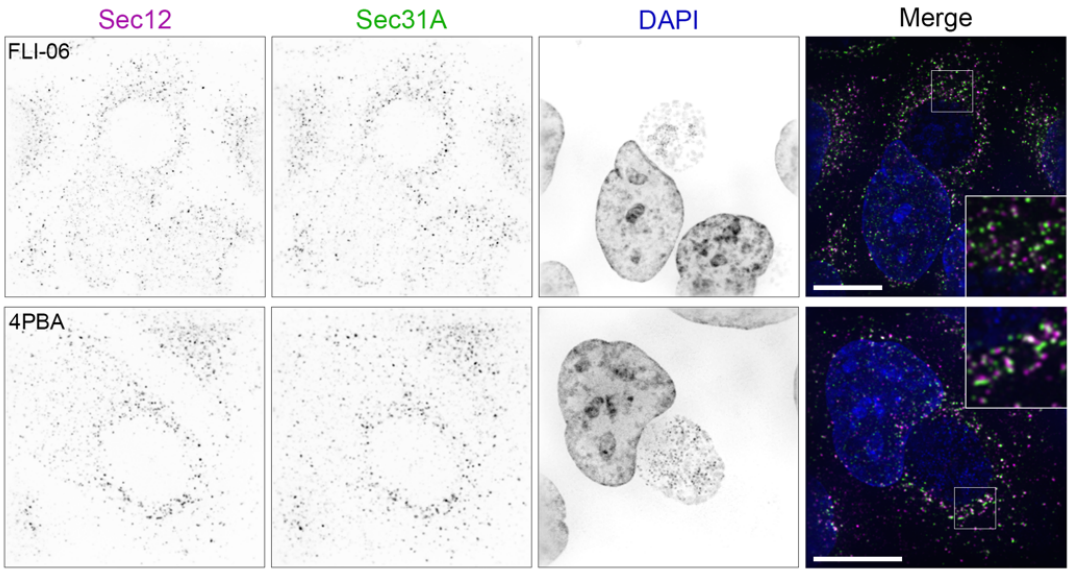


**Figure S3–8. Sec12 and Sec31A colocalize after treatment with FLI-06 or 4PBA.**

HeLa cells were infected with *C. trachomatis* and treated with 10 μM FLI-06 or 5 mM 4PBA from 20-24 hpi. Cells were then fixed with ice cold methanol and stained for Sec12 (anti-Sec12, purple in merge), Sec31A (anti-Sec31A, green in merge), or DNA (DAPI, blue in merge). Images are deconvolved merged z-series, scale = 16 μm.

# Chapter 4 – ER exit site proteins are recruited to the inclusion membrane and have disparate effects on *Chlamydia* growth

## Introduction

Although chemical inhibition and RNA interference showed that ERES function is important for chlamydial growth, microscopy showed only limited overlap between the COPII components Sec31 or Sec16, and the inclusion membrane. IncB-APEX identified the COPII proteins Tango1, Sec16, peflin, and TFG. We initially focused on Sec16 and Tango1 because they were much more well characterized for their roles in COPII vesicle formation compared to peflin and TFG. In addition to peflin and TFG, the protein PDCD6 was identified as being in close proximity to the inclusion in some of our preliminary mass spectrometry experiments using IncB-APEX. Peflin, and TFG both bind PDCD6 and all three proteins localize to ERES, but it is unclear what role they play in COPII trafficking. In the case of peflin and PDCD6 there are conflicting reports of whether they positively or negatively affect ERES transport. Sec16 and Tango1 are thought to be required for general COPII budding, yet depletion had no effect on *Chlamydia* growth. This suggests there may be a more specific ERES function for *Chlamydia* growth, or *Chlamydia* interacts with specific proteins at ERES that are not affected by depleting Sec16 or Tango1. We decided to investigate the roles of PDCD6, peflin, and TFG during *Chlamydia* infection to see if they provide additional clues to the ERES proteins that are important for *Chlamydia* growth.

Peflin and PDCD6 are members of the penta-EF-hand family, and both have five EF hand domains and two calcium binding sites in the first and third EF hands (108). PDCD6 (also called ALG-2) was first described to be involved in Fas-, glucocorticoid-, and T-cell receptor-induced cell death (109). Much of the early research on PDCD6 was focused on cell death, but some of these early findings have been called into question due to PDCD6 antibody artefacts

(110). PDCD6 was connected to ERES when it was discovered that it directly binds Sec31 in a calcium-dependent manner (111). This study suggested that PDCD6 stabilized Sec31 at ERES, but the authors did not see any effect on COPII trafficking when PDCD6 was depleted with RNA interference (111). The interaction between PDCD6 and Sec31 has been confirmed by other groups (112,113). Two subsequent studies showed that excessive PDCD6 inhibited COPII trafficking in a calcium dependent manner by preventing both budding (113) and vesicle fusion (114) in vitro. In addition, elevated calcium negatively regulated COPII budding (113). A subsequent study found that in the context of a cell, depletion of luminal calcium reduced cargo trafficking from ERES, and the interaction between Sec31 and PDCD6 was required for ER to golgi transport (115). This study used a dominant negative strategy, overexpressing PDCD6 and the PDCD6 binding region of Sec31. Knockdown of PDCD6, however, has been shown to cause a faster export of VSV-G from ERES, more in agreement with the evidence that PDCD6 negatively regulates COPII budding (116). This is far from conclusive however, as a later study showed that PDCD6 knockdown delayed secretion of different COPII cargos, SEAP and collagen (117).

It was also found that PDCD6 and peflin cooperatively regulate COPII vesicle size by promoting ubiquitylation of Sec31 under elevated calcium conditions (118). Ubiquitylation of Sec31 causes larger COPII vesicles to form, which are capable of transporting bulky procollagen out of the ER (118). It is unclear how to reconcile the different conclusions based on PDCD6 perturbation in the context of ERES function. One aspect that may partially explain the disparate data is that PDCD6 is known to form different complexes. PDCD6 can form a homodimer with itself, or a heterodimer with peflin, though only the PDCD6 homodimer bound TFG, recruiting it to ERES (119). This suggests that if PDCD6 is present in a homodimer it may function distinctly from a PDCD6/peflin heterodimer, so PDCD6 may inhibit or enhance ERES function depending on its binding partner. This would not fully explain the opposite conclusions reached by different studies regarding PDCD6 either enhancing or inhibiting COPII vesicle

formation, but it does suggest that the PDCD6-ERES relationship may be more complex than one or the other.

Peflin and PDCD6 are paralogs but the functional role of peflin in ERES has only recently been studied. Peflin was first identified based on sequence similarity to the penta-EF hand family, with highest similarity to PDCD6 (120). The main molecular difference between PDCD6 and peflin is the hydrophobic N-terminus of peflin, which consists of nine nonapeptide repeats (120). Like PDCD6, peflin also binds calcium, and peflin is thought to localize to the cytoplasm in low calcium conditions, then translocate either to membranes or the cytoskeleton upon calcium binding (121). Both peflin and PDCD6 were unstable without the EF5 domain, with truncated versions being degraded in the proteasome (121). It was proposed that the EF5 domain promotes dimerization and thus stabilization of these proteins (121). Interestingly, there seems to be a regulated amount of peflin within the cell, as ectopic overexpression of peflin led to a decrease in endogenous peflin levels, and much higher levels of peflin overexpression were attained when PDCD6 was also overexpressed (121). Peflin is ubiquitinated by $CUL3^{KLHL12}$ ubiquitin ligase, but this has not been studied in the context of regulating peflin levels (118). In the context of collagen secretion, peflin knockdown by RNA interference led to decreased secretion (118). Peflin knockdown also led to increased VSV-G export, suggesting an inhibitory role in COPII trafficking (122). It seems likely that, as with PDCD6, there may be multiple levels of regulation of peflin in the context of ERES, such that a knockdown does not fully explain the function of the protein in the context of COPII trafficking.

TFG, or Trk-fused gene, was first discovered because in certain cancers it forms a fusion protein with the NTRK1 tyrosine receptor kinase through a chromosomal rearrangement (123). A yeast-two-hybrid screen for binding partners of TFG amino acids 1-193 revealed that TFG binds NEMO and TANK, proteins that modulate NF$\kappa$B activity (124). These interactions were confirmed in human cell lines, and it was also shown that overexpression of TFG led to higher NF$\kappa$B activity after stimulation with TNF$\alpha$ (124). Contradicting this, a later study showed that

depletion of TFG using a short hairpin RNA led to an increase in NFκB and IFNβ activity (125). This result is not necessarily contradictory on a biological level, as overexpression of other ERES proteins had an inhibitory effect, so TFG overexpression may result in reduced functionality, mimicking TFG depletion. *Chlamydia* is known to suppress NFκB activity but it is not fully understood how this occurs (46). During Sendai virus infection, TFG interacts with TRIM25, a critical component of RIG-I antiviral signaling (125). This suggests that TFG may have different binding partners during infection with viruses or bacteria. A final study connecting TFG and innate immunity showed that TFG drives IFNβ production and can be targeted for lysosomal degradation by TRIM68 ubiquitination (126).

In the context of ERES, the Audhya group showed in *C. elegans* and human cells TFG directly interacted with Sec16 to allow proper assembly of COPII subunits, and was required for COPII cargo secretion (127). They showed TFG forms octameric, cup-like structures that can assemble into larger polymers within a cell, and it was suggested to promote concentration of COPII vesicles to allow them to fuse prior to fusion with the ERGIC (128). The same group found that TFG localization to ERES was mainly mediated by direct binding to the inner coat protein Sec23, and it was proposed that TFG promotes uncoating by outcompeting the COPII outer coat (129). In this model, TFG oligomers form a network near ERES and this network prevents COPII vesicles from diffusing away from ERES and the ERGIC (129). TFG binds Sec23 to compete off the Sec31 outer coat, these vesicles then get fully uncoated by an unknown mechanism and can fuse together and reach the ERGIC (129). A competing model from the Stephens group proposed that TFG oligomerization allows large ERES to form, promoting secretion of large cargo like procollagen (130). This model is supported by data showing that upon TFG depletion, ERES are more dispersed throughout the cell and do not form clusters seen in control cells (130). There was no defect in secretion of most model COPII cargo during TFG depletion, however there was a decrease in procollagen secretion (130). This led to the hypothesis that TFG allows clustering of ERES, and these larger clusters are able to more

efficiently secrete procollagen. Overall, TFG is localized to ERES and seems to have a functional role in COPII trafficking, but it remains to be seen if TFG is required for general secretion or only for specific cargo.

Although TFG, peflin and PDCD6 have clear connections to ERES, further studies will be required to resolve some of the conflicting models of how these proteins function. Both TFG and peflin bind PDCD6 so these proteins may be forming a complex on the inclusion membrane. Since TFG has been shown to oligomerize and form a scaffold to keep COPII vesicles near the ERGIC, perhaps it could also keep COPII vesicles near the inclusion membrane. Studying how these proteins relate to *Chlamydia* infection may reveal novel findings relevant to basic biology in the context of COPII trafficking.

## Results

### Localization of TFG and TFG mutants

To investigate the role of PDCD6, peflin, and TFG in *C. trachomatis* infection, we first sought to determine if the localization of these proteins resembled other ERES proteins that we investigated. First we used an antibody to test TFG localization (Figure 4–1). TFG localized to punctae that looked very similar to Sec16 and Sec31 in *Chlamydia*-infected cells, with a concentration of ERES around the inclusion membrane (Figure 4–1). To check if TFG localization was dependent on its interaction with Sec23 or PDCD6, we made plasmids with either full length TFG, or a truncated version that is missing 20 amino acids on the C-terminus corresponding to the Sec23 binding site (referred to as TFG1-380) (129). We also made a point mutant with an R106C amino acid change; this mutant is unable to bind PDCD6 (119). These three versions of TFG were flag-tagged and transiently transfected into HeLa cells. Transfected cells were infected with *C. trachomatis*, then fixed at 24 hpi and stained for immunofluorescence. We found that full length TFG formed larger punctae than were observed

with the antibody targeting endogenous TFG (Figure 4–2). This is consistent with data from the literature showing that TFG forms oligomers, and suggests that high levels of TFG may oligomerize into larger punctae. The distribution of TFG R106C was indistinguishable from wild type TFG; thus, PDCD6 binding does not seem to have a major effect on TFG localization in *Chlamydia*-infected cells (Figure 4–2). Interestingly, the TFG1-380 protein had a very different localization (Figure 4–2). It was largely not in punctae, but localized throughout the cytoplasm with a portion accumulating on the inclusion membrane (Figure 4–2). This suggests that in the absence of Sec23 binding, other TFG binding partners may be able to recruit TFG to the inclusion membrane. An alternative explanation is that full length TFG may be transiently recruited to the inclusion membrane, but in the absence of Sec23 binding it is unable to efficiently dissociate from the inclusion.

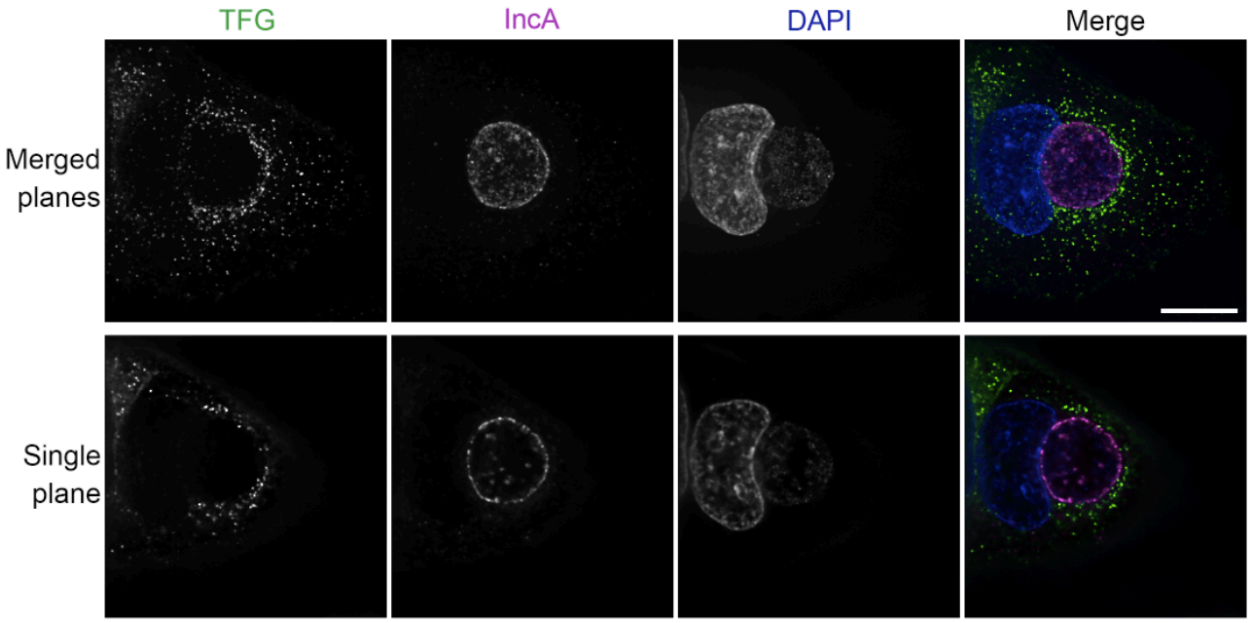


**Figure 4–1. TFG localizes to ERES and distributes around inclusion membrane.**

HeLa cells were infected with *C. trachomatis* and fixed at 24 hpi. Cells labeled with anti-TFG (first column, green in merge), anti-IncA (second column, purple in merge), and DAPI (blue). TFG was concentrated around inclusion membrane, marked by IncA, and sometimes overlapped with IncA. Images are 60x magnification, deconvolved z-series. Top row is merged z-series, bottom row is single plane.

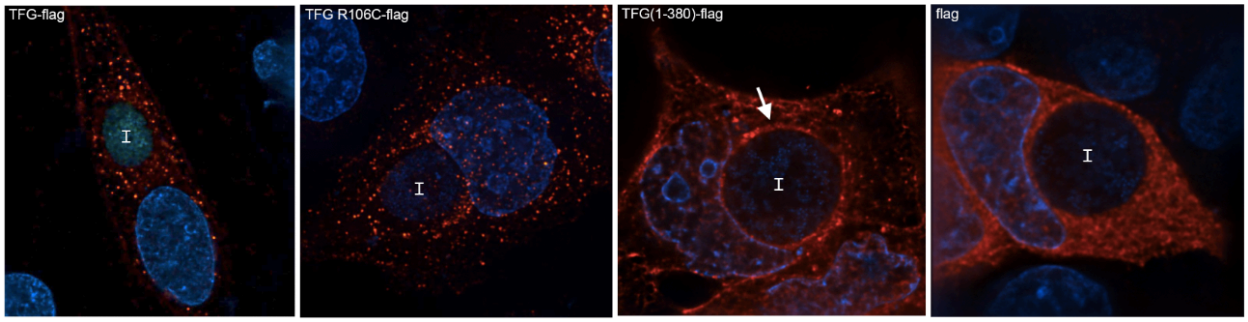


**Figure 4–2. TFG accumulates on inclusion membrane when Sec23 binding is abrogated.**

HeLa cells were transfected with plasmids expressing flag-tagged full length TFG (amino acids 1-400), flag-tagged TFG without the Sec23 binding region (amino acids 1-380), or an empty vector expressing the flag tag. Cells were infected with *C. trachomatis*, fixed at 24 hpi and stained for immunofluorescence. Overexpressed proteins were labeled with an anti-flag antibody, nuclei and inclusions (labeled with I) were labeled with DAPI. Full length TFG localized to punctae similar to other ERES proteins. Truncated TFG lacking the Sec23 binding region formed a ring (arrow) around the inclusion membrane. Flag tag was ubiquitously distributed throughout the cell. Images are 60x magnification, single planes from deconvolved z-series.

### PDCD6 localization with calcium perturbation

We next made a plasmid to express a PDCD6-GFP fusion to allow live imaging of this protein. We transfected HeLa cells with this construct, then infected with *C. trachomatis* and assessed PDCD6 localization in living cells at 24 hpi. PDCD6 localization was different from other ERES proteins (Sec16, Sec31, and Sec12), a significant portion localized throughout the cytoplasm and nucleus, as well as punctae corresponding to ERES (Figure 4–3A). In live infected cells, there was a faint accumulation of PDCD6 along the inclusion membrane (Figure 4–3B). Since PDCD6 is recruited to ERES when bound to calcium, we tested the localization of PDCD6 when intracellular calcium was increased using thapsigargin or chelated using BAPTA/AM. Confirming what has been shown previously (uninfected cells), increasing intracellular calcium decreased the amount of cytoplasmic/nuclear PDCD6 and increased the amount of PDCD6 forming punctae characteristic of ERES (Figure 4–3B). Increasing intracellular calcium levels with thapsigargin greatly increased the association of PDCD6 with

the inclusion membrane (Figure 4–3B). This indicates that PDCD6 dynamically associates with the inclusion membrane in a calcium dependent manner. Supporting this, when intracellular calcium was chelated there was no visible association of PDCD6 with the inclusion membrane or ERES (Figure 4–3B). With reduced calcium PDCD6 was evenly distributed throughout the cytoplasm and nucleus.

Since peflin has been reported to either antagonize or cooperate with PDCD6, we wanted to check how peflin localized under the same conditions. Unfortunately, we observed peflin localization was disrupted when fused to a fluorescent protein, with mScarlet-peflin not localizing to ERES and not resembling the localization of endogenous peflin that has been shown by antibody or epitope tagged peflin (118). We were unable to maintain the localization of PDCD6-EGFP following fixation, so an epitope tagged peflin likely would not work well for testing localization during calcium perturbation. Further testing of peflin constructs may resolve this issue and determine whether peflin is also recruited to the inclusion membrane under elevated calcium levels. It has been shown that TFG is recruited to ERES based on its interactions with PDCD6, so it should be tested if TFG is also increased on the inclusion membrane following thapsigargin treatment.

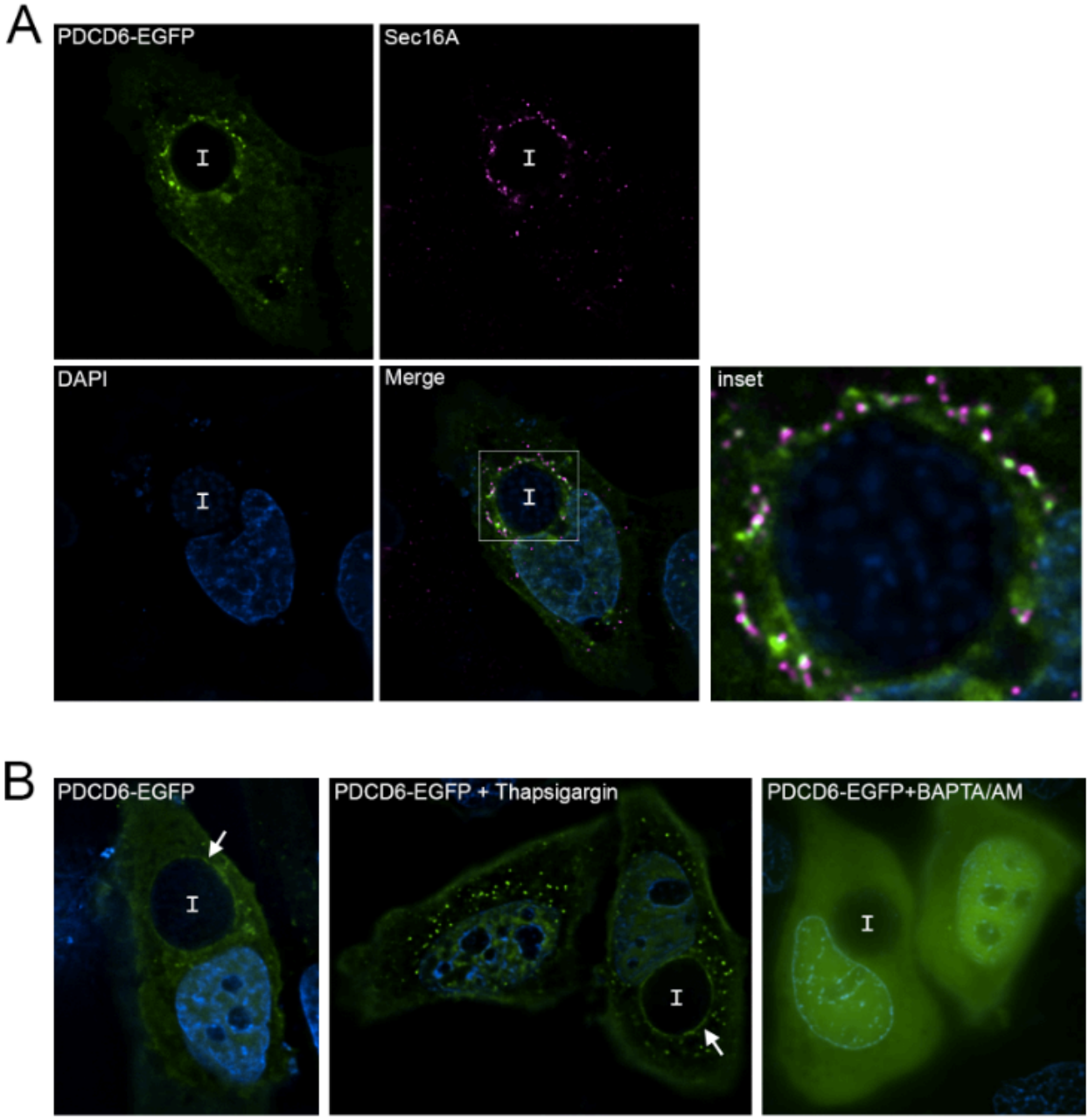


**Figure 4–3. PDCD6 localizes to ERES and the inclusion membrane in a calcium-dependent manner.**

HeLa cells were transfected with a plasmid expressing PDCD6-EGFP, then infected with *C. trachomatis* for 24 hours. Images are 60x magnification, single plane from deconvolved z-series. (A) Cells were fixed and stained with anti-Sec16A antibody (purple) and DAPI (blue). PDCD6 (green) was distributed throughout the cell and also localized to punctae that overlapped with Sec16A. (B) Live cells were incubated for 1 hour in Ringer's solution (first panel), Ringer's solution with 2 μM Thapsigargin (middle panel), or calcium-free Ringer's with calcium chelator BAPTA/AM (last panel). Representative images were taken of live cells in solutions listed. DNA was labeled with Hoechst (blue). Inclusions labeled I, arrows indicate regions of inclusion membrane with PDCD6 associated.

**Depletion of peflin and PDCD6**

As an alternative to testing peflin co-localization with PDCD6 during infection, we used RNA interference to investigate whether PDCD6 and peflin knockdown led to *Chlamydia* growth phenotypes. Peflin knockdown showed similar effects to Sec12 or cTAGE5, reducing IFU by 54.3% compared to a scrambled control (Figure 4–4A). Unexpectedly, PDCD6 had a different effect from all other ERES proteins tested, and knockdown resulted in 60.2% enhanced production of infectious progeny (Figure 4–4A).

To test the effect of peflin knockdown on PDCD6 localization we transfected HeLa cells with siRNA oligos targeting peflin, incubated the cells 72 hours, then infected with *C. trachomatis* and fixed the cells at 24 hpi to process for immunofluorescence. We used a PDCD6 antibody to avoid potential artefacts from fusion protein overexpression. In cells depleted of peflin we observed frequent enrichment of PDCD6 in large spots adjacent to chlamydial inclusions (Figure 4–4B). In the control cells these punctae were rarely observed; however, large aggregates of PDCD6 were observed in some cells (Figure 4–4B). This aggregation did not seem to be specific to infected cells, and was also observed in uninfected cells.

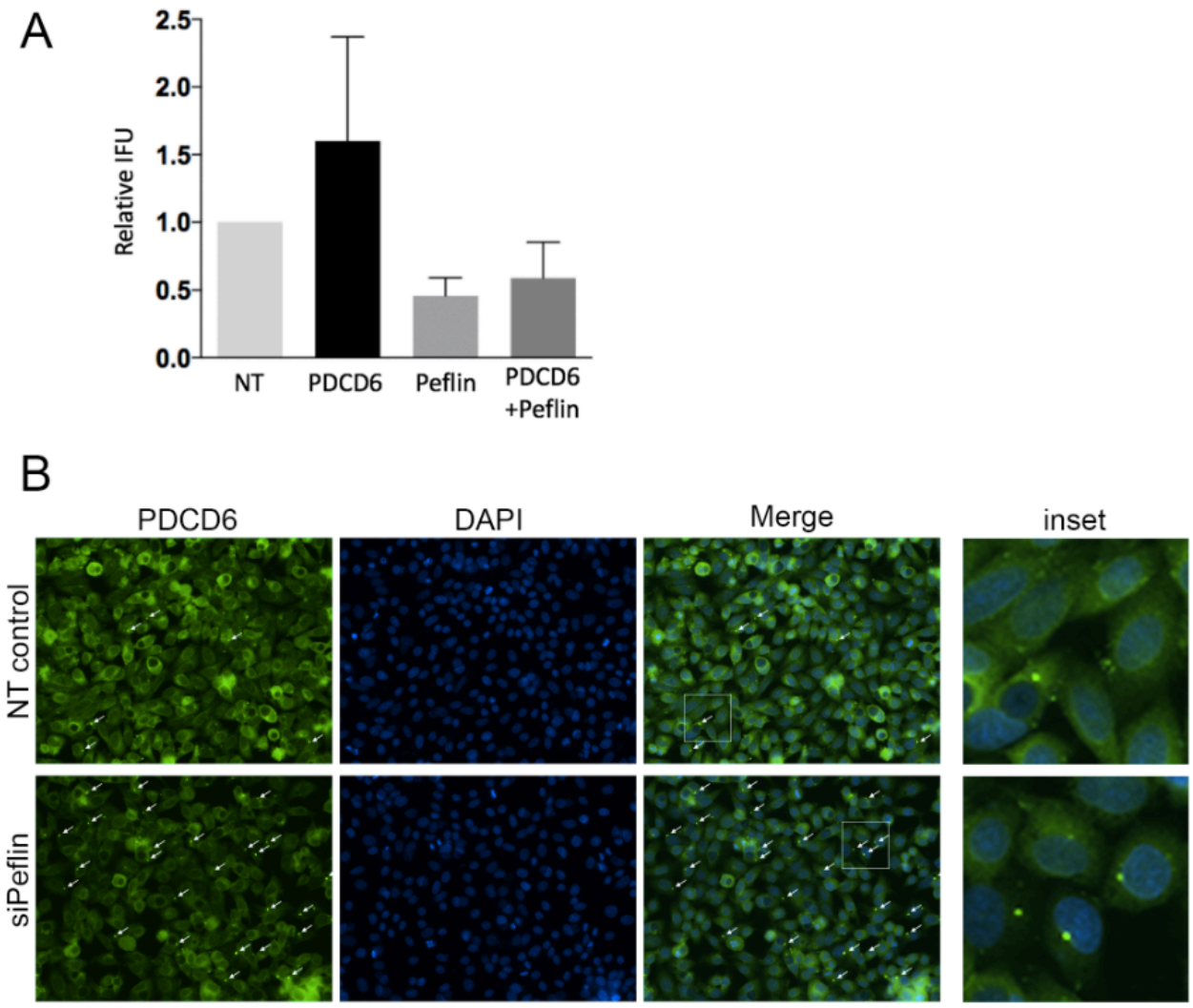


**Figure 4–4. Knockdown of PDCD6 and peflin have opposing effects on *Chlamydia* growth.**

HeLa cells were transfected for with siRNA oligonucleotides targeting PDCD6, peflin, or non-targeting control. After 72 hours, cells were infected with *C. trachomatis* for 48 hours (A) or 24 hours (B). (A) Cells were lysed at 48 hours and serial dilutions of lysate were plated on fresh monolayer of HeLa cells to measure IFU. Knockdown of PDCD6 resulted in enhanced IFU production compared to control, while peflin knockdown decreased IFU production. N = 3. (B) Cells were fixed at 24 hpi and stained with anti-PDCD6 (green) and DAPI (blue). Arrows indicate large punctae of PDCD6. Top row is representative image of cells transfected with non-targeting control, bottom row are transfected with oligonucleotide targeting peflin. Images are 20x magnification.

## Discussion

Peflin, PDCD6, and TFG are functionally enigmatic in the context of ERES regulation, but at least in the case of PDCD6 and TFG they seem to overlap with most of the inclusion

membrane compared to other markers of ERES such as Sec16 and Sec31 which overlap in small punctae along the inclusion membrane. It is difficult to translate what the association of a truncated TFG to the inclusion means in relation to endogenous TFG. There is a predicted splice variant of TFG that is only 184 amino acids, compared to the 400 amino acid full length TFG. The antibody used in our studies was a monoclonal raised against the C terminus so it would not show the localization of the shortened splice variant. No studies have investigated the relative abundance or localization of this splice variant, but if it is expressed it may be recruited to the inclusion membrane. Further studies with could show if this variant is expressed in *Chlamydia*-infected cells and if its localization is similar to the TFG1-380 protein.

PDCD6 is recruited to both ERES and the inclusion membrane in a calcium dependent manner, and it would be informative to determine what binding partners allow PDCD6 recruitment to the inclusion, or if PDCD6 interacts directly with an inclusion membrane localized *Chlamydia* effector protein. In the literature, previous studies have not examined calcium-dependent interactions with the inclusion, but calcium-dependent associations may extend beyond PDCD6 and could be an important context to include in future pulldown experiments. For affinity purification of 58 predicted Incs there were several Incs that did not reveal any binding partners under the conditions tested, but perhaps doing a pulldown in elevated calcium could reveal novel protein-protein interactions (40).

A redistribution of PDCD6 to single foci within cells following peflin knockdown has not been reported. This localization pattern resembled an aggresome, a structure that forms when there is an excessive amount of misfolded or unstable protein that overwhelms the proteasome (131). There is generally only a single aggresome per cell, and it localizes in the perinuclear region near the MTOC, which is consistent with the PDCD6 punctae observed during peflin knockdown (131). Due to previous studies showing that PDCD6 and peflin are stabilized through dimerization we hypothesize that in the absence of peflin, PDCD6 is unable to form stable PDCD6-peflin dimers, leading to a pool of unstable PDCD6 getting targeted for degradation. We

did not observe a reduction in PDCD6 by western blot at 72 hours post transfection, but other studies did report that there were reduced levels of PDCD6 following peflin knockdown (118,122). It is possible in our system we checked PDCD6 levels too early after transfection, which would fit well with aggresome kinetics. When the proteasome gets overwhelmed and an aggresome forms, this aggregate is resistant to degradation, but it eventually gets degraded through aggrephagy, a form of selective autophagy (131,132). Further studies should examine PDCD6 foci for aggresome markers such as vimentin, ubiquitin, and association with the MTOC (132).

Peflin function remains unclear and future studies should confirm if it is inhibiting or enhancing ERES function and COPII vesicle production. In *Chlamydia*-infected cells, peflin knockdown seemed to mimic the knockdown of other ERES components that would cause reduced COPII vesicle trafficking following depletion, but it should be tested whether peflin, Sec12, or cTAGE5 knockdown all cause reduction in COPII cargo export in infected cells. Previous studies have shown that peflin function can be regulated by ubiquitin, with ubiquitinated peflin binding PDCD6 in a calcium dependent manner while unmodified peflin does not seem to be affected by calcium (118). Determining peflin localization during *Chlamydia* infection may help determine if PDCD6 and peflin are both recruited to the inclusion membrane in a calcium dependent manner, and determine if peflin is antagonizing PDCD6. Testing peflin ubiquitination during *Chlamydia* infection may provide another layer of regulation of ERES during infection. If peflin is ubiquitinated it may suggest a need for secretion of large cargo, as has been shown in the context of collagen secretion (118). *Chlamydia* has been shown to de-ubiquitinate proteins on the inclusion membrane, so it could also prevent large cargo secretion by de-ubiquitination of peflin or Sec31 (133).

Finally, although TFG and peflin have been shown to bind PDCD6 in other contexts, it should be confirmed that they also bind each other in *Chlamydia*-infected cells (118,119). It is also unclear if TFG, peflin, and PDCD6 are all present in the same complex, or if TFG and peflin

independently interact with PDCD6. It would likely be very informative to compare pulldowns of each protein in uninfected versus infected cells, both under normal and elevated calcium levels. This could provide protein targets to investigate as mediators of inclusion-ERES interactions.

## Materials and Methods

### Antibodies and reagents

All reagents were purchased from Thermo Fisher Scientific (Rockford, IL) unless otherwise noted. Primary antibodies used in this study and their catalog numbers: Sec16A (Bethyl Laboratories, Montgomery, TX; A300-648A-M), IncA (gift from Daniel Rockey), Flag (Millipore Sigma; F1804), PDCD6 (Proteintech, Rosemont, IL; 12303-1-AP). Secondary antibodies used: Goat anti-Mouse DyLight 594, Goat anti-Rabbit Alexa 488.

### Plasmid constructs

Plasmids were isolated using the Qiaprep Spin Miniprep kit or the HiSpeed Plasmid Midi kit (Qiagen, Germantown, MD).

TFG constructs were made in the pEBFP2-N1 backbone, with an N-terminal flag fused to TFG, TFG1-380, or TFG R106C. At C-terminus of TFG variants was P2A sequence, followed by EBFP2. pEBFP2-N1 was a gift from Michael Davidson (Addgene plasmid # 54595).

PDCD6-EGFP was made in pEGFP-C1 backbone. PDCD6 was placed at C-terminus of EGFP.

### Immunofluorescence and live cell microscopy

For immunofluorescence microscopy, cells were rinsed in HBSS, then fixed for 15 minutes in 3.7% paraformaldehyde in HBSS. Cells were rinsed 2 times in HBSS, then permeabilized with 0.5% triton X-100 for 15 minutes, and blocked in 1% bovine serum albumin

(BSA) in PBS for 20 minutes. Samples were incubated with primary antibodies for 1 hour at room temperature in blocking buffer, then rinsed 3 times in blocking buffer, then incubated 45 minutes at room temperature with secondary antibodies in blocking buffer. DAPI was used to stain DNA, and added during the secondary antibody step. Cells were imaged on a Nikon Ti-E inverted microscope and images were captured on a Hamamatsu camera controller C10600. Images were processed using Volocity software (PerkinElmer, Waltham, MA).

For live imaging of PDCD6-EGFP in steady state or increased intracellular calcium, cells were incubated in Ringer's solution (155 mM NaCl, 4.5 mM KCl, 1 mM MgCl2, 2 mM CaCl2, 10 mM D-glucose, 5 mM Hepes, pH 7.4) for 1 hour at 37°C. For increased intracellular calcium, 2 μM Thapsigargin (Millipore Sigma) was added to Ringer's solution. For depleted intracellular calcium, cells were incubated in calcium-free Ringer's solution (155 mM NaCl, 4.5 mM KCl, 3 mM MgCl2, 10 mM D-glucose, 1 mM EGTA, 5 mM Hepes, pH 7.4) containing 50 μM BAPTA/AM. After 1 hour, Hoechst was added to solutions to label DNA, then cells were imaged on a Nikon Ti-E inverted microscope and images were captured on a Hamamatsu camera controller C10600. Images were processed using Volocity software.

**siRNA and plasmid transfections**

For siRNA transfections, HeLa cells were plated in 24 well plates to 60-80% confluence. For 24 well plates, 50 μL Opti-MEM (Gibco) medium containing 5 pmol siRNA oligonucleotides and 1.5 μL Lipofectamine RNAiMAX was added to each well. Following transfection, cells were incubated for 72 hours at 37°C prior to infection or protein analysis by western blot. Oligonucleotides were Dharmacon siGenome smartpools of 4 different oligonucleotide sequences.

For mammalian plasmid transfections, HeLa cells were plated in 4 well chamber slides (Nunc Lab-Tek), and infected with *C. trachomatis* L2. Immediately after infection, each well

was transfected with 50 µL Opti-MEM containing 500 ng plasmid and 1.5 µL Lipofectamine 2000.

**Quantitative PCR analysis**

For qRT-PCR confirming siRNA knockdown, HeLa cells were plated in 24 well plates, and transfected with siRNA oligos as described above. Cells were incubated for 72 hours, then cell pellets were frozen until RNA extraction.

RNA was extracted using the Qiagen RNeasy mini kit (Qiagen). cDNA was made using the iScript cDNA synthesis kit (Bio-Rad). qRT-PCR reactions were set up with SsoAdvanced Universal SYBR Green Supermix (Bio-Rad) and run on the StepOnePlus Real-Time PCR system (Applied Biosystems, Foster City, CA). GAPDH was used as the housekeeping gene, and the ΔΔCT method was used to calculate relative expression.

**Supplemental Information**

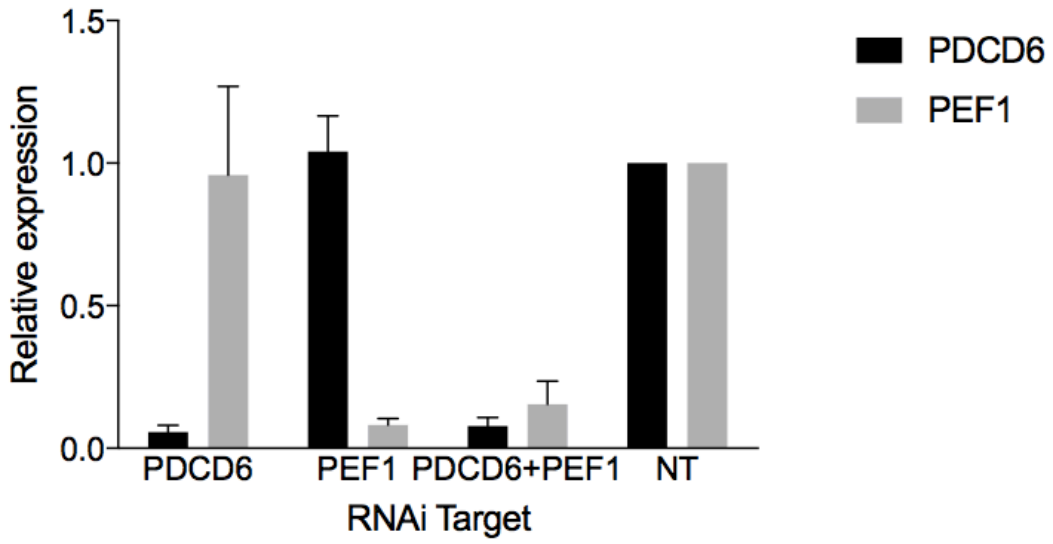


**Figure S4–1. PDCD6 and peflin were efficiently depleted.**

HeLa cells were transfected with oligonucleotides targeting PDCD6, peflin (PEF1) or non-targeting control. After 72 hours, cells were lysed and RNA was extracted. Relative expression was measured using qRT-PCR.

# Chapter 5 – Conclusions and Future Directions

## Summary of Findings

This dissertation presents a novel data set of proposed *Chlamydia trachomatis* inclusion membrane associated proteins. We explored one identified host pathway from this data set and highlighted the important functional interaction between the *Chlamydia* inclusion membrane and ER exit sites. We combined our proteomics data set with previous mass spectrometry experiments, creating a comprehensive list of host proteins that may have important roles during infection. This will provide a valuable resource for developing new hypotheses about how *Chlamydia* is able to survive within the host cell.

Chapter 2 presents the adaptation of the APEX system of proximity-dependent biotinylation and provides many novel host proteins associated with the *Chlamydia* inclusion at three time points during infection. We detected 89 proteins at 8 hpi, an early time point that has never been studied using mass spectrometry techniques. Determining which of these proteins are required for *Chlamydia* growth could provide host targets to manipulate to decrease *Chlamydia* growth at a stage before significant replication has occurred. The 16 hpi time point is also earlier than the other mass spectrometry study using infected cells, so the 179 proteins identified at that time also provide host proteins to study in context of early infection. Overall the 452 proteins identified by IncB-APEX contribute not only novel host proteins that may be important for *Chlamydia* growth but also corroborates some of the proteins found by AP-MS or inclusion-MS (40,42). While each study on its own likely contains false positives, proteins identified by more than one of these different techniques represent higher confidence inclusion-associated proteins to investigate further. Especially for the proteins identified by AP-MS which have a proposed Inc binding partner, as *Chlamydia* genetic techniques advance there will be more opportunities for connecting host pathways to specific Incs.

ERES proteins were labeled by IncB-APEX at all three time points during infection. Chapter 3 investigates the functional consequence of impairing ERES function during infection, and examines the localization of well characterized ERES markers. We found that depletion using RNA interference of two ERES regulatory proteins impaired growth, but depletion of other proteins thought to be required for COPII secretion had no effect on *Chlamydia* growth. This suggests that *Chlamydia* may not necessarily require general COPII secretion, but may require a certain subset of vesicles or may require certain proteins to be present at ERES to properly interact with these sites. Chemical inhibition of COPII budding or COPII cargo sorting during infection led to a dramatic reduction in *Chlamydia* infectious progeny. The effect seen from dysregulating COPII cargo sorting supports the RNA interference, suggesting that general secretion of COPII vesicles is not sufficient to allow normal *Chlamydia* growth. Importantly, none of the effects seen during RNA interference or chemical inhibition seemed to be related to inhibition of golgi vesicle formation or membrane contact sites with the ER, two pathways that have been shown to be important for *Chlamydia* growth (9,12).

IncB-APEX identified three proteins that have been connected to ERES but have no clearly defined functions with COPII trafficking. Chapter 4 investigates the role of these proteins during infection and finds that in certain contexts two of these proteins are more highly recruited to the inclusion membrane than the ERES markers studied in Chapter 3. PDCD6 was recruited to the inclusion in a calcium-dependent manner, and TFG was recruited in the absence of the Sec23 binding domain. Peflin has proven difficult to express from a plasmid and has limited antibodies available, so it the localization of peflin during infection is still unclear. Interestingly, two of these proteins, PDCD6 and peflin, have opposing effects on *Chlamydia* growth. Depletion of peflin using RNA interference had a similar effect to depletion of other ERES proteins Sec12 and cTAGE5, with a reduction in infectious progeny. PDCD6 knockdown, however, led to an increase in infectious progeny.

Overall, APEX has been a valuable tool for studying *Chlamydia*-host interactions and has identified ERES as a novel pathway required for *Chlamydia* growth. This dissertation contributes a more thorough understanding of the proteins associating with the inclusion membrane, at earlier stages during infection than have been previously studied using mass spectrometry. Further investigation of proteins identified by IncB-APEX could reveal many other ways that the inclusion interacts with host proteins.

**Future directions of inclusion membrane proteomics**

Many proteins identified by IncB-APEX should be studied further to determine their functions during *Chlamydia* infection. Several interesting groups of proteins are highlighted in the Discussion section of Chapter 2. The proteome of the inclusion membrane remains incomplete. IncB-APEX detected many proteins that have been previously shown to be recruited to the inclusion membrane, but it also missed many proteins. APEX is a highly flexible and with further experimentation it would likely yield many more inclusion-associated proteins. In addition to APEX, there are several versions of other enzymes that perform proximity-dependent biotinylation that may be useful for investigating *Chlamydia* pathogenesis.

One obvious next step is to express APEX tagged to different Incs. Our preliminary data indicated that CT223-APEX and IncB-APEX identified very similar proteins, but there are likely Incs that would yield different results. Expressing a microdomain-localized Inc at a level that maintained a microdomain-specific localization could identify proteins associated with microdomains. As *Chlamydia* genetic techniques improve, APEX could be integrated into the genome, allowing fusion to proteins that will be expressed at endogenous levels.

In the past few years multiple Incs have been knocked out and these knockouts had different effects on *Chlamydia* growth. For a few Incs, knockout led to premature lysis of the inclusion or host cell death (134,135). Premature cell death or vacuolar lysis seems to be mediated by innate immune activation (134,135). For the Inc CpoS, it only dampened the

immune response to the inclusion it was located, rather than in the whole cell (135). If a cell had one inclusion without CpoS and one inclusion with CpoS it would still undergo cell death (135). This implies there are specific protein-protein interactions at the inclusion membrane that allow inhibition of immune responses to the inclusion. APEX could be used to determine what proteins are lacking or recruited in the knockouts that leads to premature inclusion lysis or cell death. The knockout strains could be transformed to express APEX tagged to an unrelated Inc like IncA, and a complemented version of the knockout could also transformed to express the exact same APEX construct. Biotinylation of these two strains may reveal the differences in proteins that leads to the knockout phenotype. Inclusion lysis and host cell death generally occurred around 18 hpi, so testing proteins prior this time point would prevent severe differences in host cell viability. In addition to these Inc knockouts that have severe phenotypes, APEX may be able to identify proteomic differences in Inc knockouts that have no apparent phenotype.

Most in vitro *C. trachomatis* studies are done using serovar L2, the causative agent of lymphogranuloma venereum, but the most common human infections are caused by the sexually transmitted serovars D-K (136). Additionally, the A-C serovars cause ocular infections (136). There are also different species of *Chlamydia*, with *Chlamydia pneumoniae* and *Chlamydia psittaci* also infecting humans and causing respiratory infections (137). *C. psittaci* mainly infects birds, but can infect humans (138). There are other species of *Chlamydia* that infect animals, such as *C. muridarum* (mice), *C. suis* (pigs), *C. abortus* (sheep), and *C. caviae* (guinea pigs) (138). It could be very informative to compare the proteins associating with the inclusions of some of these different serovars and species of *Chlamydia*. This information could determine what responses are general to these intracellular pathogens, and what protein-protein interactions arose from host adaptation, as *C. trachomatis* is thought to be highly adapted to the human host. It is not possible to genetically transform many of these species or serovars, both for biological reasons and the regulatory limitations on introducing antibiotic resistance into

human pathogens. For this reason, it would likely make more sense to fuse APEX to a host protein that is known to be recruited to the inclusion membrane. Then these host cells could be infected with different *Chlamydia* serovars or species to determine what proteins are shared or unique. This could inform which proteins within the host have become associated with *C. trachomatis* during its adaptation to the human host, as well as human proteins that may have evolved in response to repeated *Chlamydia* infection.

All of the studies in this dissertation were performed in HeLa cells, so doing similar experiments in primary cells, or even different cell lines would allow differentiation between more universally important proteins, rather than cell-type specific interactions. In an in vivo infection epithelial cells of the upper genital tract mucosa would be exposed to different cytokines, such as IFN-γ. *Chlamydia* growth is reduced in vitro with IFN-γ treatment and it has been shown that different host proteins associate with *Chlamydia* inclusions following IFN-γ treatment (139,140). The enzyme TurboID is an optimized version of the BirA enzyme used for BioID; TurboID and BioID also perform proximity-dependent biotinylation but continuously biotinylate proteins in close proximity, rather than during a quick reaction like APEX does (141,142). The benefit of these systems are that they can be used in vivo since hydrogen peroxide is toxic. Testing proteins associated with the inclusion in a mouse model of infection may be most representative of a human infection.

APEX and proximity-dependent biotinylation are powerful tools for studying host-pathogen interactions. These tools will allow mapping of the chlamydial inclusion proteome under different conditions without significant genetic manipulation, which would be very time consuming in *Chlamydia*. Besides the experiments listed here, there are many more ways to use APEX to resolve questions about how *Chlamydia* is able to grow and survive within cells.

**Future directions of ERES-inclusion interactions**

This dissertation has identified that ERES are important for chlamydial growth, but the main questions remain of why they are important, and how these interactions are mediated. Determining which *Chlamydia* and host proteins are directly binding would be an important next step towards elucidating how and why ERES-inclusion interactions occur, and whether the inclusion is interacting with ERES on the ER or COPII vesicles. Since many proteins are trafficked through ERES and the functions of ERES proteins are not well understood it is difficult to determine why this interaction may affect *Chlamydia* growth. With an improved understanding of the basic biology of ERES and COPII trafficking, it may become easier to figure out what is happening during *Chlamydia* infection.

To figure out which proteins are directly mediating inclusion-ERES interactions, simple pulldowns may yield valuable results. Since we now know that PDCD6 and TFG1-380 are strongly recruited to the inclusion membrane, they are top candidates for pulling down during infection to identify binding partners. These proteins accumulate along the entire inclusion membrane, at least when overexpressed, and it therefore seems likely that they directly or indirectly bind a *Chlamydia* protein on the inclusion membrane. PDCD6 is thought to translocate to membranes upon calcium binding, so it is also possible that it is directly binding lipids in the inclusion membrane (108). Doing pulldowns with elevated or depleted calcium may reveal how PDCD6 or TFG are targeted to the inclusion membrane, and if these binding partners are necessary for the interactions between the inclusion and ERES. It may also be informative to use the IncB-APEX *Chlamydia* and biotinylate the inclusion membrane in the presence of the ERES inhibitors or after knockdown of specific ERES proteins.

It is curious that the primary infection during chemical inhibition of ERES or knockdown of ERES proteins largely appears normal. Unless inhibitors are added very early during infection, the inclusion grows at a normal rate despite very few infectious progeny forming. Genome copy number indicated that after treatment with the inhibitors there are many

organisms present that are not infectious. It is unclear if these are RB that failed to convert to EB, or these are EB that are not infectious. The standard way to identify RB or EB is through electron microscopy. Examining the presence of the different developmental forms after treatment with ERES inhibitors would determine if there were reduced EB present. If the RB to EB transition is not blocked, it would be interesting to try and detect differences between normal EB and those formed in the presence of the inhibitors. Proteomics or lipidomics of purified EB following treatment with ERES may reveal structural differences that are abrogating infectivity. In addition to proteomic or lipid differences, glycosylation of proteins in the *Chlamydia* outer membrane is also thought to be important for infectivity (143–145). Abrogation of essential modifications of EB that confer infectivity could explain the discordance between inclusion size and IFU following treatment with ERES inhibitors.

There are several connections between TFG and innate immune signaling, such as IFNβ and NF$\kappa$B activation. Innate signaling during ERES inhibition with FLI-06 or 4PBA has not been studied, but if it results in enhanced activation of an immune response to *Chlamydia* this could explain the reduction in *Chlamydia* growth. Conversely, it has been shown that certain levels of immune signaling are beneficial to *Chlamydia* growth so ERES inhibition could affect growth by decreasing signaling. For example, caspase-1 activation through the NLRP3 inflammasome is required for optimal *Chlamydia* growth in vitro (146). Recently, a genome wide RNAi screen of host genes found that knockdown of several pro-inflammatory signaling proteins resulted in highly reduced *Chlamydia* growth (147). Knockdown of proteins such as IRAK1, TLR2, PYCARD, and I$\kappa$B should reduce inflammatory signaling, yet unexpectedly this had a negative effect on *Chlamydia* growth (147). TFG has had mixed results in how it effects innate immune signaling, but further study of ERES knockdowns and inhibitors could determine if ERES have a role in the immune response to *Chlamydia*, and if this contributes to the reduction in chlamydial growth.

In addition to the several hypotheses outlined here, there are many other proteins that get trafficked through COPII vesicles that may be responsible for the growth defect seen during ERES inhibition. Further inquiry into the protein-protein interactions between *Chlamydia* and ERES, or differences between bacteria grown in the presence of ERES inhibitors may indicate alternative mechanisms of *Chlamydia* growth disruption.

**Final thoughts**

APEX is a powerful tool for studying the inclusion membrane proteome at different times during infection. The work in this dissertation has identified many novel host proteins associated with the inclusion membrane, and we have investigated a small subset of these proteins that are involved in ERES regulation. This revealed an important requirement of ERES function for *Chlamydia* growth that is distinct from known interactions between *Chlamydia* and ER membrane contact sites or the golgi. Further investigation into ERES in the context of *Chlamydia* infection is necessary to determine how these sites are affecting *Chlamydia* growth. Investigation of other proteins identified by APEX will likely yield other important host pathways that could provide valuable targets for disrupting *Chlamydia* growth.

## References


1. Gerbase a C, Rowley JT, Heymann DH, Berkley SF, Piot P. Global prevalence and incidence estimates of selected curable STDs. Sexually transmitted infections. 1998.
2. Geisler WM. Duration of Untreated, Uncomplicated *Chlamydia trachomatis* Genital Infection and Factors Associated with Chlamydia Resolution: A Review of Human Studies. J Infect Dis. 2010;
3. CDCP. 2016 Sexually Transmitted Diseases Surveillance. Centers for Disease Control and Prevention. 2017.
4. Workowski KA, Bolan GA. Sexually transmitted diseases treatment guidelines, 2015. CDC - MMWR Recommendations and Reports. 2015.
5. AbdelRahman YM, Belland RJ. The chlamydial developmental cycle. FEMS Microbiology Reviews. 2005.
6. Fields KA, Hackstadt T. The Chlamydial Inclusion: Escape from the Endocytic Pathway. Annu Rev Cell Dev Biol. 2002;
7. Grieshaber SS. Chlamydia trachomatis uses host cell dynein to traffic to the microtubule-organizing center in a p50 dynamitin-independent process. J Cell Sci. 2003;
8. Stephens RS, Kalman S, Lammel C, Fan J, Marathe R, Aravind L, et al. Genome sequence of an obligate intracellular pathogen of humans: Chlamydia trachomatis. Science (80- ). 1998;
9. Derré I, Swiss R, Agaisse H. The lipid transfer protein CERT interacts with the Chlamydia inclusion protein IncD and participates to ER-Chlamydia inclusion membrane contact sites. PLoS Pathog. 2011;
10. Elwell CA, Jiang S, Kim JH, Lee A, Wittmann T, Hanada K, et al. Chlamydia trachomatis co-opts GBF1 and CERT to acquire host sphingomyelin for distinct roles during intracellular development. PLoS Pathog. 2011;
11. Heuer D, Lipinski AR, Machuy N, Karlas A, Wehrens A, Siedler F, et al. Chlamydia causes

fragmentation of the Golgi compartment to ensure reproduction. Nature. 2009;

12. Hackstadt T, Scidmore MA, Rockey DD, McNew JA, Hurtado D, Sollner TH, et al. Lipid metabolism in Chlamydia trachomatis-infected cells: directed trafficking of Golgi-derived sphingolipids to the chlamydial inclusion. Proc Natl Acad Sci U S A. 1995;
13. Hackstadt T, Rockey DD, Heinzen RA, Scidmore MA. Chlamydia trachomatis interrupts an exocytic pathway to acquire endogenously synthesized sphingomyelin in transit from the Golgi apparatus to the plasma membrane. EMBO J. 1996;
14. Scidmore MA, Fischer ER, Hackstadt T. Sphingolipids and glycoproteins are differentially trafficked to the Chlamydia trachomatis inclusion. J Cell Biol. 1996;
15. Carabeo R a, Mead DJ, Hackstadt T. Golgi-dependent transport of cholesterol to the Chlamydia trachomatis inclusion. Pnas. 2003;
16. Rejman Lipinski A, Heymann J, Meissner C, Karlas A, Brinkmann V, Meyer TF, et al. Rab6 and Rab11 regulate Chlamydia trachomatis development and golgin-84-dependent Golgi fragmentation. PLoS Pathog. 2009;
17. Cocchiaro JL, Kumar Y, Fischer ER, Hackstadt T, Valdivia RH. Cytoplasmic lipid droplets are translocated into the lumen of the Chlamydia trachomatis parasitophorous vacuole. Proc Natl Acad Sci. 2008;
18. Kumar Y, Cocchiaro J, Valdivia RH. The Obligate Intracellular Pathogen Chlamydia trachomatis Targets Host Lipid Droplets. Curr Biol. 2006;
19. Beatty WL. Trafficking from CD63-positive late endocytic multivesicular bodies is essential for intracellular development of Chlamydia trachomatis. J Cell Sci. 2006;
20. Clague MJ, Urbé S. Multivesicular bodies. Current Biology. 2008.
21. Cox J V., Naher N, Abdelrahman YM, Belland RJ. Host HDL biogenesis machinery is recruited to the inclusion of chlamydia trachomatis-infected cells and regulates chlamydial growth. Cell Microbiol. 2012;
22. Wang Y, Kahane S, Cutcliffe LT, Skilton RJ, Lambden PR, Clarke IN. Development of a

transformation system for chlamydia trachomatis: Restoration of glycogen biosynthesis by acquisition of a plasmid shuttle vector. PLoS Pathog. 2011;

23. Wickstrum J, Sammons LR, Restivo KN, Hefty PS. Conditional Gene Expression in Chlamydia trachomatis Using the Tet System. PLoS One. 2013;
24. Bastidas RJ, Valdivia RH. Emancipating Chlamydia: Advances in the Genetic Manipulation of a Recalcitrant Intracellular Pathogen. Microbiol Mol Biol Rev. 2016;
25. Chen AL, Johnson KA, Lee JK, Sütterlin C, Tan M. CPAF: A Chlamydial Protease in Search of an Authentic Substrate. PLoS Pathog. 2012;
26. Snavely EA, Kokes M, Dunn JD, Saka HA, Nguyen BD, Bastidas RJ, et al. Reassessing the role of the secreted protease CPAF in Chlamydia trachomatis infection through genetic approaches. Pathog Dis. 2014;
27. Kokes M, Dunn JD, Granek JA, Nguyen BD, Barker JR, Valdivia RH, et al. Integrating chemical mutagenesis and whole-genome sequencing as a platform for forward and reverse genetic analysis of Chlamydia. Cell Host Microbe. 2015;
28. Mueller KE, Wolf K, Fields KA. Gene deletion by fluorescence-reported allelic exchange mutagenesis in Chlamydia trachomatis. MBio. 2016;
29. Mueller KE, Wolf K, Fields KA. Chlamydia trachomatis transformation and allelic exchange mutagenesis. Curr Protoc Microbiol. 2017;
30. Keb G, Hayman R, Fields KA. Floxed-Cassette Allelic Exchange Mutagenesis Enables Markerless Gene Deletion in *Chlamydia trachomatis* and Can Reverse Cassette-Induced Polar Effects. J Bacteriol. 2018;
31. Ouellette SP. Feasibility of a Conditional Knockout System for Chlamydia Based on CRISPR Interference. Front Cell Infect Microbiol. 2018;
32. Dehoux P, Flores R, Dauga C, Zhong G, Subtil A. Multi-genome identification and characterization of chlamydiae-specific type III secretion substrates: The Inc proteins. BMC Genomics. 2011;

33. Scidmore MA, Hackstadt T. Mammalian 14-3-3β associates with the Chlamydia trachomatis inclusion membrane via its interaction with IncG. Mol Microbiol. 2001;
34. Rzomp KA, Moorhead AR, Scidmore MA. The GTPase Rab4 interacts with Chlamydia trachomatis inclusion membrane protein CT229. Infect Immun. 2006;
35. Delevoye C, Nilges M, Dehoux P, Paumet F, Perrinet S, Dautry-Varsat A, et al. SNARE protein mimicry by an intracellular bacterium. PLoS Pathog. 2008;
36. Dumoux M, Menny A, Delacour D, Hayward RD. A Chlamydia effector recruits CEP170 to reprogram host microtubule organization. J Cell Sci. 2015;
37. Valdivia RH. Chlamydia effector proteins and new insights into chlamydial cellular microbiology. Current Opinion in Microbiology. 2008.
38. Al-Zeer MA, Al-Younes HM, Kerr M, Abu-Lubad M, Gonzalez E, Brinkmann V, et al. Chlamydia trachomatis remodels stable microtubules to coordinate Golgi stack recruitment to the chlamydial inclusion surface. Mol Microbiol. 2014;
39. Kumar Y, Valdivia RH. Actin and Intermediate Filaments Stabilize the Chlamydia trachomatis Vacuole by Forming Dynamic Structural Scaffolds. Cell Host Microbe. 2008;
40. Mirrashidi KM, Elwell CA, Verschueren E, Johnson JR, Frando A, Von Dollen J, et al. Global mapping of the inc-human interactome reveals that retromer restricts chlamydia infection. Cell Host Microbe. 2015;
41. Stanhope R, Flora E, Bayne C, Derré I. IncV, a FFAT motif-containing *Chlamydia* protein, tethers the endoplasmic reticulum to the pathogen-containing vacuole. Proc Natl Acad Sci. 2017;
42. Aeberhard L, Banhart S, Fischer M, Jehmlich N, Rose L, Koch S, et al. The Proteome of the Isolated Chlamydia trachomatis Containing Vacuole Reveals a Complex Trafficking Platform Enriched for Retromer Components. PLoS Pathog. 2015;
43. Burton MJ, Mabey DCW. The global burden of trachoma: A review. PLoS Neglected Tropical Diseases. 2009.

44. Torrone E, Papp J, Weinstock H, CDC. Prevalence of Chlamydia trachomatis genital infection among persons aged 14-39 years - United States, 2007-2012. MMWR Morb Mortal Wkly Rep. 2014;
45. Bastidas RJ, Elwell CA, Engel JN, Valdivia RH. Chlamydial intracellular survival strategies. Cold Spring Harb Perspect Med. 2013;
46. Elwell C, Mirrashidi K, Engel J. Chlamydia cell biology and pathogenesis. Nature Reviews Microbiology. 2016.
47. Bannantine JP, Griffiths RS, Viratyosin W, Brown WJ, Rockey DD. A secondary structure motif predictive of protein localization to the chlamydial inclusion membrane. Cell Microbiol. 2000;
48. Rockey DD, Scidmore MA, Bannantine JP, Brown WJ. Proteins in the chlamydial inclusion membrane. Microbes and Infection. 2002.
49. Lutter EI, Martens C, Hackstadt T. Evolution and conservation of predicted inclusion membrane proteins in chlamydiae. Comp Funct Genomics. 2012;
50. Mueller KE, Plano G V., Fields KA. New frontiers in type III secretion biology: The Chlamydia perspective. Infection and Immunity. 2014.
51. Moore ER, Ouellette SP. Reconceptualizing the chlamydial inclusion as a pathogen-specified parasitic organelle: an expanded role for Inc proteins. Front Cell Infect Microbiol. 2014;
52. Weber MM, Bauler LD, Lam J, Hackstadt T. Expression and localization of predicted inclusion membrane proteins in Chlamydia trachomatis. Infect Immun. 2015;
53. Rucks EA, Olson MG, Jorgenson LM, Srinivasan RR, Ouellette SP. Development of a Proximity Labeling System to Map the Chlamydia trachomatis Inclusion Membrane. Front Cell Infect Microbiol. 2017;
54. Martell JD, Deerinck TJ, Sancak Y, Poulos TL, Mootha VK, Sosinsky GE, et al. Engineered ascorbate peroxidase as a genetically encoded reporter for electron microscopy. Nat

Biotechnol. 2012;

55. Lam SS, Martell JD, Kamer KJ, Deerinck TJ, Ellisman MH, Mootha VK, et al. Directed evolution of APEX2 for electron microscopy and proximity labeling. Nat Methods. 2014;
56. Lee SY, Kang MG, Park JS, Lee G, Ting AY, Rhee HW. APEX Fingerprinting Reveals the Subcellular Localization of Proteins of Interest. Cell Rep. 2016;
57. Hung V, Zou P, Rhee HW, Udeshi ND, Cracan V, Svinkina T, et al. Proteomic Mapping of the Human Mitochondrial Intermembrane Space in Live Cells via Ratiometric APEX Tagging. Mol Cell. 2014;
58. Hung V, Lam SS, Udeshi ND, Svinkina T, Guzman G, Mootha VK, et al. Proteomic mapping of cytosol-facing outer mitochondrial and ER membranes in living human cells by proximity biotinylation. Elife. 2017;
59. Paek J, Kalocsay M, Staus DP, Wingler L, Pascolutti R, Paulo JA, et al. Multidimensional Tracking of GPCR Signaling via Peroxidase-Catalyzed Proximity Labeling. Cell. 2017;
60. Mital J, Miller NJ, Fischer ER, Hackstadt T. Specific chlamydial inclusion membrane proteins associate with active Src family kinases in microdomains that interact with the host microtubule network. Cell Microbiol. 2010;
61. Shaw EI, Dooley CA, Fischer ER, Scidmore MA, Fields KA, Hackstadt T. Three temporal classes of gene expression during the Chlamydia trachomatis developmental cycle. Mol Microbiol. 2000;
62. Nicholson TL, Olinger L, Chong K, Schoolnik G, Stephens RS. Global stage-specific gene regulation during the developmental cycle of Chlamydia trachomatis. J Bacteriol. 2003;
63. Stenner-Liewen F, Liewen H, Zapata JM, Pawlowski K, Godzik A, Reed JC. CADD, a Chlamydia protein that interacts with death receptors. J Biol Chem. 2002;
64. Breuer K, Foroushani AK, Laird MR, Chen C, Sribnaia A, Lo R, et al. InnateDB: Systems biology of innate immunity and beyond - Recent updates and continuing curation. Nucleic Acids Res. 2013;

65. Kanehisa M, Furumichi M, Tanabe M, Sato Y, Morishima K. KEGG: New perspectives on genomes, pathways, diseases and drugs. Nucleic Acids Res. 2017;
66. Thul PJ, Akesson L, Wiking M, Mahdessian D, Geladaki A, Ait Blal H, et al. A subcellular map of the human proteome. Science (80- ). 2017;
67. Szklarczyk D, Morris JH, Cook H, Kuhn M, Wyder S, Simonovic M, et al. The STRING database in 2017: Quality-controlled protein-protein association networks, made broadly accessible. Nucleic Acids Res. 2017;
68. Pedersen T. A Tidy API for Graph Manipulation [R package tidygraph version 1.1.0] [Internet]. Comprehensive R Archive Network (CRAN). 2018. Available from: https://cran.r-project.org/package=tidygraph
69. Gurumurthy RK, Mäurer AP, Machuy N, Hess S, Pleissner KP, Schuchhardt J, et al. A loss-of-function screen reveals Ras- and Raf-independent mek-erk signaling during Chlamydia trachomatis Infection. Sci Signal. 2010;
70. Abromaitis S, Stephens RS. Attachment and entry of chlamydia have distinct requirements for host protein disulfide isomerase. PLoS Pathog. 2009;
71. Lutter EI, Barger AC, Nair V, Hackstadt T. Chlamydia trachomatis Inclusion Membrane Protein CT228 Recruits Elements of the Myosin Phosphatase Pathway to Regulate Release Mechanisms. Cell Rep. 2013;
72. Agaisse H, Derré I. Expression of the effector protein IncD in Chlamydia trachomatis mediates recruitment of the lipid transfer protein CERT and the endoplasmic reticulum-resident protein VAPB to the inclusion membrane. Infect Immun. 2014;
73. Patel AL, Chen X, Wood ST, Stuart ES, Arcaro KF, Molina DP, et al. Activation of epidermal growth factor receptor is required for Chlamydia trachomatis development. BMC Microbiol. 2014;
74. Dumoux M, Clare DK, Saibil HR, Hayward RD. Chlamydiae assemble a pathogen synapse to hijack the host endoplasmic reticulum. Traffic. 2012;

75. Kim JH, Jiang S, Elwell CA, Engel JN. Chlamydia trachomatis co-opts the FGF2 signaling pathway to enhance infection. PLoS Pathog. 2011;

76. Gauliard E, Ouellette SP, Rueden KJ, Ladant D. Characterization of interactions between inclusion membrane proteins from Chlamydia trachomatis. Front Cell Infect Microbiol. 2015;

77. Hung V, Udeshi ND, Lam SS, Loh KH, Cox KJ, Pedram K, et al. Spatially resolved proteomic mapping in living cells with the engineered peroxidase APEX2. Nat Protoc. 2016;

78. Romine MF, Rodionov DA, Maezato Y, Anderson LN, Nandhikonda P, Rodionova IA, et al. Elucidation of roles for vitamin $B_{12}$ in regulation of folate, ubiquinone, and methionine metabolism. Proc Natl Acad Sci. 2017;

79. Anderson LN, Koech PK, Plymale AE, Landorf E V., Konopka A, Collart FR, et al. Live Cell Discovery of Microbial Vitamin Transport and Enzyme-Cofactor Interactions. ACS Chem Biol. 2016;

80. Matzke MM, Waters KM, Metz TO, Jacobs JM, Sims AC, Baric RS, et al. Improved quality control processing of peptide-centric LC-MS proteomics data. Bioinformatics. 2011;

81. Webb-Robertson BJM, McCue LA, Waters KM, Matzke MM, Jacobs JM, Metz TO, et al. Combined statistical analyses of peptide intensities and peptide occurrences improves identification of significant peptides from MS-based proteomics data. J Proteome Res. 2010;

82. Schindelin J, Arganda-Carreras I, Frise E, Kaynig V, Longair M, Pietzsch T, et al. Fiji: An open-source platform for biological-image analysis. Nature Methods. 2012.

83. Jensen D, Schekman R. COPII-mediated vesicle formation at a glance. J Cell Sci. 2011;

84. Zanetti G, Pahuja KB, Studer S, Shim S, Schekman R. COPII and the regulation of protein sorting in mammals. Nature Cell Biology. 2012.

85. Saito K, Yamashiro K, Shimazu N, Tanabe T, Kontani K, Katada T. Concentration of Sec12

at ER exit sites via interaction with cTAGE5 is required for collagen export. J Cell Biol. 2014;

86. Maeda M, Katada T, Saito K. TANGO1 recruits Sec 16 to coordinately organize ER exit sites for efficient secretion. J Cell Biol. 2017;

87. Celli J, Salcedo SP, Gorvel J-P. Brucella coopts the small GTPase Sar1 for intracellular replication. Proc Natl Acad Sci. 2005;

88. Kagan JC, Roy CR. Legionella phagosomes intercept vesicular traffic from endoplasmic reticulum exit sites. Nat Cell Biol. 2002;

89. Pastor-Cantizano N, Montesinos JC, Bernat-Silvestre C, Marcote MJ, Aniento F. p24 family proteins: key players in the regulation of trafficking along the secretory pathway. Protoplasma. 2016.

90. Krämer A, Mentrup T, Kleizen B, Rivera-Milla E, Reichenbach D, Enzensperger C, et al. Small molecules intercept Notch signaling and the early secretory pathway. Nat Chem Biol. 2013;

91. Yonemura Y, Li X, Müller K, Krämer A, Atigbire P, Mentrup T, et al. Inhibition of cargo export at ER exit sites and the trans-Golgi network by the secretion inhibitor FLI-06. J Cell Sci. 2016;

92. Ma W, Goldberg E, Goldberg J. ER retention is imposed by COPII protein sorting and attenuated by 4-phenylbutyrate. Elife. 2017;

93. Oslowski CM, Urano F. Measuring ER stress and the unfolded protein response using mammalian tissue culture system. Methods Enzymol. 2011;

94. Saito K, Maeda M, Katada T. Regulation of the Sar1 GTPase Cycle Is Necessary for Large Cargo Secretion from the Endoplasmic Reticulum. Front Cell Dev Biol. 2017;

95. Yu S, Satoh A, Pypaert M, Mullen K, Hay JC, Ferro-Novick S. mBet3p is required for homotypic COPII vesicle tethering in mammalian cells. J Cell Biol. 2006;

96. Hu J, Shibata Y, Zhu PP, Voss C, Rismanchi N, Prinz WA, et al. A Class of Dynamin-like

GTPases Involved in the Generation of the Tubular ER Network. Cell. 2009;

97. Voeltz GK, Prinz WA, Shibata Y, Rist JM, Rapoport TA. A class of membrane proteins shaping the tubular endoplasmic reticulum. Cell. 2006;

98. Ge L, Zhang M, Schekman R. Phosphatidylinositol 3-kinase and COPII generate LC3 lipidation vesicles from the ER-Golgi intermediate compartment. Elife. 2014;

99. Ge L, Zhang M, Kenny SJ, Liu D, Maeda M, Saito K, et al. Remodeling of ER-exit sites initiates a membrane supply pathway for autophagosome biogenesis. EMBO Rep. 2017;

100. Wylie JL, Hatch GM, Mcclarty G. Host cell phospholipids are trafficked to and then modified by Chlamydia trachomatis. J Bacteriol. 1997;

101. Hatch GM, Mcclarty G. Phospholipid composition of purified Chlamydia trachomatis mimics that of the eucaryotic host cell. Infect Immun. 1998;

102. Recuero-Checa MA, Sharma M, Lau C, Watkins PA, Gaydos CA, Dean D. Chlamydia trachomatis growth and development requires the activity of host Long-chain Acyl-CoA Synthetases (ACSLs). Sci Rep. 2016;

103. Fromme JC, Schekman R. COPII-coated vesicles: Flexible enough for large cargo? Current Opinion in Cell Biology. 2005.

104. Santos AJM, Nogueira C, Ortega-Bellido M, Malhotra V. TANGO1 and Mia2/cTAGE5 (TALI) cooperate to export bulky pre-chylomicrons/VLDLs from the endoplasmic reticulum. J Cell Biol. 2016;213(3):343–54.

105. Bindels DS, Haarbosch L, Van Weeren L, Postma M, Wiese KE, Mastop M, et al. mScarlet: A bright monomeric red fluorescent protein for cellular imaging. Nat Methods. 2016;

106. Bajar BT, Wang ES, Lam AJ, Kim BB, Jacobs CL, Howe ES, et al. Improving brightness and photostability of green and red fluorescent proteins for live cell imaging and FRET reporting. Sci Rep. 2016;

107. Bhattacharyya D, Glick BS. Two Mammalian Sec16 Homologues Have Nonredundant

Functions in Endoplasmic Reticulum (ER) Export and Transitional ER Organization. Mol Biol Cell. 2007;

108. Maki M, Kitaura Y, Satoh H, Ohkouchi S, Shibata H. Structures, functions and molecular evolution of the penta-EF-hand Ca 2+-binding proteins. In: Biochimica et Biophysica Acta - Proteins and Proteomics. 2002.

109. Vito P, Lacaná E, D'Adamio L. Interfering with apoptosis: Ca2+-binding protein ALG-2 and Alzheimer's disease gene ALG-3. Science (80- ). 1996;

110. Svetlana Tarabykina , Jens Mollerup PW and MWB. ALG-2, A MULTIFUNCTIONAL CALCIUM BINDING PROTEIN? Front Biosci. 2004;

111. Yamasaki A, Tani K, Yamamoto A, Kitamura N, Komada M. The Ca $^{2+}$ -binding Protein ALG-2 Is Recruited to Endoplasmic Reticulum Exit Sites by Sec31A and Stabilizes the Localization of Sec31A. Mol Biol Cell. 2006;

112. Shibata H, Suzuki H, Yoshida H, Maki M. ALG-2 directly binds Sec31A and localizes at endoplasmic reticulum exit sites in a Ca2+-dependent manner. Biochem Biophys Res Commun. 2007;

113. la Cour JM, Schindler AJ, Berchtold MW, Schekman R. ALG-2 Attenuates COPII Budding In Vitro and Stabilizes the Sec23/Sec31A Complex. PLoS One. 2013;

114. Bentley M, Nycz DC, Joglekar A, Fertschai I, Malli R, Graier WF, et al. Vesicular calcium regulates coat retention, fusogenicity, and size of pre-Golgi intermediates. Mol Biol Cell. 2010;

115. Helm JR, Bentley M, Thorsen KD, Wang T, Foltz L, Oorschot V, et al. Apoptosis-linked Gene-2 (ALG-2)/Sec31 Interactions Regulate Endoplasmic Reticulum (ER)-to-Golgi Transport: A POTENTIAL EFFECTOR PATHWAY FOR LUMINAL CALCIUM. J Biol Chem. 2014;

116. Shibata H, Kanadome T, Sugiura H, Yokoyama T, Yamamuro M, Moss SE, et al. A new role for annexin A11 in the early secretory pathway via stabilizing Sec31A protein at the

endoplasmic reticulum exit sites (ERES). J Biol Chem. 2015;

117. Takahara T, Inoue K, Arai Y, Kuwata K, Shibata H, Maki M. The calcium-binding protein ALG-2 regulates protein secretion and trafficking via interactions with MISSL and MAP1B proteins. J Biol Chem. 2017;

118. McGourty CA, Akopian D, Walsh C, Gorur A, Werner A, Schekman R, et al. Regulation of the CUL3 Ubiquitin Ligase by a Calcium-Dependent Co-adaptor. Cell. 2016;

119. Kanadome T, Shibata H, Kuwata K, Takahara T, Maki M. The calcium-binding protein ALG-2 promotes endoplasmic reticulum exit site localization and polymerization of Trk-fused gene (TFG) protein. FEBS Journal. 2017;

120. Kitaura Y, Watanabe M, Satoh H, Kawai T, Hitomi K, Maki M. Peflin, a novel member of the five-EF-hand-protein family, is similar to the apoptosis-linked gene 2 (ALG-2) protein but possesses nonapeptide repeats in the N-terminal hydrophobic region. Biochem Biophys Res Commun. 1999;

121. Kitaura Y, Satoh H, Takahashi H, Shibata H, Maki M. Both ALG-2 and peflin, penta-EF-hand (PEF) proteins, are stabilized by dimerization through their fifth EF-hand regions. Arch Biochem Biophys. 2002;

122. Rayl M, Truitt M, Held A, Sargeant J, Thorsen K, Hay JC. Penta-EF-hand protein peflin is a negative regulator of ER-to-Golgi transport. PLoS One. 2016;

123. Greco A, Mariani C, Miranda C, Lupas A, Pagliardini S, Pomati M, et al. The DNA rearrangement that generates the TRK-T3 oncogene involves a novel gene on chromosome 3 whose product has a potential coiled-coil domain. Mol Cell Biol. 1995;

124. Miranda C, Roccato E, Raho G, Pagliardini S, Pierotti MA, Greco A. The TFG protein, involved in oncogenic rearrangements, interacts with TANK and NEMO, two proteins involved in the NF-κB pathway. J Cell Physiol. 2006;

125. Lee NR, Shin HB, Kim HI, Choi MS, Inn KS. Negative regulation of RIG-I-mediated antiviral signaling by TRK-fused gene (TFG) protein. Biochem Biophys Res Commun.

2013;

126. Wynne C, Lazzari E, Smith S, McCarthy EM, Gabhann JN, Kallal LE, et al. TRIM68 negatively regulates IFN-β production by degrading TRK fused gene, a novel driver of IFN-β downstream of anti-viral detection systems. PLoS One. 2014;
127. Witte K, Schuh AL, Hegermann J, Sarkeshik A, Mayers JR, Schwarze K, et al. TFG-1 function in protein secretion and oncogenesis. Nat Cell Biol. 2011;
128. Johnson A, Bhattacharya N, Hanna M, Pennington JG, Schuh AL, Wang L, et al. TFG clusters COPII-coated transport carriers and promotes early secretory pathway organization. EMBO J. 2015;
129. Hanna MG, Block S, Frankel EB, Hou F, Johnson A, Yuan L, et al. TFG facilitates outer coat disassembly on COPII transport carriers to promote tethering and fusion with ER–Golgi intermediate compartments. Proc Natl Acad Sci. 2017;
130. McCaughey J, Miller VJ, Stevenson NL, Brown AK, Budnik A, Heesom KJ, et al. TFG Promotes Organization of Transitional ER and Efficient Collagen Secretion. Cell Rep. 2016;
131. Johnston JA, Ward CL, Kopito RR. Aggresomes: A cellular response to misfolded proteins. J Cell Biol. 1998;
132. Hyttinen JMT, Amadio M, Viiri J, Pascale A, Salminen A, Kaarniranta K. Clearance of misfolded and aggregated proteins by aggrephagy and implications for aggregation diseases. Ageing Research Reviews. 2014.
133. Fischer A, Harrison KS, Ramirez Y, Auer D, Chowdhury SR, Prusty BK, et al. Chlamydia trachomatis-containing vacuole serves as deubiquitination platform to stabilize Mcl-1 and to interfere with host defense. Elife. 2017;
134. Weber MM, Lam JL, Dooley CA, Noriea NF, Hansen BT, Hoyt FH, et al. Absence of Specific Chlamydia trachomatis Inclusion Membrane Proteins Triggers Premature Inclusion Membrane Lysis and Host Cell Death. Cell Rep. 2017;

135. Sixt BS, Bastidas RJ, Finethy R, Baxter RM, Carpenter VK, Kroemer G, et al. The Chlamydia trachomatis Inclusion Membrane Protein CpoS Counteracts STING-Mediated Cellular Surveillance and Suicide Programs. Cell Host Microbe. 2017;

136. Yuan Y, Zhang YX, Watkins NG, Caldwell HD. Nucleotide and deduced amino acid sequences for the four variable domains of the major outer membrane proteins of the 15 Chlamydia trachomatis serovars. Infect Immun. 1989;

137. Cillóniz C, Torres A, Niederman M, van der Eerden M, Chalmers J, Welte T, et al. Community-acquired pneumonia related to intracellular pathogens. Intensive Care Medicine. 2016.

138. Nunes A, Gomes JP. Evolution, phylogeny, and molecular epidemiology of Chlamydia. Infection, Genetics and Evolution. 2014.

139. Beatty WL, Belanger TA, Desai AA, Morrison RP, Byrne GI. Tryptophan depletion as a mechanism of gamma interferon-mediated chlamydial persistence. Infect Immun. 1994;

140. Haldar AK, Piro AS, Finethy R, Espenschied ST, Brown HE, Giebel AM, et al. Chlamydia trachomatis is resistant to inclusion ubiquitination and associated host defense in gamma interferon-primed human epithelial cells. MBio. 2016;

141. Branon TC, Bosch JA, Sanchez AD, Udeshi ND, Svinkina T, Carr SA, et al. Efficient proximity labeling in living cells and organisms with TurboID. Nature Biotechnology. 2018.

142. Roux KJ, Kim DI, Raida M, Burke B. A promiscuous biotin ligase fusion protein identifies proximal and interacting proteins in mammalian cells. J Cell Biol. 2012;

143. Lujan AL, Croci DO, Gambarte Tudela JA, Losinno AD, Cagnoni AJ, Mariño K V., et al. Glycosylation-dependent galectin–receptor interactions promote *Chlamydia trachomatis* infection. Proc Natl Acad Sci. 2018;

144. Kuo CC, Takahashi N, Swanson AF, Ozeki Y, Hakomori SI. An N-linked high-mannose type oligosaccharide, expressed at the major outer membrane protein of Chlamydia

trachomatis, mediates attachment and infectivity of the microorganism to HeLa cells. J Clin Invest. 1996;

145. Kuo CC, Lee A, Campbell LA. Cleavage of the N-linked oligosaccharide from the surfaces of Chlamydia species affects attachment and infectivity of the organisms in human epithelial and endothelial cells. Infect Immun. 2004;

146. Abdul-Sater AA, Koo E, Häcker G, Ojcius DM. Inflammasome-dependent caspase-1 activation in cervical epithelial cells stimulates growth of the intracellular pathogen Chlamydia trachomatis. J Biol Chem. 2009;

147. Rother M, Gonzalez E, Teixeira da Costa AR, Wask L, Gravenstein I, Pardo M, et al. Combined Human Genome-wide RNAi and Metabolite Analyses Identify IMPDH as a Host-Directed Target against Chlamydia Infection. Cell Host Microbe. 2018;